THE INLET VORTEX AS A SOURCE OF TONAL ROTOR NOISE

by

LENNOX JOHN LEGGAT

M.A. Sc., University of British Columbia

B. Eng., Royal Military College of Canada

A THESIS SUBMITTED IN PARTIAL FULFILMENT OF

THE REQUIREMENTS FOR THE DEGREE OF

DOCTOR OF PHILOSOPHY

in the Department

of

Mechanical Engineering

We accept this thesis as conforming to the

required standard

THE UNIVERSITY OF BRITISH COLUMBIA

December 1975

In presenting this thesis in partial fulfilment of the requirements for an advanced degree at the University of British Columbia, I agree that the Library shall make it freely available for reference and study. I further agree that permission for extensive copying of this thesis for scholarly purposes may be granted by the Head of my Department or by his representatives. It is understood that publication, in part or in whole, or the copying of this thesis for financial gain shall not be allowed without my written permission.

Department of Mechanical Engineering

The University of British Columbia
Vancouver V6T 1W5

Date December 18, 1975

ABSTRACT

The thesis describes experimental and mathematical analyses of the noise resulting from the interaction of an axial flow fan with a concentrated inlet vortex. A comparison of results from the two methods reveals the physical phenomena on which the discrete tone noise depends.

Vortices were generated with half delta wings mounted in the inlet bell mouth of an axial flow fan. Their properties of vortex strength, core radius, and core axial velocity deficit were measured in a wind tunnel. The far field spectrum of the fan noise was measured for various combinations of these three parameters, and for different radial positions of vortex entry. An investigation of the origin and effect on the sound levels of naturally occurring inlet vortices was carried out using real time blade pressure measurements and a synchronous display system.

The mathematical analysis comprised a linear two dimensional aerodynamic model of a vortex passing through a fan. The characteristics of the blade loading were calculated as a function of the span position and circumferential angle. Levels of overall noise and of the individual discrete tones were calculated. The theoretical dependence of the noise spectrum on the vortex strength, core radius, and core axial velocity deficit were determined. The variation of sound pressure level with the radial position of vortex entry was also calculated.

Comparison of the experimental and theoretical results shows that an artificially generated concentrated inlet vortex increases the overall sound level by as much as eight decibels and some harmonics to a maximum of fourteen decibels, at a typical set of operating conditions. The vortex circulation has the greatest effect on the tone level at the blade pass frequency while the axial velocity deficit exerts more influence on the higher harmonics of the spectrum. Local blade stall caused by large values of core axial velocity deficit is a suspected contributor to the observed pure tone noise at the higher harmonics.

A naturally occurring inlet vortex was tracked using the synchronous display system. It was observed to be unsteady in its structure and to move about a preferred position of entry into the fan. Its presence increased the overall far field fan noise by a minimum of three decibels and at the blade pass frequency by 4.5 decibel. No change in sound level occurred at the four significant harmonics of the blade pass frequency.

TABLE OF CONTENTS

Section Page

Section Page

Section Page

LIST OF FIGURES

Figure Pages

Figure | Page

NOTATION

A_0, A_n	Fourier coefficients
B	number of fan blades
B_0, B_n	Fourier coefficients
C_0, C_n	coefficients generated by Sears' function
c	speed of sound in air
C_h	fan blade chord
D	slope of blade chord variation function
F	period of revolution of fan (1/60 sec)
f_i	local stress vector
G	slope of blade twist variation function
H	flare constant for axial velocity deficit function
K	constant controlling radius of polar plotter
k	reduced wave number ($C_h \cdot \omega/2U$)
L	lift force
M	slope of axial inflow velocity variation function
n	harmonic number
P	acoustic pressure amplitude
P_s	surface pressure amplitude
p	acoustic pressure
p_s	surface pressure
R	fan radial variable
R_i	fan hub radius

R_t	fan tip radius
R_0	radial position of vortex entry
R	distance from rotor to far field microphone
r	vortex radial variable
r_c	vortex core radius
dS	surface element of area
T	time since birth of vortex
t	time
U	axial velocity at radius R
U_0	axial velocity at tip radius
$U_c(r)$	axial velocity deficit at vortex radius r
U_c	maximum axial velocity deficit
u_n	normal surface velocity
u_i	component of velocity vector
V_{rel}	velocity relative to fan blade
$v(r)$	vortex tangential velocity
$\underline{x}$, x_i	space co-ordinate indicating point of sound detection in the far field
$\underline{y}$, y_i	space co-ordinate used in source region
α_0	steady angle of attack
α	wing or blade steady angle of attack
α'	fluctuating angle of attack
β	effective blade twist angle, relative to plane of rotation
β_0	effective blade twist at rotor tip

Γ	vortex strength / circulation
Φ	angle between tangential velocity of vortex and component normal to fan blade, (Figure 33A)
ϕ	phase angle of filtered correlation function
ψ	angle between relative and rotational velocities
ρ	density of air
Σ	fan circumferential angle
θ	angle between surface normal and far field direction
τ	time delay between two realizations of a fluctuating variable
ν	kinematic viscosity
ω	rotational frequency, (radians/sec)
$dC_\ell/d\alpha$	aerodynamic lift transfer function
db	sound pressure level (SPL) in decibels

$$(SPL)_{overall} \quad 10 \log \frac{\overline{p^2_{overall}}}{(.0002\,\mu\,bar)^2} \equiv db$$

$$\overline{p^2_{overall}} = \sum_n \overline{p_n^2}$$

$p_n \equiv$ pressure of nth harmonic

$$(SPL)_n \quad 10 \log \frac{\overline{p_n^2}}{(.0002\,\mu\,bar)^2}$$

ACKNOWLEDGEMENT

The work described in the thesis was conducted under the supervision of Dr. T.E. Siddon. The author wishes to thank him for his advice and guidance in the research and for his continual optimism.

Thanks go also to Dr. I.S. Gartshore for his comments on the structure of vortices and to Dr. H.G. Davies for assistance with the mathematical development. The able assistance of summer student, Mr. G. Watt was most appreciated. Without the expertise of the mechanical and electrical technicians of the Department of Mechanical Engineering many aspects of the experiments could not have been carried out.

The major portion of this research was funded under the Defence Research Board of Canada Grant No. 9611-03. Some support was received from the National Research Council of Canada under Grant No. A 7106.

1. INTRODUCTION

Perhaps the most annoying, if not the most universally recognized sources of noise to one and all are the gas turbine engines which power most of today's commercial airliners. The noise is generated by unsteady aerodynamic phenomena in the inlet, combustor and jet exhaust of the engine. In first and second generation turbojets the main noise producing area was the jet exhaust. Here intense fluctuating shears developed in the mixing region between the exhaust jet and the ambient air. The associated turbulence is responsible for the broad band rumble that characterizes jet noise. With the introduction of the new high bypass ratio turbofan engines, especially to be found on the "jumbo" jets, the exhaust velocities have been reduced substantially resulting in less shear stress fluctuation in the mixing region and less noise. This reduction in exhaust noise has had the effect of emphasizing sound radiation from another area; the inlet fan. Under certain operating conditions such as approach and taxi fan noise dominates the overall noise produced by the jet engine.

Fan noise is not only of major concern in aircraft propulsion technology, but it also has been a topic of much research pertaining to noise generation in ventilation systems and cooling systems for internal combustion engines. Although the conditions under which fan rotors operate vary substantially, their noise producing mechanisms may be similar; for example, the effect of a series of struts downstream of a ventilating fan may

be similar to the effect of a downstream stator section in a turbo-jet engine.

1.1 Fan Noise Generation

The noise generated aerodynamically by fans can be separated into discrete tone and broad band radiation. Often the tonal radiation tends to stand out over the broad band noise, dominating the annoyance factor associated with fan noise. These two types of noise are a result of force fluctuations on the fan rotor and stator elements. The blade forces can be resolved into time varying lift and drag components, radiating noise normal and tangential to the blade elements respectively. Under certain conditions such as high axial flow Mach number or high rotor tip Mach number, unsteady Reynolds' stresses associated with the combination of the potential flow field of the rotor and a solenoidal velocity field produced by an inlet distortion may also be significant[1].

Noise problems that plagued early fan design, such as the interaction of stator or inlet guide vane wakes with a downstream rotor, have been identified and analysed both mathematically and experimentally. As a result, modern designs minimize these effects through a set of permissible and non-permissible design criteria. Yet despite efforts which have produced sweeping changes in the design of fans, intense pure tones persist especially in the on-axis direction where, in theory, there should be none. It seems apparent that other phenomena are contributing to the discrete

frequency peaks in the spectra of the fan noise, overriding the classical rotational noise first described by Gutin[2].

A comprehensive review of the state of the art relating to fan noise was published by B.D. Mugridge and C.L. Morfey in 1971[3]. The concept of intake flow distortions was discussed in the section entitled "Flow Distortions Responsible for Tone Generation". The process is explained as follows: "Although adjacent blade rows are an obvious source of flow distortion, they may not be the main cause of interaction tones. Potential flow distortions can arise from asymmetry in the duct surrounding the fan; for example, there may be a circumferential variation in rotor tip clearance and hence a periodic fluctuation in blade loading. Other possible disturbances are cross flow,wakes from upstream bends or obstructions in the inlet duct, and streamwise vortices sucked into the fan from nearby solid surfaces. In all cases, efficient acoustic radiation will result at blade passing frequency if the circumferential wavelengths of the flow distortions are similar to the rotor blade spacing. Low frequency modulation of the flow distortion causes band spreading of the radiated tones, and in fact most of the energy in what appears to be a discrete tone may be associated with unsteady velocity distortions which would not be detected by a mean velocity traverse."

1.2 The Inlet Distortion

During the past four years much interest has been directed towards the subject of various types of inlet distortions interacting with a fan rotor[1,4,5,6,7,8,9,10]. Analyses have in general been initiated on the notion of randomly occurring turbulence being drawn past the rotor, or a spatially fixed velocity field anomaly being encountered by the rotor. These approaches have a common basis in that inlet distortions are represented in terms of a spatial sum of very many discrete frequency components, each with its own characteristic spatial structure. Experimental and analytic approaches to the problem have shown that, where axial length scales of an inlet distortion are sufficiently long, an increase will occur in discrete tone radiation at the blade pass frequency and its harmonics. In conditions where single rotors are operating in free air, turbulence with axial length scales of up to 100 feet have been measured[6,9]. Some have suggested that these stretched inflow distortions may in fact be vortices[7,8]; either produced by the elongation of inlet turbulence in the potential sink flow of the fan inlet, or originating at a solid surface near the fan inlet, forming the well known ground vortex[11,12]. In the latter case, as pointed out by Siddon and Leggat[7,8], the distortion is perhaps best modelled as a discrete potential anomaly entering the inlet plane at a fixed position, rather than as a randomly occurring field of inlet vorticity.

Little is known about the true nature of the velocity field associated with the elongated inlet eddy and even less about its

effect on fan rotor loading, and the harmonic levels of the resulting far field sound. This uncertainty is complicated by the fact that vortices are difficult to detect even when they are relatively stationary.

1.3 Scope of Work

This thesis comprises a theoretical and experimental analysis of the inlet vortex/rotor interaction phenomenon. It is hoped that such a study will increase our understanding of the physical processes involved, provide a means to predict noise resulting from vortex blade interaction, and offer insight into some of the unanswered questions put forth by other researchers in the field.

Experimentally, the problem has been explored by introducing known distortions into an axial flow fan. Concentrated vortices of known circulation, core radius, axial velocity deficit and position of entry are generated by a half delta wing. The resulting far field, on-axis sound pressure level is measured for different combinations of vortex parameters. Also, real time polar plots of blade pressure measurements (sychronized to the rotational frequency of the fan) have provided information about the spatial extent and length of naturally occurring and artificially imposed vortices.

A linearized aerodynamic theory has been developed to describe the interaction of a Rankine-type vortex with a fan rotor. Empirical parameters describing the geometry of the fan blade were included and far field on-axis noise spectra calculated in terms of vortex parameters. This model has also provided information

regarding the span-wise distribution of unsteady loading over each blade and around the circumference of the fan, as the vortex passes through the rotor disc. Both experimental and theoretical approaches will be described in detail. Parametric results are discussed and compared. Limitations imposed by the idealized model and their influence on the accuracy of predictions are also considered.

In sequence then, the thesis begins with a discussion of pertinent background material, reviews the extent of previous research, and gives a description of the apparatus and experimental method employed. Then the mathematical model of rotor/vortex interaction is outlined. A presentation of results lends evidence to the inlet vortex theory and contributes to the physical understanding of the problem. Finally there is a discussion of the extent of agreement between the theory and experiments with some comments about the limitations of the mathematical model.

2. BACKGROUND

Before describing the analysis undertaken it is necessary to discuss the results of others who have conducted studies into the problem of inflow distortion/rotor interaction. Major works in this area will be reviewed, from the initial analytic studies to recent experimental investigations which support the notion of stretched eddies or vortices in the inflow of axial flow fans.

2.1 Inlet Turbulence

Mani was one of the first to attempt to model the interaction of a turbulent velocity field with a fan rotor[4]. His work was motivated by experimental findings of Sofrin and McCann[12], and Filleul[14]. Both reported on increase in sound level in fans with an increase in turbulence intensity. Mani postulated that the unsteady velocity fluctuations produced by the turbulence being sucked into a fan would produce "non-stationary fluctuations in angle of attack on the blade row resulting in unsteady forces [on the blades], and noise radiation."[4] He developed a two dimensional model of a fan rotor in the presence of a turbulent inflow. For convenience he chose to model the inflow turbulence as homogeneous and isotropic. His rotor model consisted of a row of flat plate airfoils at incidence. The analysis was carried out in the frequency domain in that the turbulence was treated as a superposition of harmonic shear waves. Sears' lift response

function for an airfoil encountering a sinusoidal gust was used to determine the unsteady blade forces resulting from the incident shear waves. This function predicts a diminishing lift coefficient with increasing frequency or wave number.

Among several significant results, Mani found that peaks in the resulting far field noise spectra appeared at the blade passage frequency and its first harmonic multiple whenever the ratio of the length scale of the turbulence to the transverse spacing between the blades exceeded 0.5. For values of this ratio less than 0.5 the spectra were broad band in nature; the discrete tone phenomena did not radiate constructively.

2.2 Inlet Distortions

Lowson was concerned with the estimation of noise produced when a rotor operated in the presence of a discrete inflow distortion. His particular interest was in the prediction of pure tone noise caused by the interaction of a compressor rotor with the wake of a stator stage[16].

Lowson started with a previously derived result for sound radiated by a fluctuating point source in arbitrary motion[17]. He then allowed this point force function to repeat periodically as would the force on a fan blade when rotating continually through a steady pattern of inflow velocity distortion. In this way Lowson was able to predict the harmonics of the noise radiated by the fluctuating forces on the rotor. He deduced a transfer function

between the inlet velocity distortion harmonic order and the noise, also by using Sears' sinusoidal gust lift response function. However, at that time, the necessary input information pertaining to the characteristics of stator wakes was lacking. Therefore the approach was not pursued further. Lowson's method is useful for predicting the noise given the unsteady blade forces, but it did not treat the complete problem from the input, the velocity distortion; to the output, the noise.

To overcome this deficiency, Lowson subsequently devised an experiment wherein inflow distortions could be measured in a frame of reference rotating with the rotor. These data were used in the calculation of an aero-acoustic transfer function.

He attached a hot wire anemometer to one blade of an unducted rotor mounted in an anechoic chamber. This enabled him to measure the harmonic levels present in the fluctuating velocity relative to the rotor blade. By subtracting these harmonic levels from the acoustic harmonic amplitudes measured in the far field, he was able to determine the magnitude of the transfer function between input velocity distortion and radiated noise. He compared these data with the results obtained from his mathematical model described earlier which employed Sears' function. The comparison is shown in Figure 1. The distribution of points taken as one group collapse to the vicinity of the straight line described by the theory. The agreement is best at conditions of high rotor solidity and rpm (i.e. a seven bladed rotor turning at 1200 and 1600 rpm).

At this point it is useful to consider the employment of the Sears' aerodynamic response function. The function describes the variation of the magnitude and phase of the aerodynamic lift transfer function ($dC_{\ell}/d\alpha$) with reduced wave number k. It describes the sectional lift expected of a two dimensional (infinite span) airfoil when inserted into a velocity field with sinusoidal gusts of a particular wave number acting perpendicular to the chord of the airfoil section (Figure 3) As wave number increases the up wash and down wash effects tend to produce a partial cancellation of incidence-induced lift changes, due to cyclic shedding of countersign circulation (that is essentially a consequence of inadequate compliance with the Kutta condition at the trailing edge). Turbulence incident on an airfoil may be modeled using this Sears' function to describe the variation of force response on each blade section as a function of streamwise wavelength for each element of the spatial (wave number) spectrum. The model assumes the gust field to be locally two dimensional; that is spanwise scale effects are neglected.

Perhaps the most interesting result of Lowson's work was the shape of the inlet relative velocity spectrum (Figure 2). There are as many as forty higher harmonics of the rotational frequency. Strong energy content at high harmonic numbers is indicative of an inflow distortion of small lateral extent and giving a pulse like shape in the time domain (A train of delta functions has a relatively "flat" distribution of harmonic levels). Such a spectrum would not be expected of an isotropic turbulent

velocity field of large scale, but is more characteristic of long skinny eddies crossing the rotor plane.

The work of both Mani and Lowson presents positive evidence that naturally occurring inflow distortions, whether they be due to random atmospheric turbulence or to a spatially discrete inflow distortion may be major sources of rotor noise. The purpose of Mani's model was to "present a systematic approach to determine the effect of turbulence as a noise generator due to its impingement on a blade row." His results show that pure tone peaks at multiples of the blade pass frequency increase in magnitude with an increasing eddy length to transverse spacing between the blades ratio.

Lowson's experimental results were unique and interesting in that they prompted questions as to whether homogeneous isotropic turbulence would be capable of producing an inflow spectrum possessing so many higher harmonics.

2.3 Stretched Eddies and Vortices

Hanson[6] and Siddon and Leggat[8] had different ideas about the nature of the inflow.

Hanson used an auxiliary fan mounted far downstream of the intake bell to draw air through an experimental fan inlet. In this way he was able to measure the characteristics of the inflow at the inlet plane in the absence of a rotor. He measured both streamwise and transverse velocities with a crossed-wire hot wire anemometer. By using a visual means of cross correlation between two hot wire signals he determined that the inflow distortions were correlated

circumferentially over a maximum angle of 30 degrees around the duct axis. This corresponded to a disturbance three inches in width (lateral scale). Auto-correlations of the streamwise velocity fluctuations were conducted. These produced results indicating an integral length scale of 100 feet in the streamwise direction. Hanson considered this anisotropy in the inflow turbulence to be "critical", and "leading to short blade loading pulses (due to the narrowness of the eddies), and high coherence (due to the length of the eddies)." He thought that these long, narrow eddies originated as naturally occurring atmospheric turbulence. As the eddy is sucked into the static fan inlet, it is elongated axially and contracted transversely by the sink-like potential field at the fan mouth. Accompanying this contraction is an increase in its "transverse" velocity to conserve angular momentum.

Hodder[9] undertook a series of experiments where the length scale of the turbulence entering a fan was varied. He measured a 10 decibel decrease in the noise at the blade pass frequency and 15 decibels decrease at the first harmonic when the eddy length was shortened substantially. In the first test the axial length scale of the inlet distortion was measured to be very long in that it was cut some fifty times by the rotating rotor blades over its correlation length. The second test was conducted with a sufficiently short eddy length that it was cut, over its correlation length, by only one blade. The eddy length was shortened by inserting honeycomb into the fan inlet. The significant change in level of the two harmonics supports the theoretical findings of Mani.

Rao and Chu[10] compared Hodder's results with their theory of inlet turbulence interaction noise. Like Mani they used isotropic turbulence as an input, and found that by knowing the turbulence and fan parameters of Hodder they could predict the fundamental and first harmonic noise levels to within 1 decibel. However, their calculated harmonic spectra exhibited less band spreading than Mani's. Rao and Chu attributed this peakiness to differences in the assumptions of loading on neighbouring blades. Mani considered the problem in terms of a Fourier-Stieltjes integral of shear waves producing velocity fluctuations on the blade. He used Sears' function to obtain the resulting lift. Rao and Chu described the turbulence in terms of correlation lengths of the velocity field and then determined the spectral nature of unsteady blade forces resulting from subsequent passes of blades through the same eddy. The subtle difference of these two approaches may account for the more discrete spectrum obtained by Rao and Chu.

Measurements of fan blade unsteady pressure were carried out by both Leggat[7] and Hanson[6] on different fans. Both observed spectra with a dominant fundamental (the fan rotational frequency), and many higher harmonics (Figure 4). The presence of inlet vortices would explain these pressure spectra and Lowson's hot wire spectra.

Using a statistical distribution in position, intensity, and length of long narrow eddies entering a fan, Hanson proposed a model to predict the spectrum of noise produced by the fan/eddy interaction. He formulated the problem in terms of blade forces

produced by the eddies rather than in terms of the eddy velocity field. He used measured blade pressure data to deduce the spatial and temporal character of the fluctuating blade loads. The blade pulses were allowed to vary in intensity, length, and width over time; and in position (Figure 5). The pulse spacing in time was equal to the period of rotation of the fan. He chose parameters describing the shape and duration of the pulse train so that the computed lift spectrum for the blade matched the relative harmonic weighting of the measured blade pressure spectrum. Working with this statistical input Hanson calculated an expected energy spectrum for any far field point. In the on-axis direction his results predicted discrete tone levels at the blade pass frequency and the first harmonic rising above the calculated broad-band spectral levels (Figure 6). However, his method failed to forecast information on the second, third, fourth or fifth harmonics which were observed experimentally in the far field sound.

Concurrent with Hanson's studies came the experimental work of Siddon and Leggat[7,8]. The aim of their work was to prove the existence of expected, but as yet unmeasured sources of fan rotor noise; the effect of duct boundary layer separation in the inflow region, tip clearance modulation and inlet velocity distortions were measured. A method of cross-correlation between the blade hydrodynamic pressure and the far field acoustic pressure (causality correlation) yielded spatial source strength evaluations over the blade surfaces[7,18,19] (Appendix A). A typical source strength curve for spanwise points located at 15 percent chord behind the leading

edge is shown in Figure 7. The ordinate gives the contribution to the mean squared far field pressure ($\overline{dp^2}$) coming from each element of blade surface, dS. The cross-correlation measurements indicate a region of zero source strength at about the 3/4 span position. On the outboard side the source strength is negative, while on the inboard side it is positive. This countersign source strength behaviour indicates that the blade is experiencing a disturbance which on the time average causes force fluctuations on the blade which are out of phase with each other, in a span-wise sense. The significance of negative source strength is explained mathematically and physically by Leggat[7], but basically it indicates that the portion of the surface with negative source strength is radiating more than ±90° out of phase with the dominant part of the far field sound (coming from the positive source region).

Leggat and Siddon explained the existence of the counter-phase source strength as a consequence of a concentrated inlet vortex being physically "chopped" by subsequent blade passages. The null at the 3/4 span point would correspond to the position of the vortex core. The positive and negative source strengths on either side of the null would be caused by decreases and increases in blade angle of attack relative to the mean flow, as the blade passed through the vortex velocity field.

Such a phenomenon would not be in disagreement with the physical explanation proposed by Hodder and Hanson. Hanson said that as the eddy is sucked into the fan the transverse velocities would be expected to increase to conserve angular momentum. As Hanson

measured only one component of the unsteady transverse velocity, and as the hot wire is incapable of distinguishing direction, it is very possible that the eddies measured were well organized vortices; either concentrated ones such as ground vortices or naturally occurring vortices being stretched and aligned in the fan inflow field.

2.4 The Inlet and Tip Vortex

The presence of ground-generated inlet vortices in fans and aircraft jet engines is well documented[11,12], and has been explained using potential flow methods[12]. During flight concentrated vortices may originate from stagnation points in the boundary layer on the fuselage and enter rear mounted engines, while during taxi and run up vortices are likely to grow from both the fuselage and the ground.

The rotor/vortex interaction problem is most acute when a helicopter rotor interacts with its own tip vortices. Here the vortex generated at the tip of one rotor blade may pass close to the underside of the following blade. The associated velocity field interaction may cause efficient noise radiation. If the helicopter is hovering, the tip generated vortices will remain relatively stationary with respect to the rotor blade. The result is a fixed region on the blade over which there occurs a vortex induced stall. Broadband noise is produced. Periodic slapping occurs when the helicopter is in forward flight. The forward velocity of the helicopter tends to skew the path of the shed vortex. The vortex then is no longer stationary with respect to the blade and a periodic modulation of

the blade load results. Actual chopping of tip vortices takes place when vortices shed by a rotor intersect a tandem rotor's plane of rotation. These problems are somewhat different from the fan rotor/vortex interaction problem as the vortex influence is felt over only a small percentage of the rotor blade span; generally near the tip. Regardless, results of work concerned with this problem deserve consideration.

Leverton and Taylor[20] analyzed the vortex "chopping" phenomenon using a model helicopter rotor and two jets blowing against one another to simulate the vortex (Figure 8). They found that the harmonic levels varied as the fourth power of rotor velocity and the square of equivalent vortex strength. The simulated vortex used in the experiments would create more coherent wing loads than would be produced by a true vortex. For this reason true vortex results may prove to be somewhat different.

Patterson, Amiet, and Munch[21] cross-correlated blade pressure and far field acoustic pressure to determine the noise generating mechanisms involved when a vortex passed beneath a stationary airfoil. They found that when the vortex passed very close to the encountering blade, local blade stall developed. This process is not modulatory in time. The noise generating mechanism is associated with the passage of stalled wake eddies over the airfoil trailing edge.

Complete theoretical studies of the noise resulting from helicopter blade/vortex interaction were carried out by Widnall[22] for a vortex passing under a blade of a helicopter in forward flight.

Using linear and unsteady aerodynamic theory, she was able to predict features of the radiated noise including total power and directivity as a function of the vortex characteristics. Widnall showed good agreement between theory and experiments at low tip Mach numbers.

2.5 Role of Present Work

It is evident that there is still much to be resolved about the problem of a fan rotor interacting with an inlet distortion. It is generally agreed among researchers that long coherent eddies are responsible for much of the tonal radiation from rotors. The physical nature of these eddies; whether they should be characterized as steady or intermittent vortices or whether indeed they possess net circulation at all is not clear at this time.

Theoretical approaches to the problem predict the levels of sound at the blade pass frequency and its first harmonic, but do not agree with experiments at higher harmonics. Two dimensional methods using linear aerodynamic assumptions and employing Sears' sinusoidal gust lift response function have given acceptable predictions of the noise due to turbulence interaction. However, this approach has not been applied previously to the problem of a discrete vortex penetrating the rotor disc. The dependence of the fan noise on the vortex parameters and on the position of vortex entry into the fan are unknown.

The following Sections, Three and Four, describe the experimental and theoretical approaches respectively. The author has

presented the experimental work first as it is felt that the development of the theory falls into place more logically if the limitations of the experiments are realized. Sections Three and Four are essentially self-contained. The reader who is primarily interested in the theory may read section Four first without loss of clarity.

3. EXPERIMENTAL ANALYSIS

The experiments were designed to enable a detailed analysis of the noise produced in the far field when a vortex of known strength, axial velocity deficit and core radius was introduced into a fan. Small half delta wings at incidence were used to generate vortices of varying strength and core radius. Their properties were measured in a low-speed wind tunnel using a unique vorticity detection device. Subsequently, the wings were mounted in the fan bell mouth, and the vortex interaction effects measured for various operating conditions. On-blade fluctuating pressures were measured with and without the vortex generator installed. The resulting pressure signal was plotted in real time on a circular polar plot synchronized to the rotation of the fan. This procedure allowed the study of the interaction of naturally occurring vortices with the fan rotor, and a confirmation of the predicted blade load fluctuations due to interaction with the contrived vortices. The University of British Columbia aeroacoustic facility and other apparatus will be described prior to discussions of the experimental techniques.

3.1 Apparatus

3.1.1 Aeroacoustic Facility

All acoustic measurements were carried out in an anechoic chamber of inside dimensions 16 feet by 14 feet by 8 feet high.

The chamber is constructed of steel-fibreglass sandwich panels 4 inches thick mounted on a spring isolated concrete pad. The wedges installed in the chamber are made of semi-rigid fibreglass, and encased in a protective grid of galvanized hardwire cloth. The chamber has been calibrated and validated[23] and was found to exhibit free field (anechoic) conditions from a lower cut-off frequency of 150 Hz to a maximum measured frequency of 100 KHz. Removable hatch covers were incorporated into the initial design of the chamber to allow experiments on fan and jet noise, which involve the passage of air through the chamber.

3.1.2 Fan Rig

The research fan was located in one corner of the chamber, its centre line 30 inches from the wall wedges (Figure 9). The fan began life as a Woods of Colchester 19 inch, seven bladed axial flow fan unit. The rotor was carefully rebuilt, polished, and balanced. It operates in a remanufactured casing made from rings of cast and machined aluminum (Figure 10). The clearance between all blade tips and the casing is constant and equal to .040 inches. The earlier sheet metal shroud provided by Woods was substantially "out of round". The rotor was driven by a 10 hp direct coupled induction motor driving the rotor at a constant rate of 3600 rpm. For the vortex interaction experiments the fan was operated at a constant head of 2.54 inches of water and a flow rate of 7000 CFM with a blade stagger angle of 20 degrees. This operating point was near the optimum and gave a throat inlet velocity equal to that under which

the vortex generating wings were tested. The importance of this matching of velocities will be discussed later.

The fan casing was vibration isolated from the chamber using rubber machine mounts and a flexible coupling to the exhaust duct. The downstream diffuser section was acoustically treated to minimize extraneous noise. Variation of the fan head and flow rate was made possible by the installation of an airfoil louvre in the wind tunnel. A 1/4 inch celled hexagonal honeycomb mesh measuring 4 feet square and 6 inches in thickness was made to be installed over the air intake hatch when required. An inlet bell mouth was molded from fibreglass to an aerodynamically optimum shape giving uniform and unseparated flow at the throat[24]. It was bolted to the upstream end of the fan casing.

3.1.3 Vortex Generators

The vortices that were introduced into the fan were produced by half delta wings with sharp leading edges. The various sweep back angles and dimensions as shown in Figure 11. For testing in the wind tunnel the wings were mounted in a faired support bracket 5 1/2 inches long and 3/8 inches square.

A ball vortometer was used to measure the vortex tangential velocity at any radius (Figure 12). It consisted of a styrofoam ball .10 inches in diameter attached by a thin nylon thread to a support pin mounted to the trailing edge of the airfoil. The rotational velocity field in the wing trailing vortex causes the ball to rotate,

accelerating to an angular velocity where the net drag on the ball is close to zero. This condition corresponds to the point where the ball velocity equals the vortex tangential velocity at the particular vortex radius that the ball occupies. Simultaneous measurement of the angular velocity, ω, and the radius of the circle described by the ball, r, yielded the rotational velocity of the vortex $v(r)$ (results are discussed in section 3.2). The ball rpm was measured with a Strobotac and the circle diameter with a reflex camera mounted on a vertical traverse screw.

3.1.4 Blade Pressure Fluctuations

Measurements of the blade pressure fluctuations were made by installing a .125 inch Kulite semi-conductor pressure transducer into a brass casing which was fitted into a milled slot in the bottom of the blade. Ten pin holes .030 inches in diameter were drilled from the base of the slot through to the blade upper surface (Figure 13). A hole in the brass casing was aligned with the pin hole corresponding to the desired measuring point. The resonant frequency corresponding to the pin-hole/cavity resonator created by the volume inside the transducer casing was calculated to be 10,000 Hz, which is one order of magnitude above the highest frequency of interest in the blade pressure spectrum.

Shielded leads from the transducer were directed back along the milled slot to the hub of the fan where a two channel EKEG F.M. telemetry system was located. The slot was filled with RTV mold-making rubber. This system enables the transfer of two signals

simultaneously from the rotating fan rotor to the stationary telemetry receiver. Gain and phase shift characteristics for the system are shown in Figure 14. The two telemetry transmitters were mounted in a plexiglass housing mounted on the front end of the fan shaft. Batteries to power both the transmitters and two pressure transducers were also fixed in the housing. The rotor and rotor-mounted instrumentation were statically balanced. An aerodynamically shaped nose cone covered the hub-mounted telemetry transmitter package (Figure 10).

3.1.5 Acoustic Analysis

The far field acoustic pressure was measured at a distance of 6 fan diameters (9.5 ft) in front of the rotor plane on the fan axis, using a Bruel and Kjaer 1/2 inch microphone model 2134 (free field corrected). Calibration of the microphone was accomplished using a Bruel and Kjaer piston phone generating a pressure level of 124 db at 250 Hz. The transducer-telemetry system was calibrated using the same piston phone fitted with an adaptor designed to seal around the blade surface pin holes.

A Bruel and Kjaer narrow band spectrum analyzer with a band width equal to 6 percent of the centre frequency was used to measure the far field and on-blade pressure spectra and discrete tone amplitudes. Due to a slowly varying modulation of the rms pressure under "natural" inlet conditions, a Schlumberger time domain analyser had to be used to time average the filtered harmonic levels over a period of 30 sec. This procedure produced an improvement in the accuracy to a repeatability within $\pm$ 0.1 db.

A limited amount of correlation analysis was carried out, using a SAICOR SAI 43A correlation computer. Cross-correlations between the fan blade surface pressure and far field acoustic pressure yielded surface source strength information. The technique is described in Appendix A. Magnitudes of the source strengths at blade spanwise locations were similar to those measured before the modifications to the fan were carried out (Figure 7). This indicated that the modifications had little effect on the inlet vortex detected in earlier work.

3.1.6 Real Time Polar Pressure Display

A special analogue circuit was developed to sychronize the circumferentially varying blade pressure fluctuation to the circumferential position of the rotor blade in which the transducer was mounted. Thus a real time polar plot of the blade pressure at any rotor position could be displayed on an oscilloscope. The method incorporated two analog multipliers which multiplied the blade pressure signal by sine and cosine waves respectively of frequency equal to the fan rotational frequency. The governing equation reads as follows:

$$p(R, \omega t) = \text{const} \sqrt{\underbrace{(e_p \sin \omega t)^2}_{x} + \underbrace{(e_p \cos \omega t)^2}_{y}} + K$$

e_p is the amplified transducer voltage arising from blade pressure fluctuations. The constant accounts for the overall voltage to

pressure calibration of the system. x and y are used as inputs to the horizontal and vertical drives of an oscilloscope trace. ω is the frequency of fan rotation. K is constant which determines the radius of the polar circle. The circle distorts with time on each revolution to depict the spatial and temporal variation of blade pressure. The schematic of the system and an example of resulting polar plot are shown in Figure 15.

3.2 Determination of Trailing Vortex Characteristics

Measurements of the strength, core radii, and position of trailing vortices behind delta wings have been carried out by other researchers[25,26,27,28]. However, in these cases the results obtained were particular to the dimensions of the model and the Reynolds' number under which it was operated. For this reason, it was decided to experimentally measure the vortex characteristics corresponding to the model sizes and flow rates associated with the fan experiments.

A delta wing of 5 1/2 inch root chord was mounted in an open circuit wind tunnel with test section dimensions 6 1/2 inches by 12 1/2 inches. The vortex position relative to the wing trailing edge, tangential velocity, core radius and axial flow deficit were measured for angles of attack ranging from 10° to 30° in five degrees increments. Details of the method used to locate the vortex core relative to the wing, using a hot wire anemometer are contained in Appendix B.

3.2.1 Measurement of Core Radius and Vortex Strength

To ensure that the ball vortometer accurately followed the vortex tangential velocity, it was necessary to position the pivot point on the axis of the vortex. Using the core positional data recorded in Appendix C, the pivot point was placed at the point in space corresponding to the vortex core position for the wing angle of attack. With the tunnel at operating velocity (63.7 ft/sec), the position of the pivot point was adjusted until the rpm of the ball maximized. This last minor adjustment ensured the pivot point to be as close to the axis of the vortex as the ball vortometer was capable of sensing.

The nylon thread was extended to a length of 1.5 inches and then decreased in length by small intervals. At each interval the rpm of the ball and the diameter of the circle it swept were measured. In some cases, the ball trajectory would lie within the rotational (solid body) core. In other cases it would spin at a radius larger than the core radius where the magnitude of the tangential velocity falls as 1/r. Here the vortex velocity field behaves like that of an irrotational (ideal) vortex. When the ball was in this region the velocity gradient over the nylon thread caused the ball to spin faster than the local vortex velocity. On the other hand, when the radius of the vortometer circle became too small, stiffness in the nylon thread became important, and with decreasing circle radius the ball eventually stopped spinning. The former of these two effects became important at radii exceeding twice

the core radius of the vortex, while the latter occurred when the circle radius became less than approximately 25 percent of the core radius.

The measured data was compared with a mathematical model for real vortices obtained from vortex tube experiments:[29]

$$V(r) = \frac{\Gamma}{2\pi r}\left(1 - e^{-\frac{r^2}{4\nu T}}\right) \qquad \ldots .(3.1)$$

where Γ is the vortex strength, ν is the kinematic viscosity of air and T is the time elapsed since the birth of the vortex. T determines the vortex core radius . To achieve a comparison we referenced the measured radius of peak tangential velocity to the theoretical value. This is accomplished by setting the first derivative with respect to radius of the vortex tangential velocity equal to zero

$$\frac{dV(r)}{dr} = 0 \qquad \ldots .(3.2)$$

yielding

$$\frac{-r^2}{4\nu T} = \ln \frac{4\nu T}{2r^2 + 4\nu T} \qquad \ldots .(3.3)$$

substitution of the measured value of core radius (r_c) for r gives the value of T for which the theoretical and measured core radii will align. The strength of the vortex may then be simply calculated as follows:

$$\Gamma = \frac{2\pi r\, V(r)}{1 - e^{-\frac{r^2}{4\nu T}}} \quad . \qquad \ldots .(3.4)$$

Curves showing the amount of agreement between measured and theoretical vortex tangential velocity fields are shown in Figures 16 and 17. Here also is shown the collapse of the calculated values of vortex strength.

Curves describing the variation of vortex strength and core radius with angle of attack for the 5.5 inch wing were plotted (Figures 18 and 19). Vortex strength was found to vary linearly with angle of attack while core radius was given by the following relationship

$$\text{Log } r_c = .439\,\alpha + 1.27 \quad . \qquad \ldots .(3.5)$$

Having these relationships, it was possible to define vortex strengths and core radii for vortices generated at all angles of attack from 0 to 30 degrees, by the other three half delta wings, by measuring these properties at only two angles of attack for each wing (Figures 18 and 19). These data along with those pertaining to the vortex measurements from the 5.5 inch wing are presented in Appendix C

3.2.2 Vortex Axial Flow Deficit

The amount by which the axial (streamwise) velocity decreased inside the vortex core was measured by traversing a hot wire anemometer

laterally through the core. The spatial extent and magnitude of the deficit was found to vary with the wing angle of attack. The core remained very tight and the deficit was difficult to detect until the wing angle of attack increased to the point where trailing vortex bursting was expected[30]. At this point the spatial extent of the deficit increased rapidly with angle of attack (Figure 20). The magnitude of the deficit is tabulated in Appendix C. Deletions in this data for wings at low angles of attack indicate that the magnitude of the deficit could not be measured. For these cases the vortex had not burst.

The term "vortex bursting" refers to a transition that occurs in delta wing trailing vortices when the wing is operated at high angles of attack. The vortex core changes from laminar to turbulent. The transition is accompanied by a spreading of the radial extent of the axial velocity deficit in the vortex core, and an increase in the growth rate of the vortex core radius with time. The stability of the vortex deteriorates more quickly than for the laminar case. The result is a more rapid break up of the vortex field.

The onset of bursting is useful because it allows two types of vortices to be tested (laminar and turbulent cores). Not only may the effect of vortex strength on the noise be examined, but also the contribution of various forms of vortex cores and percentage velocity deficits.

3.2.3 Discussion of Vortex Velocity Fields

The wind tunnel measurements of the half delta wing trailing vortices provided a range of circulation values from a minimum measured strength of 7.5 ft^2/sec (r_c=.625 inches) to a maximum of 40 ft^2/sec (r_c = 1.23 inches). The vortex axial velocity deficits varied from the limit of being undetectable with a hot wire (no vortex bursting) to a maximum of 82 percent velocity deficit.

The agreement of the measured data with the mathematical vortex model was good in most cases. Therefore, this model was used as the vortex input to the theoretical analysis of the problem with the values for Γ and r_c being based on the calibration experiments.

The hot wire measurements of axial velocity deficits may be considered accurate only in cases where the deficit region is wide compared to the length of the wire. However, in cases with tight cores such as the 5.5 inch wing at 10° angle of attack (Figure 20), the axial velocity measurement is probably somewhat inaccurate because the active portion of the hot wire sensor ($\simeq$.05 inches) was probably larger than the true core radius. Less confidence can be placed in the magnitude of the deficit in these cases. The position of the vortex core, however, is thought to be reasonably accurate.

3.3 Vortex/Rotor Interaction Experiments

The experiments were designed to determine the effect of the vortex parameters of vortex strength, core radius, and axial velocity deficit on the overall on-axis fan noise resulting from a

single vortex passing through the rotor disc. We also studied the dependence of the far field noise level on the radial position of vortex entry into the fan.

As the results of these experiments were to be compared to those derived by the mathematical model, it was necessary to ensure that conditions in the fan inlet were as similar as possible to those under which the vortex characteristics had been measured in the wind tunnel. Furthermore, it was necessary to ensure that other forms of naturally occurring distortions be minimized to the ultimate degree.

The former of these two conditions was achieved as follows. The half delta wings were mounted in the throat of the fan inlet bell mouth 2 inches from the fan rotor (Figure 21). This distance corresponded to the position where all vortex parameters were measured relative to the wing in the wind tunnel. The operating point of the fan and duct system was altered with the controlling louvre until the axial inflow velocity at the bell throat matched the velocity used for the wind tunnel tests (63.7 ft/sec). At this condition the fan was operating with a static head of 2.54 inches of water with a blade stagger angle of 20°. The presence of contaminating noise being generated as a result of an interference between the upstream potential field of the rotor and the delta wing surface was found to be minimal. No increase in sound level was detected at all the harmonics with the half delta wing at 0° angle of attack compared with the case of no delta wing inserted.

The effect of naturally occurring distortions was minimized by placing the honeycomb over the anechoic chamber hatch. The result was a decrease in the overall sound pressure level of 3 db and in the blade pass frequency of 4.5 db. No effect was apparent at the higher harmonics. A decrease in the degree of fluctuation in the magnitude of the overall sound pressure level with time accompanied the insertion of the honeycomb. The resulting base-line spectrum is shown as the solid line in Figure 22. (No imposed vortex).

3.3.1 Dependence of Noise on Vortex Parameters

Tests were carried out for each of the half delta wings mounted at angles of attack varying from 10° to 30° (both burst and unburst vortices). A vortex with positive circulation (counter-clockwise rotation) was generated by the wing at positive angles of attack, and vice versa for negative angles of attack. The fan rotor was also turning counter-clockwise as viewed from the inlet.

A change in the angle of attack of one wing produced a change in all three vortex parameters of interest: core radius, circulation strength, and axial velocity deficit. Operating all four wings at the same angle of attack resulted in a change in vortex circulation and axial velocity deficit from wing to wing, but no change in core radius. In a few cases, wings operating at different angles of attack would produce vortices of equal vortex strength, but varying core radius and axial velocity deficit. It is apparent, then, that the effect of all three vortex parameters may not be studied independently, but must be analyzed in groups of two and three.

Overall far field sound levels and spectra were measured for wing angles of attack, both positive and negative, in 5° increments. The far field microphone was at the on-axis position at a distance of six fan diameters. Typically the overall levels increased by anything from 1 to 8 db and some harmonics showed an increase of up to 14 db as the angle of attack was increased from 0 to 30 degrees. Figure 22 contrasts the effect on the far field spectrum for vortices of identical characteristics except that their direction of rotation is reversed in the two cases. Notice that the vortex of negative (clockwise) rotation creates two new harmonic peaks (2100 and 2520 Hz). This result is for only two conditions, but they are representative of the trends observed in all the trials. They serve to give an overall impression of the effect of the vortices. A tabulation of the effect of the varying vortex parameters on the overall level and blade passing harmonic levels is presented in Appendix D.

The trends of positive and negative vortex sense do not show any common features. Therefore they will be discussed separately. A parametric analysis was carried out of the expected lift fluctuation amplitude on the blade (Appendix E). This produced a way of scaling the dimensional dependence of acoustic noise levels relative to the vortex properties. Two terms involving the three vortex parameters evolved: ($\Gamma U_c r_c$ and $\Gamma U_o r_c$). The overall noise levels for both positive and negative vortex sense were plotted against each of the two terms. The data collapsed most favourably against the grouping $\Gamma U_c r_c$. The curves for these data are shown

in Figure 23. Vortices of negative sense (rotation opposite to that of the fan) effect the overall noise level more strongly than do positive vortices at the higher values of $\Gamma U_c r_c$ while the opposite is true at low values of $\Gamma U_c r_c$. Unfortunately, the magnitude of the discrete tone levels of the measured blade pass frequency and its higher harmonics did not collapse well when plotted against either of the two parametric groupings calculated in Appendix E. This is not surprising, however, as each frequency will possess its own functional dependence on the three vortex properties (Γ, U_c and r_c); and therefore, the data may collapse against one grouping of the parameters, but more likely some compromise of the two groupings. Most of the discrete frequency sound levels show an increase in amplitude with an increase in vortex strength, core radius, and axial velocity deficit.

The effect on the overall noise of changing only the vortex circulation and axial velocity deficit parameters is shown in Figure 24. Here each set of four points (white circles, black triangles, etc.) represents the noise level produced when each of four vortices of equal core radii, but increasing vortex strength pass through the fan rotor. The four equal core radii vortices were produced by the four half delta wings of equal root semi-span operating at the same angle of attack. The axial velocity deficit in the vortex increases as the root chord of a half delta generating wing decreases. Therefore in any set of four points, the axial velocity deficit decreases as the vortex strength increases.

Take for example the set of white squares for a vortex strength with positive sense. Here as the vortex strength increases, the resulting noise level increases very little. It would seem that the effect on the noise of the increase in the vortex strength is being cancelled by the effect of the decrease in axial velocity deficit. This trend is generally true for all sets of points for the overall sound pressure level case.

Now look at Figure 25 which shows the variation of amplitude of the 1680 Hz harmonic with changes in vortex strength. There is a large increase in harmonic amplitude with increasing vortex strength for both positive and negative vortex sense. For the case of negative vortex sense and the white squares, a doubling a vortex strength causes a 8 db increase in the sound pressure level. The reason for this trend is not immediately obvious. On first look it is clear that the blade loading at 1680 Hz is very sensitive to changes in the vortex strength, but there are no obvious physical explanations. The results of the mathematical model may help to clarify this trend in the data.

In Figure 26, an entirely different trend is displayed. Here the sound pressure level at the blade pass frequency actually decreases with increasing vortex strength. If the axial velocity deficit were the dominant mechanism contributing to the sound level at this frequency, then this behaviour would be expected. That is, as the vortex strength increases, the dominant distortion, velocity deficit, decreases; and so the sound level should decrease. Intuitively, however, we know that because the axial velocity deficit tends to be small in spatial extent compared to the vortex tangential

velocity field, it should contribute more favourably to the higher harmonics of the spectrum. This result is indeed a paradox, and it too must await the results of the mathematical model for a proper explanation.

3.3.2 Dependence of Noise on Position of Entry

The change in the far field noise spectrum with vortex position of entry was measured by introducing the vortex into the fan at a number of different radial positions. The 5 1/2 inch wing was mounted on one of a series of thin flat plates. The plate was then placed in the throat of the bell mouth so as to cut the circular inlet plane as does a chord of a circle (Figure 27). The wing was set at incidences of plus and minus 30°. When the radial position of entry was to be changed, the wing was mounted on a longer flat plate thus bringing it closer to the hub of the fan. At each radial position the effect of the plate alone on the far field noise spectrum was measured. The effect was significant at all harmonics, when the plate was 2 inches in front of the fan rotor. When moved upstream to a distance of 4 inches the effect was very much less significant. For the worst case its presence changed the overall level by .6 db. The worst increase in a single frequency was 2.3 db at 840 Hz. The minimum increase in the sound pressure level was produced when the test vortex (Γ=30 ft^2/sec, r_c=0.078 ft, U_c/U = 77%) was introduced into the fan at a radius of R/R_t= .45. The result was a 4 db increase in the overall noise level. The lowest increase for a single frequency was 3 db for the 1680 Hz harmonic. The increase in sound level resulting from the introduction of the mounting plates are shown in Appendix D.

In Figures 28 and 29 is plotted the resultant variation in sound level produced when the vortex was introduced at radial positions varying from a minimum fan radius of .36 ft (R/R_t = .45) to a maximum of .64 ft (R/R_t = .81). Figure 28 shows the effect of positive sense vortices and 29 of vortices of negative sense. In both graphs the trend is for the overall sound pressure level and that of the fundamental tone to decrease uniformly as the vortex approaches the root of the fan blades. The higher harmonic levels tend to cross over each other as the radial position of vortex entry is varied. Discussion of this phenomenon would best be left until results of the mathematical model can be presented simultaneously.

3.3.3 Fluctuating Blade Pressures

A study of the effect of the imposed vortex and naturally occurring ground or atmospheric vortices was made possible using the blade pressure measuring apparatus described earlier in Section 3.1.6. The pressure transducer was mounted in the fan blade .6 inches from the blade tip. This point was deemed most suitable as it corresponded to the region on the fan blade where the pressure fluctuations and acoustic source strength had been found to be strongest. These results come from earlier work[7]. The source strength curve of Figure 7 shows that the magnitude of the source strength is greatest between non-dimensional fan radii of .86 and .97. The present measuring point is at a non-dimensional fan radius of .93. At this point the effect of naturally occurring vortices should be most apparent.

Tests were run with imposed vortices of positive and negative sense ($\Gamma = \pm 20$ ft^2/sec, $r_c = .65$ ft, $U_c/U = 75\%$). The pressure measuring hole was .324 inches outboard of the vortex core radius. The vortex generator was then removed from the fan. Measurements were repeated for the clean running fan both with the honeycomb in place over the anechoic chamber hatch and with it removed. Pictures taken of the oscilloscope trace under these four conditions are shown in Figure 30.

For the imposed vortex with circulation sense opposite to that of the fan rotor, the pressure on the upper surface decreases on encounter with the vortex (Figures 30A, 31A). The vortex tangential velocity at the pressure tap is rotating opposite to the rotation of the fan. The resulting increase in the ωR component felt by the blade section causes an increase in the local angle of attack. The result is an increase in sectional lift which involves a decrease in the pressure on the upper surface of the blade section. A vortex of opposite circulation sense produces the opposite sequence of events and leads to an increase in the pressure in the region of the vortex (Figures 30B, 31B). Figures 30C, 31C and 30D, 31D contrast the effect of placing the honeycomb over the anechoic chamber hatch. Figure 30C shows a substantially greater degree of blade pressure fluctuation than is apparent in Figure 30D. It is this fluctuation that is responsible for the 3 db increase in far field noise level produced when the honeycomb is removed from the anechoic chamber hatch.

A series of 16 mm exposures of the variation of the blade surface pressure signal are shown in Figure 32. The figure shows what appears to be a large naturally occurring vortex entering the

lower portion of the fan generally near 5 o'clock position. It is indicated by a localized "hump" on the polar plot. It can be seen after examination of Figure 32 that this characteristic hump (marked for convenience) is recurrent over time and persists for several revolutions. The camera shutter speed was 1/50 sec and the film speed was 18 frames per sec. Therefore each exposure displays approximately one revolution of the fan rotor. Two revolutions occur between frames. In the series of exposures shown in Figure 32, the characteristic hump persists for about four consecutive frames, or twelve revolutions of the rotor.

The double-humped blade pressure signature produced by the vortex is indicative of a vortex of positive sense (i.e. counter-clockwise rotation) entering the fan inboard of the pressure tap. It possesses a significant axial velocity deficit. The positive sense vortex circulation causes a decrease in angle of attack at the instrumented blade section, and an increase in pressure on the blade upper surface. However, as the blade passes through the core of the vortex it experiences a decreases in axial velocity and a resultant increase in angle of attack. This explanation accounts for the dimple (suction) between the two humps.

The spatial extent of the natural vortex varied although it usually encompassed about 60° on the inlet plane, with a core radius covering about 30° or 1.48 inches. In contrast, the largest vortex generated by the half delta wings possessed a smaller core radius of 1.15 inches.

The fact that the double humped pressure signature is recurrent over time indicates that the vortex is moving continually over the face of the fan in a preferred area (the lower sector of the inlet). The group of five marked frames shown in Figure 32 not only show this motion of the vortex, but also suggest that the vortex strength is changing with time. The magnitude of the pressure signature increases and then decreases as successive frames are encountered.

These irregular increases and decreases in the rate of vortex rotation, coupled with the varying position of vortex entry into the fan are probably responsible for the low frequency modulations in the far field overall sound level which were relatively sporatic and as large as 6 db over a time interval of one sec.

If the vortex were as strong and persistent as the photographs indicated, then it could only have been generated by the gathering of vorticity from the boundary layer on a nearby surface (i.e., a floor vortex). The closest and largest surface present was the floor of the laboratory outside the hatch of the anechoic chamber. Fine styrofoam beads were sprinkled over the floor while the fan was running at maximum flow rate. The beads were seen to rotate over the surface of the floor in concentric clockwise trajectories. Their rate of rotation varied somewhat, in an erratic fashion. Also the position on the floor over which the circulation centered, tended to move about, as the vortex wandered to regions of high vorticity concentration.

3.4 Remarks on Experimental Analysis

The experiments described above have provided a good information base on the problem of rotor/vortex interactions, but the results obtained are only applicable to the physical conditions under which the experiments were conducted. Some of the experimental results are functionally dependent upon a group of parameters, rather than just one. A mathematical model would help in the extension of the results beyond the experimental limitations and in the determination of how the vortex physical properties affect rotor noise.

4. MATHEMATICAL ANALYSIS

A linearized, two dimensional model was developed to describe the interaction of a fan rotor with a single inlet vortex. The model leads to predictions of the discrete tone noise levels and helps to explain some of the results obtained in the previous section. Furthermore, the model is general enough to be used as a building block for other more complex combinations of vortices and rotors.

4.1 General Method

The sectional load variation is a function of span-wise position for a single blade as it completes one revolution. This loading is then applied to all seven blades taking into consideration the appropriate time lag for vortex encounter by each blade. This rotor loading function is then used to predict the far field overall and discrete tone sound pressure levels. A completely closed-form analytic approach was attempted, but proved to be too complicated in end form to be of general use. Therefore, a hybrid solution was developed. The sectional loading on a blade was determined analytically by superimposing the incident velocity fields. The remainder of the problem (Fourier analysis and radiation calculations) was solved numerically using the UBC IBM 370 computer.

4.2 Mathematical Formalism

The geometry of the vortex entry into the fan is shown in Figure 33A. The vortex is fixed in space, entering the fan at a radial position, R_0, and at a 3 o'clock circumferential angle (Σ=0). Counter-clockwise circulation is taken as positive. The vortex tangential velocity v(r) is a function of its radius, r, measured from the vortex centre. The fan is spinning with counter-clockwise rotation and angular velocity ω. Its tip radius is R_t and hub radius R_i (the fan radial variable is R).

4.2.1 Fan Blade Geometry

In the analysis the sectional lift on each blade was calculated as a function of radial position.. Radial changes in blade shape result from variations in chord, twist, and zero lift line. These were measured and accounted for as follows. The chord variation was modelled as a linear function.

$$C_h = C_{h_0} + D(R_t - R) \quad . \qquad \ldots .(4.1)$$

The change in twist and zero lift line were lumped together to give an effective linear twist function

$$\beta = \beta_0 + G(R_t - R) \quad . \qquad \ldots .(4.2)$$

The equation describes the measured variation in blade twist over the span. It was found to increase linearly as the blade root was approached.

The sectional shape of the airfoil was measured and found to be closed to a NACA 4412 wing section[31,32], which has a lift curve slope of 5.72 per radian over a range of Reynolds numbers from 83,000 to 3,000,000. The fan blade sectional Reynolds' numbers varied from 340,000 to 560,000 for the test flow rate.

4.2.2 Velocity Fields

The blade was subjected to two pairs of orthogonal velocity components relative to the moving blade element. The steady components comprise the axial (inflow) velocity and the local rotational velocity. Both of these steady components were modulated by velocity disturbances imposed by the time varying vortex field (relative to the blade). The axial velocity was modulated by the velocity deficit in the vortex core. The velocity, ωR, resulting from the fan rotation was modified cyclically by the circulatory velocity field of the vortex.

The axial velocity deficit of the vortex core was modelled by fitting a Gaussian function to measured profiles of the deficit. The form of equation which suited the measurements of the burst vortex cores was

$$U_c(r) = U_c \, e^{-H(\frac{r}{r_c})^2} \qquad \ldots (4.3)$$

Here $U_c(r)$ is the local velocity deficit and U_c is the maximum value of the deficit at the vortex centre. The vortex core radius is given by r_c, and H is an empirically derived constant which describes the rate of flare of the deficit with vortex radius. A comparison of this function with experiment is shown in Figure 20.

The mathematical form of the tangential velocity field was discussed earlier and is given by

$$v(r) = \frac{\Gamma}{2\pi r} \left(1 - e^{-\frac{r^2}{4\nu T}}\right) . \qquad \ldots .(4.4)$$

In calculating the sectional lift versus time, we are only interested in the component of v(r) which is tangential to the blade element trajectory (i.e. that which produces an upwash fluctuation on the local blade element). This component acts perpendicular to the span of the blade and is given by $v(r) \cos \Phi$ (see definition of Φ, Figure 33A). It contributes to the instantaneous lift on the blade, whereas the span-wise component is inconsequential to the lift, according to our two dimensional model. In terms of the fan parameters, this upwash component of the vortex velocity may be expressed as follows:

$$v(r) \cos \Phi = \frac{\Gamma}{2\pi r} \left(1 - e^{\frac{-r^2}{4\nu T}}\right) \left(\frac{R - R_0 \cos \Sigma}{r}\right) . \qquad \ldots .(4.5)$$

where:

$$r^2 = R^2 - 2R\,R_0 \cos \Sigma + R_0^2 \quad . \qquad \ldots . (4.6)$$

The angle Σ locates the position of the quarter chord span line in the rotor plane.

The rotational velocity of the fan remained constant, but the axial velocity, $U(r, \omega t)$, was found to decrease relatively linearly with decreasing fan radius at the one fan operating condition used. It was decided to model this effect with the equation

$$U(R,t) = U_0 - M(R_t - R) - U_c(r) \quad . \qquad \ldots . (4.7)$$

Here U_0 is the axial velocity measured at the fan rotor outer extremity. The velocity drop to the rotor hub amounts to 18 percent. Figure 33B depicts the variation in blade relative velocity due to the vortex velocity components, which will occur upon each vortex encounter. Note that $U(R,t)$ incorporates the cyclic variation of the axial velocity deficit, $U_c(r)$.

4.2.3 The Quasi-Steady Lift Equation

The instantaneous section lift on the blade may now be expressed using the lift equation of linearized aerodynamics:

$$\frac{dL}{dR}(R,t) = \frac{1}{2} \rho\, V^2_{rel}(R,t) \frac{dC_\ell}{d\alpha}(k)\, \alpha(R,t)\, C_h(R) \quad . \qquad \ldots . (4.8)$$

where

$$V_{rel}^2(R,t) = U^2(R,t) + (\omega R - v(r)\cos\Phi)^2 \quad \ldots .(4.9)$$

The instantaneous angle of attack

$$\alpha(R,t) = [\beta(r) - \psi] - \alpha' \quad \ldots .(4.10)$$

$$= \alpha_0 - \alpha' \quad \ldots .(4.11)$$

where α_0 is the steady angle of attack

$$\alpha' = \mathrm{Tan}^{-1}\frac{U(R,t)}{\omega R - v(r)\cos\Phi} - \mathrm{Tan}^{-1}\frac{U(R,t)}{\omega R} \quad \ldots .(4.12)$$

$$= \mathrm{Tan}^{-1}\left[\frac{U\, v(r)\cos\Phi}{\omega^2R^2 - \omega R\, v(r)\cos\Phi + U^2}\right] \quad \ldots .(4.13)$$

Having expressed the cyclic variations of velocity and angle of attack in terms of known geometric properties of the fan, the time varying lift over the entire blade is written as:

$$L(t) = \frac{1}{2}\rho\frac{dC_\ell}{d\alpha}(k)\int_{R_i}^{R_t} C_h\,[U^2 + (\omega R - v(r)\cos\Phi)^2]^* \cdot$$

$$*\left[\alpha_0 - \left(\frac{Uv(r)\cos\Phi}{\omega^2R^2 - \omega R\, v(r)\cos\Phi + U^2}\right)\right]dR \quad \ldots .(4.14)$$

L(t) is a repetitive pulse-like function of time for each blade. The amplitude of the circumferential lift variation for each blade is identical. However, because the blades encounter the vortex one after the other, the lift fluctuation on one blade leads that of the follow-

ing blade by 1/B of the period of revolution. Therefore, the method of analysis was to sum the contributions to the far field noise from lift fluctuation on each of the blades. (As shown in the following Section).

4.2.4 The Acoustic Transfer Function

In terms of the fluctuating force on the B blades of the fan rotor, the far field acoustic pressure is given by

$$p(R,t) = \frac{\cos\theta}{4\pi Rc} \sum_{n=0}^{B-1} \left[\frac{dL}{dt} \left(t + n\frac{F}{B}\right)\right]_{t-\frac{R}{c}} \quad \ldots .(4.15)$$

where θ is the angle between lift vector, L(t), and the far field measuring point. F is the period of revolution of the fan. This result comes from Curles surface integral solution[33]. Its origin is briefly described in Section 1 of Appendix A. Equation 4.15 sums the fluctuating lifts from the B blades. It is valid only where the distances from each blade to the far field measuring point are equal (i.e. an on-axis evaluation point). If an off-axis point is chosen, we must sum the lift fluctuations from the blades accounting for the phase difference caused by the variation in path length for each blade. This problem will not be considered in the present work.

Using Equation 4.15 it is possible to calculate the far field, on-axis, acoustic pressure in terms of the fluctuating rate of change of lift on a single blade.

The notion of using the total blade force fluctuation to calculate acoustic radiation is valid if the compact source condition is met. That is, the quarter wave length of the frequencies of interest must be long compared to the differences in path length to the far field measuring point between the fan tip and hub. This condition holds for the range of frequencies being considered here.

The aerodynamic lift transfer function $dC_\ell/d\alpha$ is a function of reduced wave number k[15], which is itself dependent on frequency and the radial position of the blade section. Ideally the wave number spectrum of the cyclic sectional incidence variation should have been calculated at each blade section. The calculated amplitudes would then have been multiplied by the appropriate value of the lift transfer function. However, this procedure proved to be lengthy and very costly in computer time. Calculations of the rate of change of lift over the blade sections showed the maximum effects were at the fan radial position where the vortex was being ingested (Figure 34). For this reason it was argued that a span-wise variation in the magnitude of the lift transfer function would have little effect on the integrated blade loading. We therefore used a frequency weighting of $dC_\ell/d\alpha$ appropriate to the blade chord and relative velocity at the point of vortex entry.

The resulting acoustic pressure signal is expanded in a Fourier series. The relationship between the rate of change of lift on the blades; and the far field acoustic pressure is linear. Therefore the lift transfer function is carried through the analysis to the point where the acoustic spectrum is evaluated. At this time it is incorporated into the analysis as a function of frequency. An elaboration of this method follows.

4.2.5 Inclusion of Sears' Function

Because the Sears' function ($dC_\ell/d\alpha$) is not a function of time it may be taken outside the summation sign in Equation 4.15 (refer to Equation 4.14 for the dependence of $L(t)$ on $dC_\ell/d\alpha$). The process for inserting the appropriate values of the function into Equation 4.15 is to expand the periodic far field acoustic pressure into a Fourier series using a constant value for $dC_\ell/d\alpha$ (i.e. the lift curve slope for zero frequency limit, $k \to 0$)

$$p(R,t) = \frac{A_0}{2} + \sum_{n=1}^{\infty} A_n \cos n\omega t + B_n \sin n\omega t \quad . \qquad \ldots . (4.16)$$

Sears' function is a function of reduced wave number

$$k = \frac{C_h}{2} \frac{\omega}{V_{rel}} \quad . \qquad \ldots . (4.17)$$

For each discrete frequency, ω, there is a appropriate correction factor C_n.

$$C_n = \frac{dC_\ell}{d\alpha}(k) \Big/ \left(\frac{dC_\ell}{d\alpha}\right)_{k=0} . \qquad \ldots .(4.18)$$

The far field discrete frequency tone levels

$$P_n(R,\omega) = C_n \sqrt{A_n^2 + B_n^2} \qquad \ldots .(4.19)$$

and the correct far field acoustic pressure is

$$p(r,t) = C_0 \frac{A_0}{2} + \sum_{n=1}^{\infty} C_n A_n \cos n\omega t + C_n B_n \sin n\omega t \qquad \ldots .(4.20)$$

4.3 Results of the Analytic Study

The nature of the model is such that there exist infinite possibilities for the variation of fan and vortex parameters. In order to illustrate the most essential features of the interaction, a planned approach to the verification and application of the model was devised and followed.

The verification consisted of examining results at various steps of the development of the problem, and eventually of comparing the calculated overall and discrete tone levels with those measured (as discussed in Section 3). In this way the physical elements of the problem were revealed and assessed at each point of the development. The degree of agreement with experimental results gave a final test of the validity of the model.

The model was used to determine the contribution of each of the vortex properties (axial velocity deficit, core radius, and vortex strength) to the overall and discrete tone sound pressure levels. The effect on these levels of varying the radial position of vortex entry into the fan was also determined.

4.3.1 Empirical Constants and Numerical Solution

In Section 4.2 expressions were developed to describe the blade twist, chord, inflow velocity profile, and axial velocity deficit. At the fan operating point chosen for the experimental work, the empirical constants in the expression were determined as follows:

Chord (Equation 4.1)

C_{h_0} = .287 ft

D = .177

Blade Twist (Equation 4.2)

β_0 = .388 radians

G = .238 radians/ft

Axial Velocity Deficits (Equation 4.3)

H = 3.65

U_c = is different for each vortex

Inflow Velocity (Equation 4.7)

U_0 = 63.7 ft/sec

M = 20.2/sec .

The numerical solution to the problem uses sixty stations over the span of the fan blade and four hundred twenty around the circumference of the fan. Simpson's rule is employed to integrate lift over the span of the blade. A first central difference method determines the first derivative of the integrated lift with respect to time.

The UBC computer library programme entitled FCF carries out the Fourier analysis of the far field acoustic pressure. It is a curve fitting routine which calculates a Fourier series fit to a specified function using the fast Fourier transform alogrithm. The calculated Fourier series coefficients give the real and imaginary parts of the spectrum. Their modulus renders the discrete tone acoustic pressure amplitudes.

4.3.2 Verification of the Model

In this section, there will be frequent reference to the loading on the blade sections. The reader it reminded that the sectional lift was calculated using a constant value for the lift transfer function (5.76/radian). The effect on the solution of the wave number dependence of the lift transfer function was not incorporated into the model until the far field acoustic pressure was expanded in a Fourier series. The magnitude of the loading curves, therefore,represent the lift exclusive of the effects of the unsteady aerodynamics. Figure 35 shows the time dependent loading over the span of the blade at the circumferential angle $\Sigma = 0$. In the case

shown, the vortex sense is negative (opposite rotation to the fan) and the curves are plotted so that the contributions of the vortex circulation and axial velocity deficit may be viewed separately. The vortex and fan conditions were selected to match the experimental test employing the 5.5 inch half delta wing at an angle of attack of -20° (Γ = -20 ft^2/sec, r_c = .065 ft, U_c = 47.8 ft/sec). The vortex circulation effectively decreases the steady loading inboard of the core and increases it on the outboard side. The axial velocity deficit causes a significant increase in loading in the region of the vortex core (the resultant increase in angle of attack overrides the decrease in the relative velocity). However, it has no strong effect outside the vortex core limit.

The circumferential variation in sectional loading for the same fan conditions is shown in Figure 36. The solid lines show the loading on a blade section (R/R_t = .94) outside the vortex core for positive and negative values of vortex circulation sense. The effect of the axial velocity is not felt at this position of fan radius. However, the loading on a blade section that passes through the vortex core region is quite different (R/R_t=.83 , dashed curve). The axial velocity deficit creates a sharp spiky increase in lift. The contribution from the vortex velocity is insignificant in this region.

According to Equation 4.15, the acoustic radiation from each blade depends on the rate of change of force on that blade. The derivative of the circumferential total blade lift with respect

to time is shown in Figure 37, for both positive and negative vortex sense. Both curves are odd functions symmetric about the vortex core circumferential position ($\Sigma = 0$) the two antisymmetric spikes in the region of the core result from the axial velocity deficit. The positive and negative magnitude shoulders outboard of the spikes are caused by the positive (solid line) and negative (dashed line) sense vortices.

By evaluation of Equation 4.15, the resultant far field pressure signal is obtained due to the lift fluctuations on the seven bladed rotor. The waveform for one complete rotor cycle is shown in Figure 38. The corresponding pure tone spectra are given in Figures 39 and 40 for positive and negative circulation sense respectively. For comparison with the predicted levels, experimental values are shown as a solid line. The dotted lines on top of the solid lines at 2100 and 2520 Hz in Figure 39 indicate that this measured harmonic level dropped below the broad band noise level. The solid lines represent the level after correction was made for the six percent band pass filter. The true discrete tone levels at these frequencies may lie anywhere in the dotted line regime. The agreement between spectra is good; that is, generally within two to three db.

Having followed the progression of the mathematical development through the initial stages of the problem it became apparent that the results made sense physically. The directions, relative magnitudes and spatial extents of the time varying lift forces due to the vortex encounter agree with our intuitive expectations. The

agreement between experiment and theory for this one case is very respectable. The difference between predicted and measured overall levels in a set of twenty-five different comparisons rarely exceeded 5 db.

4.3.3 Variation of Sound Level with Vortex Entry Position

The radial position of vortex entry was varied (in the theoretical model) from a minimum radius of .35 ft(R_0/R_t=.44) to a maximum of .70 ft(R_0/R_t=.88). The calculated variations in overall SPL are shown in Figures 41 and 42 for negative and positive vortex sense respectively. Both sets of curves show an increase in level with an increasing radial point of entry. For the case of positive vortex sense (Figure 42) the rate of increase of overall SPL rises as the fan tip is approached (i.e., the curve is concave upwards). However, the overall level for negative vortex sense (Figure 41) droops down as the maximum radius is reached. The decrease is caused by a drop out in the level of the fundamental blade pass tone occurring at a radial position of .70 ft(R_0/R_t = .88).

An unexpected result such as this one (i.e., for a vortex of negative sense) deserves some attention. The far field acoustic pressure is directly proportional to the varying blade lift (Equation 4.15). By studying a sequence of the time history of dL/dt curves for conditions of increasing radius of vortex entry (approaching the drop-out radius), we obtain some insight into the physical nature of the anomaly.

For the negative sense vortex in accordance with Figure 35, it is evident that the increase in lift resulting from core velocity deficit and outboard "upwash" effect is partially cancelled by a reduction of lift due to the downwash effect experienced inboard of the vortex core. For particular spectral components of the distortion velocity field, it is possible to imagine a perfect spanwise cancellation, such that dL/dt integrated over the blade span goes to zero, when the vortex penetrates the rotor disc at a unique value of R. (Figure 43). The consequence of this cancellation is evident in Figure 41 for the fundamental blade pass tone.

On the other hand, for a vortex of positive sense, such a dropout cannot occur because the upwash field is now inboard of the vortex core. Moving the vortex towards the tip increases the amount of upwash induced lift, and produces an increase in the rate of change in SPL. This effect produces the concave up curve observed for the overall SPL, blade pass frequency, and its first harmonic (Figure 42).

4.3.4 Variation of Sound Level with Vortex Parameters

A set of computer calculations were carried out to determine the effect of vortex parameters on the overall sound pressure level and its pure tone spectrum. An arbitrary vortex of core radius 0.6 in, ($r_c/R_T = .063$) axial velocity deficit of 25 ft/sec ($U_c/U_0 = 39\%$) and vortex strength of 20 ft^2/sec was chosen as a datum. The fan operating conditions remained as described in Section 4.3.1. One of the vortex parameters was varied in magnitude while the other two were held constant. The resulting sound levels were calculated.

The parameters were varied as follows: core radius from .12 inches to 1.2 inches, axial velocity deficit from 5 ft/sec (7.8%) to 50 ft/sec (48%), and vortex strength from 4 ft^2/sec to 40 ft^2/sec, for both positive and negative vortex sense. The upper limits of these ranges corresponded to the maximum measured experimental values. The vortex entered the rotor at a radial distance of .65 ft(R_0/R_t = .82; within the previously noted dropout region). This position corresponded to the distance used in most of the experimental analysis of the vortex interaction noise. The predicted overall and discrete tone sound pressure levels are plotted against each varying parameter in turn.

The overall levels for positive and negative vortex sense are shown in Figures 44 and 45 respectively. They are plotted against a combined parameter, $\Gamma U_c r_c$, for convenience only and not to justify a linear interdependence on the parametric grouping. As discussed already in Section 3, such a simplistic dependence is probably not a realistic approximation for the general influence of the vortex properties on the noise levels.

It is interesting to note that in Figure 44 (Γ positive) for values of $\Gamma U_c r_c$ greater than 25 ft^4/sec^2, the r_c and U_c curves have approximately the same shape. Thus the overall SPL appears to be equally sensitive to changes in U_c and r_c. However, the sound level appears to exhibit much less variation with vortex circulation, Γ. Below 25 ft^4/sec^2, the r_c curve also flattens out. In this region the overall SPL seems to be only sensitive to changes is U_c.

Figure 45 shows that for the case of negative vortex sense, the overall SPL is almost totally independent of the vortex strength, and equally sensitive to changes in U_c and r_c.

As previously discussed the vortex-induced up and down wash inboard and outboard of the vortex core causes resultant increases and decreases in the span-wise loading on the fan blade (Figure 35), as the vortex is encountered. In cases where the difference between positive and negative loading is large, changes in vortex strength will contribute significantly to changes in the overall SPL. (i.e. for R_0/R_t values approaching the hub or tip). However, if the circulation influence cancels almost perfectly along the span, then the effect of changing the vortex strength will be minimal, and the core deficit effect will dominate the noise radiation.

The blade shape determines the sectional loading. Therefore the characteristics of the design (i.e. variation of blade chord from root to tip, blade twist function) and the radial position of vortex entry do have a profound influence on the degree of cancellation that is actually realized.

With these points in mind, and referring to Figure 45 it is apparent that for the case of negative vortex strength (with core radius of 0.6 inches and entering at R_0/R_t=.82), the span-wise acoustic radiation resulting from the vortex circulation must be mutually cancelling. A change in vortex strength produces very little change in the overall sound pressure level.

Figure 46 shows results for the fundamental blade pass frequency levels with negative vortex sense. The results here

confirm the foregoing explanation. As the core radius is increased the sound level passes through a sharp minimum at a value of $\Gamma U_c r_c$ equal to 25 ft^4/sec^2, the value for the datum vortex. Variation of the axial velocity deficit or the vortex strength appears to change the value of the grouping $\Gamma U_c r_c$ at which the drop out occurs. Computation of sound level versus $\Gamma U_c r_c$ at other harmonic frequencies indicates that the fundamental tone is the frequency most affected by the cancellation, as was the case with the drop out, dependent on the position of vortex entry (Figure 41). However, the curves in Figure 46 show that this null may occur for a variety of parameter combinations at one position of vortex entry (R_0/R_t = .82).

The variation of the fundamental tone level for positive vortex sense is shown in Figure 47. For values of $\Gamma U_c r_c$ less than 20 ft^4/sec^2, a change in the vortex strength causes the greatest change in the tone level. For values greater than 20 ft^4/sec^2, changes in Γ, r_c and U_c have roughly equivalent effects, with r_c showing the strongest influence.

Data similar to that given in Figures 44, 45, 46 and 47 were calculated and plotted for the higher harmonic levels (840 Hz, 1260 Hz, 1680 Hz, 2100 Hz, and 2520 Hz). At the highest frequencies (2100 Hz and 2520 Hz), the sound levels were dominantly influenced by changes in axial velocity deficit. The curves for 1680 Hz are shown in Figures 48 and 49. The harmonic level is seen to be equally sensitive to changes in both axial velocity deficit and core radius. The lower harmonic amplitudes (840 Hz and 1260 Hz) are most sensitive to changes in the vortex core radius. These curves are tabulated in Appendix F.

4.3.5 Magnification of Input Errors

The curves of SPL vs $\Gamma U_c r_c$ also serve to indicate the sensitivity of the model to errors in the specification of the input vortex parameters. The degree of confidence in the ability of the model to predict accurate noise levels depends upon the amount by which input errors in the vortex parameters are magnified. The overall sound levels for both positive and negative vortex strength seem to be relatively insensitive to errors in the input circulation, but more susceptable to errors in the core radius and velocity deficit. Over estimation of the vortex circulation (using 20 ft^2/sec instead of 16 ft^2/sec) produces an error in the predicted overall level of only +1 db for positive vortex sense and +2 db for negative sense. The frequency component most sensitive to input error appears to be the fundamental, for negative vortex sense. Here a twenty percent error in the vortex circulation strength would cause a 14 db error in the predicted level. This high magnification of error is caused by the drop out discussed earlier where small changes in the distribution of blade loading cause large changes in output.

4.4 Remarks on the Mathematical Analysis

The value of this analysis of the vortex/rotor interaction problem is dependent upon the degree of realism in the mathematical simulation. There are numerous limitations on the simple linearized approach taken here. However, the model is viewed as an essential first step to understanding the problem. At this time, a more

rigorous extension of analysis does not seem feasible. The following section discusses the degree of agreement between theoretical and experimental results, and underscores some of the areas in which the mathematical model might be viewed as inadequate.

5. DISCUSSION OF RESULTS

Direct comparison of experimental and theoretical results can be made in the areas of cyclic blade loading, far field noise spectra, and the dependence of the noise level on the radial position of vortex entry. These features of the study will be discussed, and an attempt will be made to explain the discrepencies between theory and experiment. The capabilities and limitations of the model will emerge as a by product of the discussion.

5.1 Blade Loading

It was not possible to measure the chord-wise loading at a section experimentally. However, the time history of the pressure fluctuation of the imposed inlet vortex may be determined from the polar diagrams, as in Figure 30. Recall that for these experiments, the vortex parameters were $\Gamma = 20\ ft^2/sec$, $U_c/U_0 = 75\,\%$, $r_c = 0.65\ ft$ and position of entry, $R_0/R_t = .82$. The angular extent of the pressure increase on the upper surface of the airfoil was about 60 to 70 degrees of rotation (measured from zero crossing to zero crossing). The measured extent of the corresponding decrease in lift predicted by theory is 72 degrees (Figure 35). It is difficult to compare the magnitudes of the loading directly, as the chord-wise pressure distribution over the airfoil at the instant of peak suction is

unknown. However, it can be approximated by using known thin-airfoil loading functions. The measured decrease in suction on the airfoil upper surface at 15 percent chord was .015 psi (an increase in the pressure coefficient of .09 on a steady value of -1.2). This would correspond to an angle of attack change of about -0.4 degrees on a two-dimensional thin airfoil ($dC_\ell/d\alpha = 5.72$). The corresponding decrease in sectional lift is approximately 2.1 lb/ft. On our fan blade at the appropriate span-wise point, the theoretical minimum sectional lift (corrected for the Sears' function effect) was about 3.1 lb/ft for similar operating conditions. The circumferential sectional lift (theoretical) and pressure (experimental) variations are plotted for comparison in Figure 36. The experimental pressure plot is relatively symmetric about $\Sigma = 0$ as is the section lift graph. There is actually a decrease in the pressure in the region of $\Sigma = \pi/4$. The negative fluctuation in the surface pressure is thought to be a result of the decrease in velocity in the delta wing wake below the vortex centre (Figure 20). This anomaly in the axial velocity deficit profile is probably caused by the shear layer being shed from the trailing edge of the delta wing vortex generator.

The double humped blade pressure signature observed on the polar plots for naturally occurring inlet conditions (called "natural vortex", Figure 32) was simulated surprisingly well with the analytic model. The result is shown in Figure 50. The radial blade position was selected in the mathematical model so that it passed through the core of a positive sense vortex, but far enough away (on the outboard side) from the vortex axis to ensure that contributions to the fluctuating lift from both the axial velocity

deficit and vortex circulation were approximately equal. (U/U_c = 39.2%, Γ = 20 ft^2/sec, r_c = .065 ft, R_0/R_t = .82). The experimental pressure signature was measured at a radius R_0/R_t = .94.

The spiky increase in lift in the core (predicted theoretically) is consistent with the experimentally observed decrease in pressure. However, the "humps" of the experimental vortex are broader than those of the theoretical vortex. This result suggests that the natural vortex is larger than the theoretical vortex, but the actual extent of the natural vortex may not be determined using only one blade-mounted pressure transducer.

5.2 Far Field Noise Spectra

The theoretical model predicted the measured overall noise levels to within 5 db for twenty-five comparisons with experimental data where the vortex properties and the position of entry were varied. The average discrepency was 3.5 db. In all cases, the measured levels were higher than the calculated ones. As the theory considers the interaction of the rotor and one vortex only, and the experiment involves the generation of noise in excess of the clean running fan noise level (80.7 db), the base noise level of the fan adds to the noise produced by the rotor/vortex interaction. This may in part account for the discrepancy between theory and experiment.

The comparison of levels at the discrete tone frequencies fell within the 5 db limit with two exceptions; at the blade pass frequency and the third harmonic frequency (1680 Hz), for negative source strength.

At the fundamental frequency, for $\Gamma = -20$ ft^2/sec, the theoretical prediction fell 10 db short of the measured value (Figure 40). Here the vortex was being introduced in the tip region of the blade ($R_0/R_t = .82$). As previously discussed in Section 4, a drop-out occurs in the theoretical prediction of the fundamental level in the region. As the position of entry of the vortex is moved toward the hub of the rotor, the agreement between theory and experiment improves, to within 3 db (compare Figures 29 and 41).

Experimentally, a drop-out in level is not seen to occur at large radii for negative vortex sense (Figure 29). To understand this difference we recall the explanation of the drop-out phenomenon given in Section 4. As the negative sense vortex is moved outward radially, the outboard, upwash-induced lift fluctuation is developed over a diminishing fraction of the total blade span, while the inboard downwash-induced negative lift fluctuation grows increasingly dominant. Thus the localized, core-deficit induced lift fluctuation can be totally cancelled at some circumferential positions by the residual, circulation induced load fluctuation (of opposite sign), for a specific radial position of vortex entry.

The foregoing picture is predicted by our idealized two dimensional blade element theory. In actual fact, however, the outboard upwash effect of the vortex does not merely vanish as the outboard segment of the blade diminishes in size. As the vortex circulation field is crowded into a narrowing space between the core filament and the bell-mouth wall, the local vortex velocities are amplified, so that an almost total cancellation of vortex

circulation effects remains operative. The residual core-induced lift fluctuation ensures that a drop-out cannot occur.

This explanation of the relative roles of the circulation induced upwash effects, and core deficit induced load fluctuations helps to explain the somewhat paradoxical results shown in Figure 26 and discussed in Section 3.3.1.

At small negative values of Γ, the increasing circulation seems to induce an increase in tone level. However, the fundamental tone sound pressure level was seen to eventually decrease as vortices of equal core radius, but increasing negative strength and decreasing axial velocity deficit were introduced into the fan at a radius of .65 ft ($R_0/R_t = .82$). As the axial velocity deficit decreased, the contribution to the upwash produced lift on the blade also decreased. The effect of the accompanying rise in the magnitude of the vortex circulation tended to cancel over the span of the blade. The net change in lift over the span due to the circulation, if any, was small. The resulting decrease in axial velocity deficit produced upwash has the same effect on the far field noise as does the decrease in upwash when a theoretical vortex is moved radially outwards. That is, there is a decrease in the amplitude of the fundamental frequency.

Discrepancies between theory and experiment at the third harmonic (in some cases a difference of 7 db) are not immediately explainable. Figure 25 indicates a rapid increase of sound level with negative sense vortex strength, whereas Figures 28 and 29 both show that as the vortex is moved radially outwards, the third harmonic

frequency becomes dominant over all tone levels, except for that of the fundamental (blade pass) frequency.

5.3 Radius of Vortex Entry

The agreement between theory and experiment for positive (Figures 42 and 28 and negative (Figures 41 and 29) vortex sense is best near the blade tip, with the exception of the fundamental tone for negative vortex sense. Inboard of the radial position $R_0/R_t = .7$, however, the theoretically predicted sound levels tend to be lower than those measured. For example, at $R_0/R_t = .5$, the fourth harmonic frequency (2100 Hz) experimentally measures 69 db (negative sense vortex) while its theoretically predicted level is 48.5 db, far below the level produced for natural inlet condition (no vortex) which was 66.4 db. Therefore, some other mechanism is dominating the noise levels for small R, even when the artificial vortex is imposed.

The experimental curves of harmonic sound levels tend to cross over and generally show no simple trend as the vortex is moved toward the tip. In contrast, the predicted levels increase smoothly as the tip is approached, and except for the fundamental frequency for negative vortex sense, do not cross over one another. This discrepency is most surely a consequence of the combination of a vortex crowding effect at larger R, as discussed earlier, and a possible non-linear (stalling) effect, to be discussed in the next subsection.

5.4 Local Blade Stall

The cross-overs in the curves of harmonic level versus radial position (Figures 28 and 29), together with the unusual increase in the third harmonic sound level may be explained by a local stall on the blade. This stall would be induced by the sudden incidence change arising from the velocity deficit in the vortex core. The vortex used to generate the curves of Figures 28 and 29 had a maximum axial velocity deficit of 49.1 ft/sec. When coupled with the steady velocity fields at each radial position, this core deficit could produce a momentary increase in angle of attack which might exceed the critical stalling angle for the blade section. The calculated momentary peak incidences range from 17 degrees at $R_0/R_t = .42$ to 16 degrees at $R_0/R_t = .82$. According to airfoil measurements on blade profiles similar to ours (NACA 4412)[31], stall should begin at an angle of attack of about 12 degrees for our range of Reynolds' numbers (340,000 to 560,000).

As mentioned in the Background Section, local blade stall can provide a strong sound generating mechanism in helicopter, rotor/vortex interactions. However, the detailed nature of such a phenomenon is not easily predicted theoretically because of uncertainty about the time dependent behaviour of three dimensional separated flows. Since our vortices pass right through the rotor disc, there appears to be a high likelihood for such non-linear localized effects. If this conjecture were correct, then it would appear that fluctuating blade stall may affect the harmonic levels in different ways at

varying radii of vortex entry. For example, near the tip (R_0/R_t=.82) the stall could cause the observed emergence of the third harmonic (1680 Hz) as the second strongest tone in the noise spectrum (Figures 28 and 29). Presuming this statement to be true, let us try to explain the results of Figure 25 where at $R_0/R_t = .82$, increases in the negative sense circulation results in a more rapid increase in the third harmonic levels than for the other pure tones.

For the four half delta wings operating at angles of attack of 30, 25, and 20 degrees, the generated vortices all had "burst" cores and exhibited large axial velocity deficits at the rotor plane distance. It is at these large angles of half delta wing incidence that we observe the rapid increase in harmonic level with increasing vortex strength. Perhaps the core deficit is large enough to initiate the cyclic stall.

The effect of the tangential velocity of the negative sense vortex is to increase the local angle of attack outboard of the vortex centre. Here the relative velocities are higher than on the inboard portions of the wing. This situation may be exaggerated by the boundary-induced crowding of the vortex rotational velocity. The effect of increasing Γ is to increase the tangential velocities, and so, there will be a spreading of the extent of stall in the tip region. Since the relative velocity is higher as we approach the tip, the stall becomes more intense with increasing R_0.

For a positive sense vortex, the circulation tends to reduce the angle of attack outboard of the vortex core, and to increase it on the inboard side. However, the increased angle of attack is

in a region of lower relative velocity, and so the noise radiated by the stall, even if it occurred, would be expected to be less intense compared to the case for negative vortex sense.

This physical explanation may account for the rapid increase in harmonic level with increasing vortex strength for negative sense vortices. A somewhat weaker increase is observed for positive sense vortices. Such a non-linearity in the blade lift function would appear to have its greatest effect at the third harmonic at $R_0/R_t = .82$. Perhaps this occurs because the circumferential spatial extent of the separation is such that it contributes energy preferentially to the third harmonic. Stated very simply, at $R_0/R_t = .82$ the relative velocity seen by a blade section is 253 ft/sec. For this velocity, the circumferential wave length that contributes most efficiently to the 1680 Hz harmonic is 1.8 inches. The extent of the stall producing axial velocity deficit (core diameter), for the vortices generated, ranges from 1.3 inches to 2.3 inches.

6. CONCLUSIONS AND RECOMMENDATIONS

The phenomenon of rotor/vortex interaction in an axial flow fan was studied both experimentally and theoretically. The effect of naturally occurring and artificially generated vortices on the unsteady blade loading and on the far field sound was examined.

The quantitative agreement between predicted and measured overall and discrete tone sound levels established the value of using, as a first model, the case of a steady spatially fixed vortex passing through a fan rotor. The chosen model is entirely linear in its formulation, and does not account for boundary or blade to blade confinement effects. It is incapable of predicting the non-linear consequences of cyclic blade stall, should these occur in reality. There is no evidence to confirm that such stall actually occurs when a large scale natural vortex is drawn through a fan. However, where the point of vortex origin is close to the fan (as is the case when vortices originate on a runway or on the fuselage of an aircraft and are drawn through the intake fan) the magnitude of the vortex axial velocity deficit in the plane of the fan rotor may be great enough to cause a local stall, and significant increases in the tonal sound radiation.

Measurements of the naturally occurring "floor vortex" field showed that the inlet disturbance fluctuated slowly and

randomly about certain mean positions of entry into the fan. There was also some low frequency modulation of the vortex strength, apparently being influenced by the large scale external disturbances in the aerodynamics laboratory. These time varying characteristics account for some of the observed irregularity in the overall and discrete tone levels.

The mathematical model does not account for temporal modulations of vortex strength and position. The theoretical acoustic waveform is steady with time. When the honeycomb was placed over the anechoic chamber inlet hatch, a 3 db decrease in the overall sound level was realized. Thus the externally generated "floor vortex" was at least partially suppressed. However, it is probable that additional inlet vorticity was still being generated from corners and obstructions within the chamber itself. Therefore, a more realistic model would be one incorporating more than one inlet vortex. Each would possess time varying vortex properties and position of entry into the fan. This model would then exhibit the band spreading of the discrete tones observed experimentally, and would also produce a broad band contribution to the noise spectrum (as in Hanson[6]).

Artificially generated vortices were employed to check the validity of the model. In reality, however, the model should be useful for describing the interaction of natural vorticity with any rotor. A knowledge of the structure of naturally occurring vortices is therefore required. Vortex characteristics may be determined by the simultaneous measurement and polar display of blade surface pressure signals from more than one surface position; or alternatively by using

modern techniques of laser velocimetry (non-intrusive detection of velocity fields). Comparison of the two or more polar plots at the same instants of time over a period of many fan revolutions would enable the tracking of the magnitude of the vortex strength and its position of entry.

Evaluation of the spatial extent of the blade/vortex interaction is possible using cross-correlation between two surface pressure signals. Measurement of the pressures near the blade trailing edge might also indicate if the naturally occurring vortex is producing a local, time modulated stall.

The vortex circulation and axial flow deficits combine to produce a counter-phase unsteady loading over the blade span. The description of the instantaneous distribution of blade load serves to confirm the validity of the source strength curve (Figure 7) obtained by Leggat and Siddon. The postulation that a floor vortex was entering the fan at a preferred position ($R_0/R_t = .75$) now appears to be confirmed.

The results of the experiment and theory indicated that the changes in the far field sound level resulting from changes in vortex strength were confined to the blade passage frequency (neglecting the effect of stall). The magnitude and spatial extent of the axial velocity deficit determined the sound levels at the higher harmonic frequencies. Previous models of inflow distortions interacting with rotors[4,6,10] have been successful in predicting the blade pass frequency and its first harmonic levels but have been

unable to calculate the observed peaks at the higher harmonic frequencies. The present model, however, does predict significant sound levels with reasonable accuracy up to the fifth harmonic of the blade pass frequency for the cases considered.

In view of the above discussion, the following recommendations are proposed.

6.1 Theoretical Extensions

1. The single vortex model should be refined to include the effects of the bell mouth boundary on the vortex tangential velocity. This addition to the model may be made by including an image vortex of opposite sense the same distance outboard of the blade tip, as the real vortex is inboard.

2. The rotor/vortex interaction model should be extended to include the effects of more than one vortex,and also to account for the time varying vortex properties and position of entry.This modification may be implemented by using random functions of vortex properties or alternatively by employing a statistical approach similar to that carried out by Hanson[6].

6.2 Experimental Extensions

3. The present two channel instrumented blade should be redesigned to enable a more rapid means of relocating the pressure transducers in the blade. In the present system, the brass casing which protects the transducers must be placed in the milled blade slot so that the hole penetrating the side of the casing is aligned with the hole communicating to the upper surface of the blade. A proper alignment of the two holes proved to be difficult to achieve and therefore was time consuming. Having completed the redesign, pressure measurements could be made conveniently at many blade surface locations. Experiments to determine the structure of the observed floor vortex, and to test for local blade stall (as described above) could then be carried out.

4. Further investigation into the origin of the on-axis discrete tone noise is required. Elimination of the "floor vortex" by inserting the honeycomb did not cause the blade passage frequency and its harmonics to disappear. The installation of a fine wire mesh cone over the fan inlet may help to reduce vorticity originating inside the chamber.

If the mathematical model is modified, and if the blade instrumentation is improved, a powerful means will exist for the continuation of research on the sources of discrete tone fan noise.

REFERENCES

1. MANI, R. "Isolated Rotor Noise due to Inlet Distortion/Turbulence," Final Progress Report Prepared for the National Aeronautics and Space Administration, Lewis Research Centre, June 1974.

2. GUTIN, L. "On the Sound of a Rotating Propeller," Translation of "Uber da Schallfeld einer Rotierenden Luftschraube," Physikalishe Zeitscher ift der Sonjetunion, Band 9, Heft 1, 1936; NASA Tech. Memo. No. 1195, 1945.

3. MUGRIDGE, B.D. and MORFEY, C.L. "Sources of Noise in Axial Flow Fans," Journal of the Acoustical Society of America, Vol. 51, No. 5, 1972, pp. 1411-1426.

4. MANI, R. "Noise Due to the Interaction of Inlet Turbulence with Isolated Stators and Rotors," Journal of Sound and Virbation, Vol. 17, No. 2, July-August 1971, pp. 251-260.

5. LOWSON, M.V. "Studies of Noise Radiation by Rotating Blading," Proceedings of the Interagency Symposium on University Research in Transportation Noise, March 28-30, 1973, pp. 211-224.

6. HANSON, D.B. "Spectrum of Rotor Noise Caused by Atmospheric Turbulence," Journal of the Acoustical Society of America, Vol. 56, No. 1, 1974, pp. 110-126.

7. LEGGAT, L.J. Experimental Investigations of On-Axis Discrete Frequency Fan Noise, M.A. Sc. Thesis, University of British Columbia, October, 1973.

8. SIDDON, T.E. and LEGGAT, L.J. "Blade Load Modulation as a Source of Discrete Frequency Fan Noise," Proceedings of Internoise '73, August, 1973, pp. 176-185.

9. HODDER, B.K. "Investigations of the Effect of Inlet Turbulence Length Scale on Fan Discrete Tone Noise," NASA Tech. Memo. X-62,300, September, 1973.

10. RAO, G.V.R., CHU, W.T., and HODDER, B.K. "Rotor Noise Due to Inflow Turbulence," AIAA Paper No. 73-632, July, 1973.

11. PLUCINSKY, J.C. "Quiet Aspects of the Pratt and Whitney Aircraft JT15D Turbofan," Presented at the Society of Automotive Engineers Business Aircraft Meeting, Wichita, Kansas, April, 1973.

12. COLEHOUR, J.L. and FARQUHAR, B.W. "Inlet Vortex," Journal of Aircraft, Vol. 8, No. 1, January, 1971, pp. 39-43.

13. SOFRIN, T.G. and McCANN, J.C. "Pratt and Whitney Experience in Compressor Noise Reduction," Presented at the 72nd Meeting of the Acoustical Society of America, 1966.

14. FILLEUL, N. le. S. "An Investigation of Axial Flow Fan Noise," Journal of Sound and Vibration, 3(2), 1966, pp. 147-165.

15. SEARS, W.R. "Some Aspects of Non-Stationary Airfoil Theory and Its Practical Application," Journal of the Aeronautical Sciences, 8(2), February, 1941, pp. 104-108.

16. LOWSON, M.V. "Theoretical Analysis of Compressor Noise," Journal of the Acoustical Society of America, 47(2), 1970, pp. 371-385.

17. LOWSON, M.V. "The Sound Field for Singularities in Motion," Proc. Roy. Soc., (London), A286, 1965, pp. 559-572.

18. SIDDON, T.E. "Surface Dipole Strength by Cross Correlation Method," Journal of the Acoustical Society, Vol. 53, No. 2, February, 1973, pp. 619-633.

19. RACKL, R. Two Causality Correlation Techniques Applied to Jet Noise, Ph.D. Thesis, University of British Columbia, April, 1973.

20. LEVERTON, J.W. and TAYLOR, F.W. "Helicopter Blade Slap," Journal of Sound and Vibration 4(3), 1966, pp. 345-357.

21. PATTERSON, W.R., AMIET, R.K., and MUNCH, C.L. "Isolated Airfoil - Tip Vortex Interaction Noise," Presented at the AIAA 12th Aerospace Sciences Meeting, January, 1974.

22. WIDNALL, S. "Helicopter Noise Due to Blade-Vortex Interaction," Journal of the Acoustical Society of America, Vol. 50, No. 1, 1971, pp. 354-365.

23. SIDDON, T.E., HOGLUND, L., and DAVIS B. "Validation Report; UBC Anechoic Chamber and Jet Noise Facility," Submitted to General Electric Company Limited, Aircraft Engine Group, November, 1974.

24. SMITH, R.H. and WANG C. "Contracting Cones Giving Uniform Throat Speeds," Journal of the Aeronautical Sciences, October, 1944.

25. ELLE, B.J. "An Investigation at Low Speed of the Flow Near the Apex of Thin Delta Wings with Sharp Leading Edges," Performance Sub-Committee, Aeronautical Research Council (U.K.), Perf. 1621, F.M. 2629, January, 1958.

26. MARSDEN, D.J., SIMPSON, R.W., and RAINBIRD, W.J. "An Investigation into the Flow over Delta Wings at Low Speed with Leading Edge Separation," Report No. 114, The College of Aeronautics, Cranfield, U.K., February, 1958.

27. FINK, P.T. and TAYLOR, J. "Some Low Speed Experiments with 20 Degree Delta Wings," Performance Sub-Committee, Aeronautical Research Council, Perf. 1382, F.M. 2339, September 1955.

28. LAMBOURNE, N.C. and BRYER, D.W. "The Bursting of Leading Edge Vortices - Some Observations and Discussion of the Phenomenon," Fluid Motion Sub Committee, Aeronautical Research Council, F.M. 3085, ARC 22, 775, April, 1961.

29. HALL, M.G. "The Structure of Concentrated Vortex Cores," Royal Aircraft Establishment, Tech. Memo. Aero. 869, January, 1965.

30. SUN, Y.C. Experimental Investigation of the Field About Sharp-Edged and Rectangular Wings, M.A.Sc. Thesis, University of British Columbia, December, 1961.

31. ABBOTT, I.H. and VON DOENHOFF, A.E. Theory of Wing Sections, Dover Publications Inc., New York, 1959.

32. JACOBS AND SHERMAN, NACA Report, No. 586, 1937.

33. CURLE, N. "The Influence of Solid Boundaries Upon Aerodynamic Sound," Proc. Roy. Soc., A 231, 1955, pp. 505-514.

34. LIGHTHILL, M.J. "On the Sound Generated Aerodynamically, II, Turbulence as a Source of Sound," Proc. Roy. Soc. A 222, 1954, pp. 1-32.

35. KRAICHNAN, R.H. "Noise Transmission from Boundary Layer Pressure Fluctuations," Journal of the Acoustical Society of America, Vol. 25, 1957, pp. 65-80.

APPENDIX A

RADIATION SOLUTION AND SOURCE ANALYSIS BY CAUSALITY CORRELATION*

In the diagnosis of multistage systems such as turbomachines one is frequently faced with determining which components of a system contribute most to the overall generate sound. Spectral analysis of the noise and systematic modification of machine parts have in the past provided limited information. A proven means of source localization is the causality correlation technique[7,18,19]. It establishes a causative relationship between individual noise source phenomena and the overall sound radiated in a given direction; thus yielding quantitative information on acoustic source distributions, their local spectra and scales of coherence. The theoretical development of the causality approach was carried out by Siddon. A complete derivation of the technique,applied to surface generated aerodynamic noise,may be found in reference 18. A condensed version follows.

A1. Relationship Between Surface Pressure and Far Field Sound

Starting with Curle's generalized solution[33] to the Lighthill equation[34], it follows that the sound resulting from the interaction between a flow and surface S is given by the following far field

*This Appendix is included to provide the reader with an abbreviated presentation of the derivation of Equation 4.15 and an explanation of the technique used to obtain the curve in Figure 7.

$$p(\bar{x},t) = \frac{1}{4\pi xc} \int_S \left[\rho \dot{U}_n c + \frac{x_i}{x} \frac{\delta}{\delta t} (f_i + \rho u_i u_n)\right]_{t-\frac{x}{c}} dS \quad \ldots . (A1)$$

(Here we have discarded the volume-distributed quadrupole sources). In cases where the surfaces are non-vibrating and have rigid steady motion, the terms involving surface velocities u_n and u_i vanish. If the surface stress is dominated by its normal component (and it generally is[35]) a simple relationship results

$$p(\bar{x},t) = \frac{1}{4\pi xc} \int_S \cos\theta \left[\frac{\delta p_s}{\delta t} (t - \frac{x}{c})\right] dS \quad \ldots . (A2)$$

If the dimensions of S are small compared to the wavelength of the highest frequency of interest in the radiated sound, the variation in retarded time over the surface may be neglected, and $R \simeq x$. The integral in Equation A2 now describes the resultant force exerted by the fluid on the surface. If the surface is an airfoil in a flow, the force on the airfoil may be resolved into instantaneous lift and drag force components. When the drag force is negligible, Equation A2 may be written as

$$p(R, t) = \frac{1}{4\pi Rc} \left[\frac{\delta L}{\delta t} \right]_{t - \frac{R}{c}} . \qquad \ldots . (A3)$$

A2. Causality Formalism

If both sides of Equation A2 are multiplied by the acoustic pressure at a new time t', time averaging yields:

$$\overline{p(t)p(t')} = \frac{1}{4\pi xc} \int_S \cos\theta(\underline{y}) \left[\overline{\frac{\delta p_s}{\delta t}(\underline{y}, t - \frac{x}{c}) \, p(\underline{x}, t')} \right] dS(\underline{y}) . \qquad \ldots . (A4)$$

Then assuming p and p_s are statistically stationary random variables

$$\overline{p\,p(\tau)} = -\frac{1}{4\pi xc} \int_S \cos\theta \left[\frac{\delta}{\delta\tau} \overline{p_s\, p} \; (\tau - \frac{x}{c}) \right] dS; \; \tau = t - t' . \qquad (A5)$$

We evaluate the mean square acoustic pressure by setting $\tau = 0$

$$\overline{p^2}(x) = -\frac{1}{4\pi x c}\int_S \cos\theta \left[\frac{\delta}{\delta\tau}\overline{p_s p}\right]_{\tau=-\frac{x}{c}} dS \quad . \qquad \ldots . (A6)$$

Thus the contribution to the mean square sound pressure at a far field point $\underline{x}$, arriving from the surface element $ds(\underline{y})$, when p_s is being measured, is given by the integrand of A5. This quantity may be viewed as the strength of the acoustic source at that point, and for the case where the dipole radiation from the surface is predominant, (as is the case in applications such as rotor noise), it is called the surface dipole source strength

$$\frac{\overline{dp^2}}{dS} = -\frac{\cos\theta}{4\pi x c}\left[\frac{\delta}{\delta\tau}\overline{p_s p}\right]_{\tau=-\frac{x}{c}} \qquad \ldots . (A7)$$

The distribution of source strength results in an acoustic model fixed to the geometry of the surface. The surface may then be considered as an array of acoustic sources of various strengths.

Initial experiments showing the validity of this approach were carried out by Siddon[18] in the investigation of broad band noise radiated from a flat circular plate embedded in an air jet. The success of these experiments pointed the way towards the analysis of more complicated situations involving surface interaction noise as were carried out by Siddon and Leggat at a later date[8].

Typically the surface related correlation function $\overline{p_s p}(\tau)$ will have a characteristic antisymmetric shape for source fluctuations

which are broad band in spectral nature. This trend results because the acoustic radiation is proportional to the time rate of change of the surface pressure. One merely evaluates the slope of many such functions at points on the surface, at appropriate time delays, in order to generate the contours of source strength over the surface. In certain cases involving anticoherent sources, some elements of area may exhibit an apparent negative source strength. When source strengths are integrated over the surface, these negative strengths will cancel a portion of the positive strength, but the resulting integral will always be positive. In the special case where two counter phase sources exactly cancel one another, there will be no far field sound, and hence no correlation.

Where there is a strong harmonic coupling between source and far field pressure spectra, the resulting cross-correlation function will not decay quickly with time delay, but will be periodic in nature.

A3. Periodic Correlation Functions

It is useful to filter both the surface pressure and the far field signals with frequency and phase matched filters if the far field spectrum is dominated by particular frequencies, or if the distribution of a component frequency of broad band noise is to be analysed. This approach allows for the examination of the distribution of sources producing the filtered frequency. For filtered source analysis, the relative pulsation phases of sources at various positions are important.

A4. Accounting for Phase

Variation in the phase of fluid dilitations on the surface at a particular frequency can be most important when relating the source distribution to the net overall sound (at that frequency) by integration over the surface in question. If the source and far field signals are filtered, then the cross-correlation function will be sinusoidal, having a frequency identical to the centre frequency of the band pass filter. The correlation function can be represented mathematically by the expression.

$$\overline{p_s p}(\tau) = -|\overline{P_s P}| \sin\left[\omega\left(\tau - \frac{x}{c}\right) + \phi\right] . \qquad \ldots . (A8)$$

Here ϕ is the phase angle between the measured correlation function and a correlation function of the same period but with a zero crossing of negative slope at the correct time delay $\frac{x}{c}$.

Differentiation with respect to time gives

$$\frac{d}{dt}\overline{p_s p}(\tau) = -|\overline{P_s P}| \left(\omega \cos\left[\omega\left(\tau - \frac{x}{c}\right)\right] \cos\phi - \omega \sin\left[\omega\left(\tau - \frac{x}{c}\right)\right] \sin\phi\right) \qquad \ldots . (A9)$$

evaluation at the correct time delay gives

$$\frac{\delta}{\delta\tau}\overline{p_s p}\left(\tau = \frac{x}{c}\right) = -|\overline{P_s P}| \, \omega \cos\phi \qquad \ldots . (A10)$$

substitution into A6 gives

$$\frac{\overline{dp^2}}{ds} = \frac{\cos\theta \cos\phi}{4\pi x c} \omega \overline{|P_s P|} \quad . \qquad \ldots .(A11)$$

Thus for a filtered correlation, it is possible to predict the source strength at a particular source location by knowing the amplitude of the cross-correlation function, the frequency, the angle between the surface normal and the far field point, the phase angle ϕ, the speed of sound, and the distance to the field point $\underline{x}$.

APPENDIX B

LOCATION OF THE VORTEX CORE

In order to position the pivot point of the ball vortimeter correctly, it was necessary to know the location of the vortex core centre relative to the trailing edge of the half delta wing.

A hot wire was traversed vertically and horizontally through the vortex produced when the 5 1/2 inch wing was mounted in the wind tunnel. Two sets of orthogonal traverses were conducted. One with the wire oriented perpendicular to the axial flow, and the other with it parallel to the axial flow. The wire served to indicate the point of minimum velocity: in the first case, for the resultant of the axial and vortex tangential velocities and in the second for the resultant of the vertical and horizontal components of the vortex tangential velocity. The results of the two methods agreed well and are presented below.

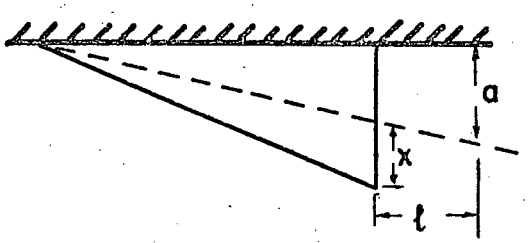

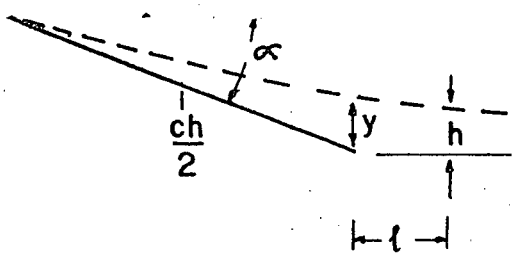

α	h	ℓ	a	x	Y
5°	$\frac{5}{32}$	$1\frac{1}{8}$	$1\frac{27}{32}$	$\frac{26}{32}$	$\frac{3}{16}$
10°	$\frac{10}{32}$	$1\frac{1}{4}$	$1\frac{27}{32}$	$\frac{27}{32}$	$\frac{3}{8}$
15°	$\frac{15}{32}$	$1\frac{5}{16}$	$1\frac{3}{4}$	$\frac{30}{32}$	$\frac{9}{16}$
20°	$\frac{17}{32}$	$1\frac{5}{16}$	$1\frac{11}{16}$	1	$\frac{21}{32}$
25°	$\frac{20}{32}$	$1\frac{3}{16}$	$1\frac{21}{32}$	1	$\frac{13}{16}$
30°	$\frac{23}{32}$	$1\frac{3}{8}$	$1\frac{17}{32}$	$1\frac{1}{8}$	$\frac{31}{32}$
35°	$\frac{24}{32}$	$1\frac{7}{16}$	$1\frac{7}{16}$	$1\frac{7}{32}$	$1\frac{1}{16}$

APPENDIX C

HALF DELTA WING VORTEX CHARACTERISTICS

Angle of Attack	Γ (ft^2/sec)	r_c (ft)	U_c (ft/sec)
4.25 inch wing			
10	7.5	.053	42.7
15	11.25	.059	51.0
20	15.0	.065	46.5
25	18.75	.073	49.7
30	22.5	.081	56.6
5.5 inch wing			
10	10.0	.057	28.1
15	15.0	.059	39.2
20	10.0	.065	47.8
25	25.0	.070	49.6
30	30.0	.078	49.1
6.875 inch wing			
10	11.9	.056	-
15	17.5	.063	38.2
20	23.75	.070	47.8
25	30.0	.079	51.0
30	36.25	.089	52.9
8.25 inch wing			
10	13.5	.057	-
15	20.3	.065	-
20	26.8	.074	38.3
25	33.75	.084	40.8
30	43.7	.096	49.7

APPENDEX D

D1. Data from Vortex Parameter Tests (all levels are SPL in decibels)

Clean Fan

	Frequency Hz					
Overall	420	840	1260	1680	2100	2520
80.9	72.2	66.1	68.9	69.6	66.4	63.8

Wing angle of attack +10°

Wing	Overall	420	840	1260	1680	2100	2520
4.25"	82.4	75.2	70.6	72.1	73.2	68.9	65.9
5.5"	82.3	75.2	69.9	71.1	73.3	67.7	65.5
6.875"	83.0	75.9	71.2	72.9	74.0	68.8	66.7
8.25"	83.2	76.1	71.1	72.5	74.8	68.8	67.0

Wing angle of attack -10°

Wing	Overall	420	840	1260	1680	2100	2520
4.25"	81.7	74.0	70.3	70.5	71.8	67.0	65.0
5.5"	81.7	73.9	70.1	70.3	72.0	66.7	64.7
6.875"	82.3	74.6	70.3	70.6	72.2	67.3	65.9
8.25"	82.0	74.2	69.7	70.3	72.7	67.0	65.8

Wing angle of attack +15°

Wing	Overall	420	840	1260	1680	2100	2520
4.25"	83.5	77.2	71.9	72.7	74.4	70.6	66.9
5.5"	83.0	76.9	70.1	71.6	74.4	70.0	67.7
6.875"	84.2	77.9	71.4	72.8	76.0	71.1	67.7
8.25"	84.4	78.0	71.6	73.0	77.7	70.8	69.0

Wing angle of attack -15°

Wing	Overall	420	840	1260	1680	2100	2520
4.25"	82.0	75.3	70.6	70.2	71.3	67.6	65.6
5.5"	81.9	74.8	68.9	69.3	71.4	68.8	66.7
6.875"	82.5	74.6	68.2	69.8	73.5	69.3	68.5
8.25"	82.7	73.4	67.2	70.9	76.0	70.7	67.7

Wing angle of attack +20°

Wing	Overall	420	840	1260	1680	2100	2520
4.25"	83.2	78.6	71.1	73.2	73.0	67.5	66.3
5.5"	83.3	78.0	69.9	72.4	75.1	67.7	66.9
6.875"	84.2	78.3	71.4	72.7	77.6	69.1	68.0
8.25"	84.6	78.7	72.4	72.6	78.3	68.1	67.7

Wing angle of attack -20°

Wing	Overall	420	840	1260	1680	2100	2520
4.25"	83.2	77.2	72.0	71.1	73.6	70.1	69.4
5.5"	83.4	76.6	70.0	70.2	76.5	71.8	68.8
6.875"	84.1	75.7	70.3	72.1	78.4	72.0	69.6
8.25"	84.1	73.3	71.5	74.5	78.9	72.2	68.1

Wing angle of attack +25°

Wing	Overall	420	840	1260	1680	2100	2520
4.25"	84.1	80.2	70.8	73.4	73.4	67.4	65.7
5.5"	83.6	78.9	69.1	72.2	76.4	66.6	65.4
6.875"	84.9	79.6	72.7	72.7	78.0	67.7	67.0
8.25"	85.0	79.5	75.0	73.9	78.6	67.9	67.1

Wing angle of attack -25°

Wing	Overall	420	840	1260	1680	2100	2520
4.25"	85.1	80.5	74.7	74.0	75.9	70.8	69.3
5.5"	84.8	79.9	73.6	70.5	79.1	70.5	70.2
6.875"	85.9	78.7	75.5	73.4	80.5	70.7	72.1
8.25"	86.3	77.1	76.7	76.4	81.8	70.4	71.7

Wing angle of attack +30°

Wing	Overall	420	840	1260	1680	2100	2520
4.25"	85.6	82.7	70.4	74.0	75.2	69.2	66.2
5.5"	85.5	82.4	68.8	72.9	76.4	69.9	68.1
6.875"	85.6	82.1	72.6	72.4	76.1	68.3	67.1
8.25"	86.2	81.3	77.6	75.2	77.5	68.8	67.0

Wing angle of attack -30°

Wing	Overall	420	840	1260	1680	2100	2520
4.25"	87.1	83.5	77.6	76.7	76.7	69.7	71.2
5.5"	87.7	84.3	77.5	71.5	80.1	71.6	74.4
6.875"	88.2	83.0	78.4	73.7	82.8	73.3	74.1
8.25"	88.9	82.0	78.6	78.8	84.0	76.5	75.0

D2. Far Field Noise Levels with Mounting Plates Inserted

Plate Radius $(\frac{R}{R_t})$	Overall	420	840	1260	1680	2100	2520
Clean fan	81.6	72.7	67.6	70.0	71.2	67.1	65.1
.94	81.7	72.4	68.0	69.9	71.7	67.2	65.2
.89	81.8	72.4	68.1	71.0	72.1	67.7	65.6
.84	81.8	72.7	68.1	69.9	72.5	67.9	66.0
.78	81.7	73.0	68.8	70.3	72.7	68.1	65.9
.73	81.8	72.4	68.7	70.1	72.1	68.3	65.8
.68	82.2	73.4	69.5	70.1	72.9	68.3	66.1
.63	82.4	74.5	69.9	70.9	71.9	68.3	66.5

APPENDIX E

PARAMETRIC ANALYSIS OF LIFT FLUCTUATION ON BLADE

— The pressure in the far field produced by a force fluctuation on a surface is proportional to the time rate of change of the total force acting on the surface.

$$p \sim \frac{dL}{dt} \qquad \ldots .(E1)$$

From Equation 4.14,

$$L(t) = \frac{1}{2} \rho \frac{dC_{\ell}}{d\alpha} (k) \int_{R_i}^{R_t} C_h \left[U^2 + \omega R - V(r) \cos \phi)^2\right]^* *\left[\alpha_o - \left(\frac{U\, V(r) \cos \phi}{\omega^2 R^2 + \omega R\, V(r) \cos \phi + (U - U_c)^2} \right) \right] dR \qquad \ldots .(E2)$$

The results of the theory indicated that the noise was primarily a function of the angle of attack fluctuations over the blade. Therefore if

$$U_c << U \text{ and } V(r) \cos \phi << \omega R,$$

then,

$$L(t) \simeq \frac{1}{2} \rho \frac{dC_\ell}{d\alpha} V^2 \left[\alpha_o - \frac{(U_o - U_c)\, V(r) \cos \phi}{V^2} \right] A \quad \ldots . (E_3)$$

ie,

$$p \simeq \frac{d}{dt} \left[\frac{1}{2} \rho \frac{dC_\ell}{d\alpha} \alpha_o V^2 A - \frac{1}{2} \rho \frac{dC_\ell}{d\alpha} A \frac{(U_o - U_c)\, V(r) \cos \phi}{V^2} \right] \quad \ldots . (E4)$$

$$\simeq - \frac{1}{2} \rho \frac{dC_\ell}{d\alpha} \frac{d}{dt} \left[U_o V(r) \cos \phi + U_c V(r) \cos \phi \right] A \quad \ldots . (E5)$$

Now the area over which the vortex acts is proportional to r_c and $V(r) \cos \phi$ is proportional to the vortex strength divided by the core radius

$$A \simeq r_c^2 \quad \ldots . (E6)$$

$$V(r) \cos \phi \simeq \frac{\Gamma}{r_c} \quad \ldots . (E7)$$

$$p \simeq - \frac{1}{2} \rho \frac{dC_\ell}{d\alpha} \frac{d}{dt} \left[U_o \Gamma r_c + U_c \Gamma V_c \right] \quad \ldots . (E8)$$

$$p \simeq -\frac{1}{2}\rho \frac{dC_{\ell}}{d\alpha}\left[U_o r_c \frac{d\Gamma}{dt} + U_c r_c \frac{d\Gamma}{dt} + \Gamma r_c \frac{dU_c}{dt}\right] \quad \ldots (E9)$$

Thus, we see that where (dU_c/dt) is large, then $U_c \Gamma r_c$ will be the parameter grouping having the strongest influence on the far field noise. However, if (dU_c/d_t) is small, then because $U_o > U_c$, the $U_o \Gamma r_c$ grouping will dominate.

APPENDIX F

TABULATION OF HARMONIC AMPLITUDE DEPENDENCE ON VORTEX PARAMETERS

(Theoretical)

Frequency 840 Hz

	Positive Vortex Sense			Negative Vortex Sense		
$\Gamma U_c r_c$ (ft^4/sec^2)	Γ Varies (db)	U_c Varies (db)	r_c Varies (db)	Γ Varies (db)	U_c Varies (db)	r_c Varies (db)
5	63.4	51.0	57.9	63.8	48.8	25.4
10	64.0	56.8	56.0	63.6	55.2	35.8
15	64.0	60.0	57.9	63.5	59.2	53.2
20	64.2	62.2	61.0	63.5	61.6	59.6
25	64.2	64.2	64.2	63.5	63.5	63.5
30	64.2	65.0	62.8	63.5	65.2	66.8
35	64.2	67.0	69.2	63.5	66.4	69.0
40	64.2	68.0	71.0	63.4	67.6	71.2
45	64.2	69.0	73.0	63.4	68.8	72.8
50	64.3	70.0	74.0	63.3	69.6	74.0

Frequency 1260 Hz

5	64.0	50.8	47.8	64.6	50.6	40.4
10	64.8	56.8	50.8	64.6	56.6	50.0
15	64.7	60.0	56.8	64.6	60.2	56.6
20	64.7	62.0	63.2	64.6	62.6	61.2
25	64.7	64.7	64.7	64.6	64.6	64.6
30	64.7	66.4	67.2	64.6	66.0	67.2
35	64.7	67.6	69.2	64.6	67.6	69.2
40	64.7	68.4	70.4	64.6	68.6	70.8
45	64.7	69.6	70.8	64.6	69.8	71.6
50	64.7	70.8	72.4	64.6	70.4	72.4

Appendix F (continued)

Frequency 2100 Hz

$\Gamma U_c r_c$ (ft^4/sec^2)	Positive Vortex Sense			Negative Vortex Sense		
	Γ Varies (db)	U_c Varies (db)	e_c Varies (db)	ΓVaries (db)	U_c Varies (db)	r_c Varies (db)
5	62.4	50.0	40.0	64.0	49.6	38.4
10	64.0	56.0	51.2	64.0	54.6	51.2
15	64.0	59.2	57.6	64.0	59.2	56.5
20	64.0	62.0	61.6	64.0	62.0	61.4
25	64.0	64.0	64.0	64.0	64.0	64.0
30	64.0	65.0	64.9	64.0	65.2	65.2
35	64.0	67.0	65.9	64.0	66.8	66.0
40	64.0	68.1	65.2	64.0	68.0	65.6
45	64.0	69.0	64.3	64.0	68.8	64.5
50	64.1	70.0	62.8	64.0	70.0	62.8

Frequency 2520 Hz

5	62.3	48.3	40.0	62.3	48.4	38.4
10	62.3	54.6	51.8	62.3	54.6	51.4
15	62.3	58.2	57.6	62.3	58.0	59.2
20	62.3	60.9	60.4	62.3	60.4	61.0
25	62.3	62.3	62.3	62.3	62.3	62.3
30	62.3	64.1	62.3	62.3	64.0	65.1
35	62.3	65.6	62.3	62.3	65.6	62.3
40	62.3	66.8	60.8	62.3	66.8	61.0
45	62.3	67.5	58.2	62.3	67.6	58.1
50	62.3	68.7	55.2	62.3	68.6	55.2

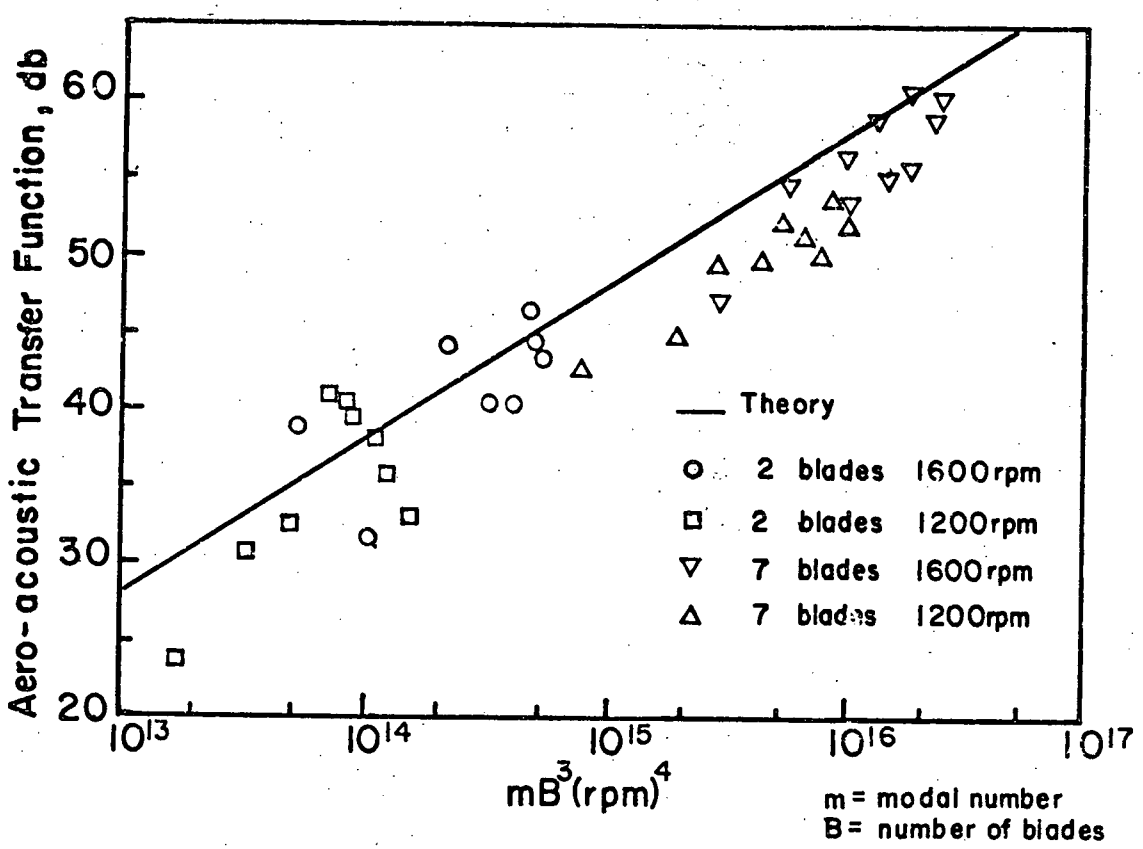

Figure 1 Lowson's Aero-acoustic Transfer Function

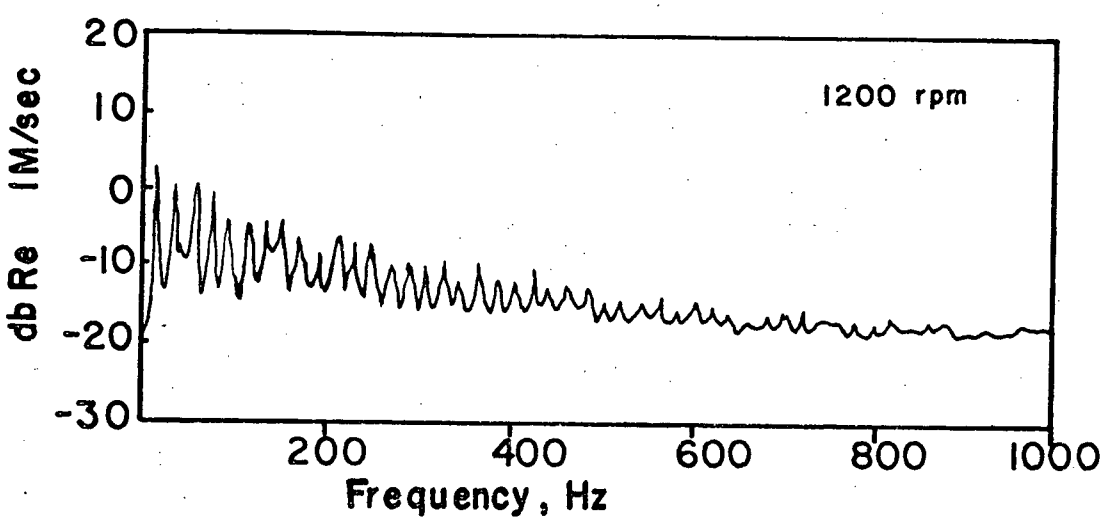

Figure 2 Blade Relative Velocity Frequency Spectrum (Lowson)

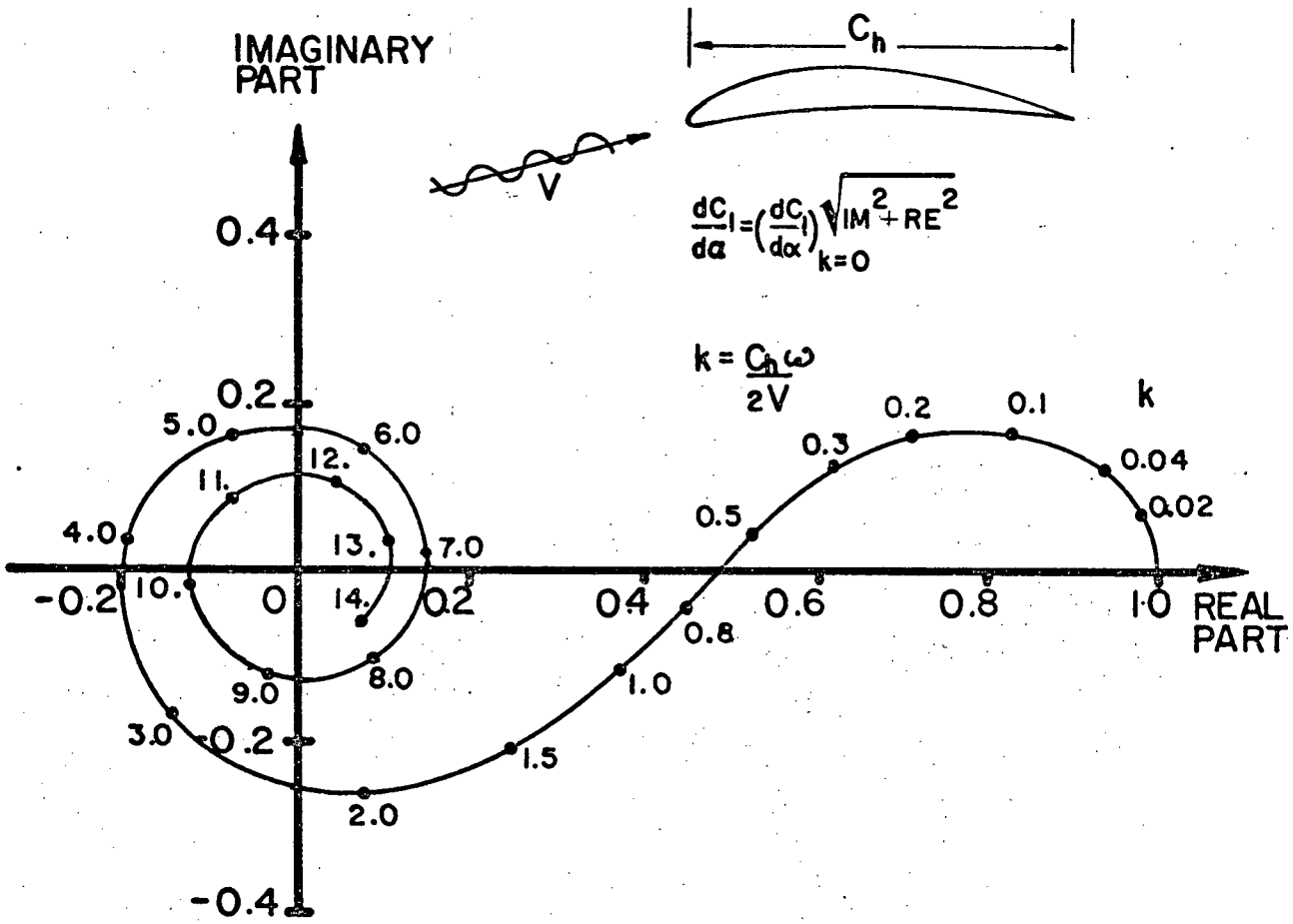

Figure 3 Sears' Aerodynamic Lift Transfer Function for an Airfoil Encountering a Sinusoidal Gust

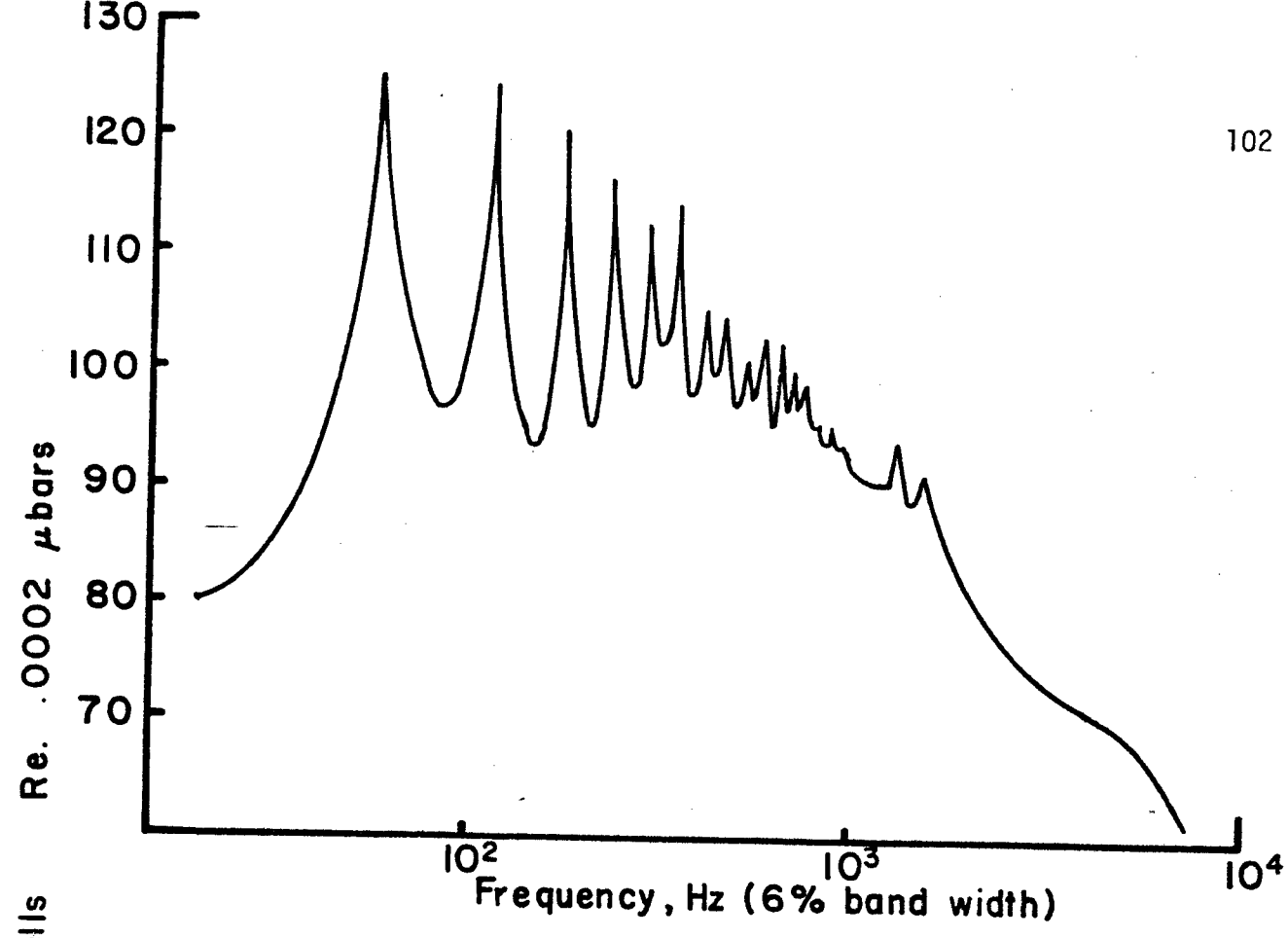

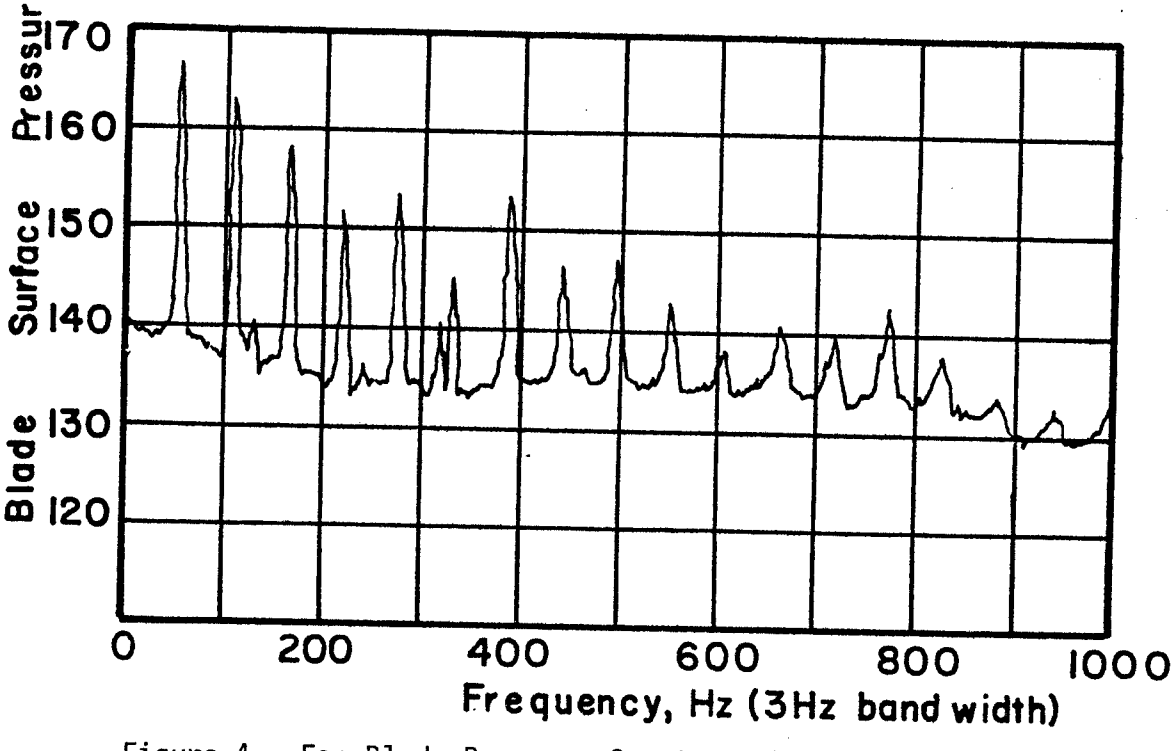

Figure 4 Fan Blade Pressure Spectra. Upper, from Leggat and Siddon; Lower, from Hanson

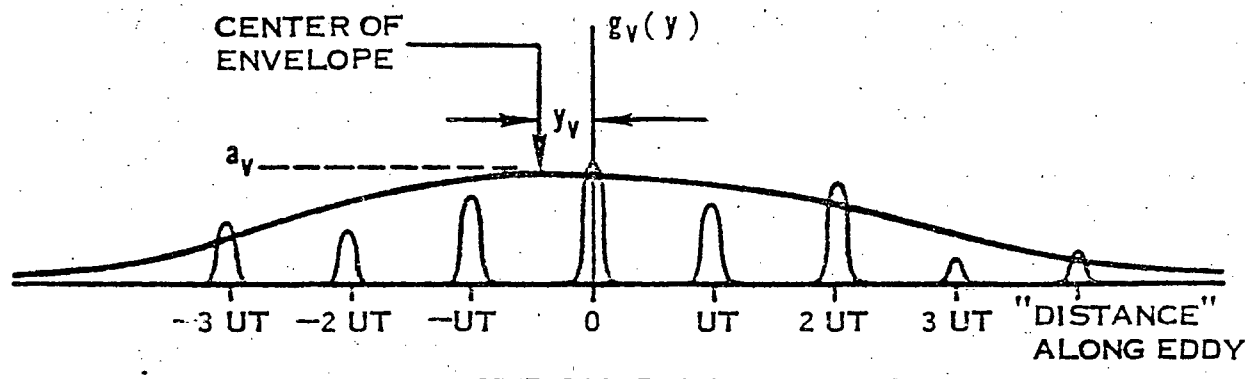

TYPICAL PULSE ENVELOPE

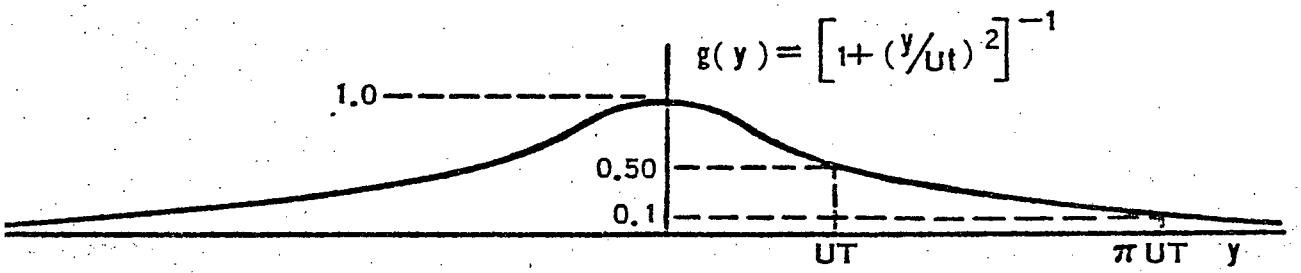

STANDARD PULSE ENVELOPE

Figure 5 Pulse Input Proposed by Hanson

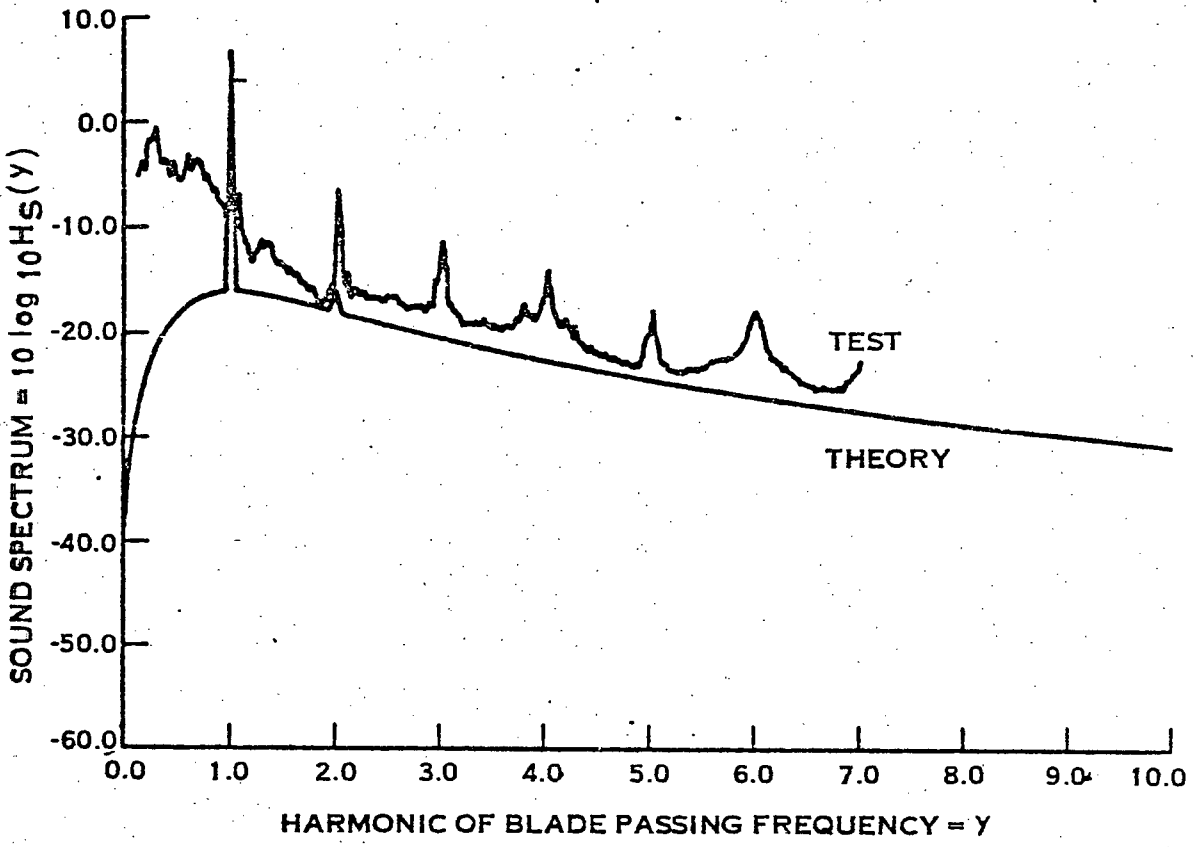

EXPERIMENTAL AND THEORETICAL
SOUND SPECTRA ON ROTOR AXIS

Figure 6 Comparison of Theory and Experiment (Hanson)

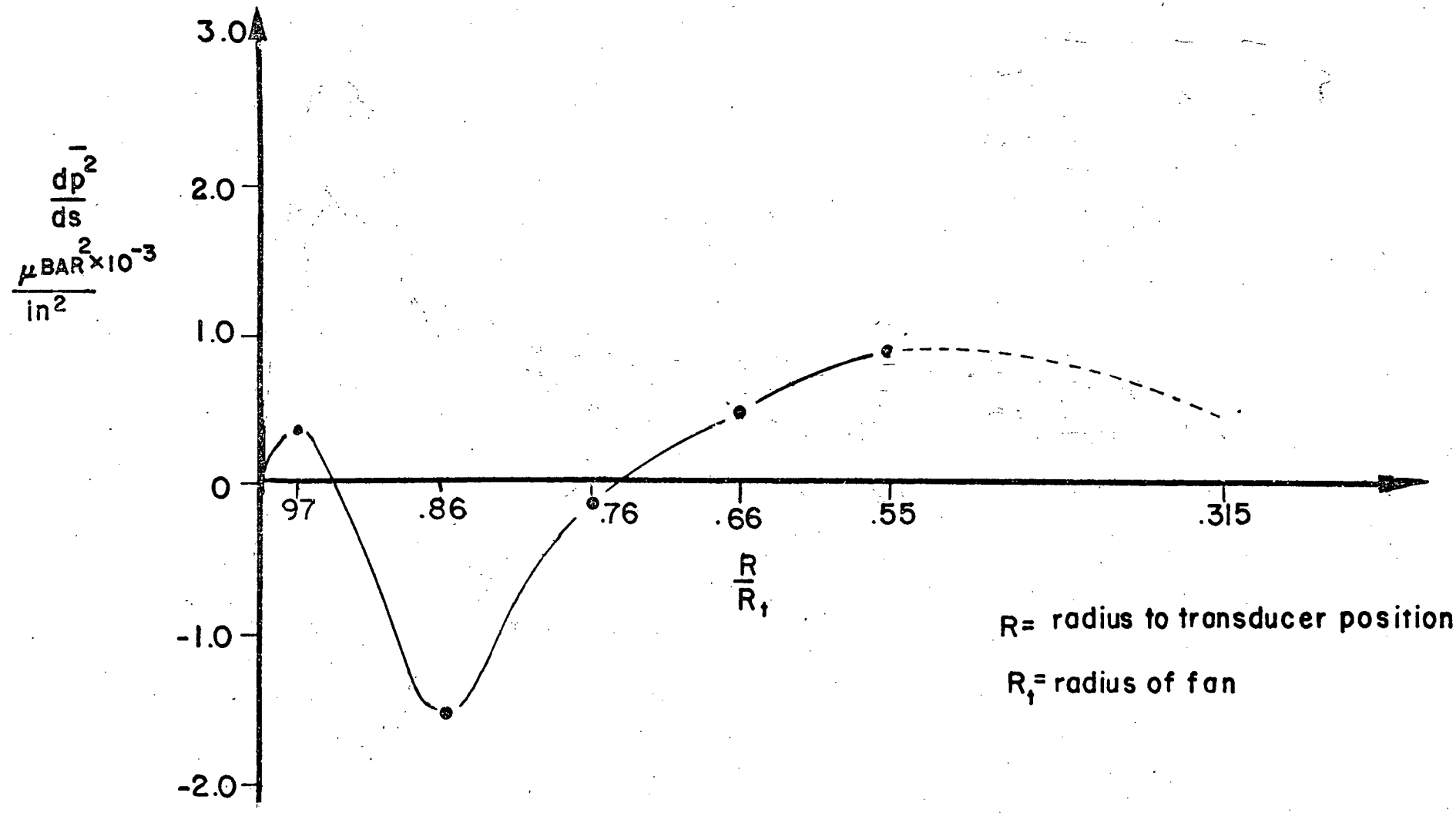

Figure 7 Spanwise Source Strength of 420 Hz Tone at 15 Per Cent Chord

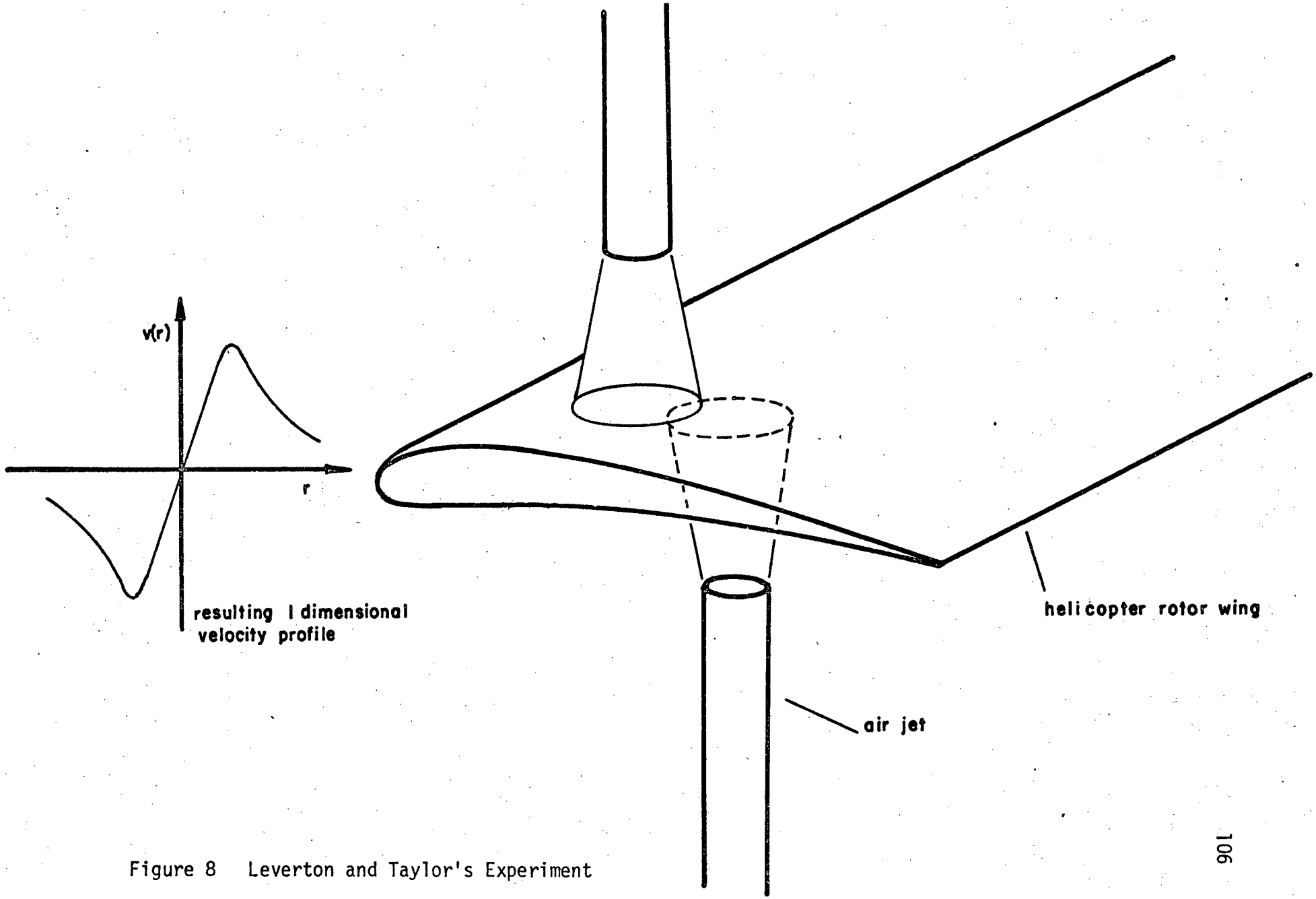

Figure 8 Leverton and Taylor's Experiment

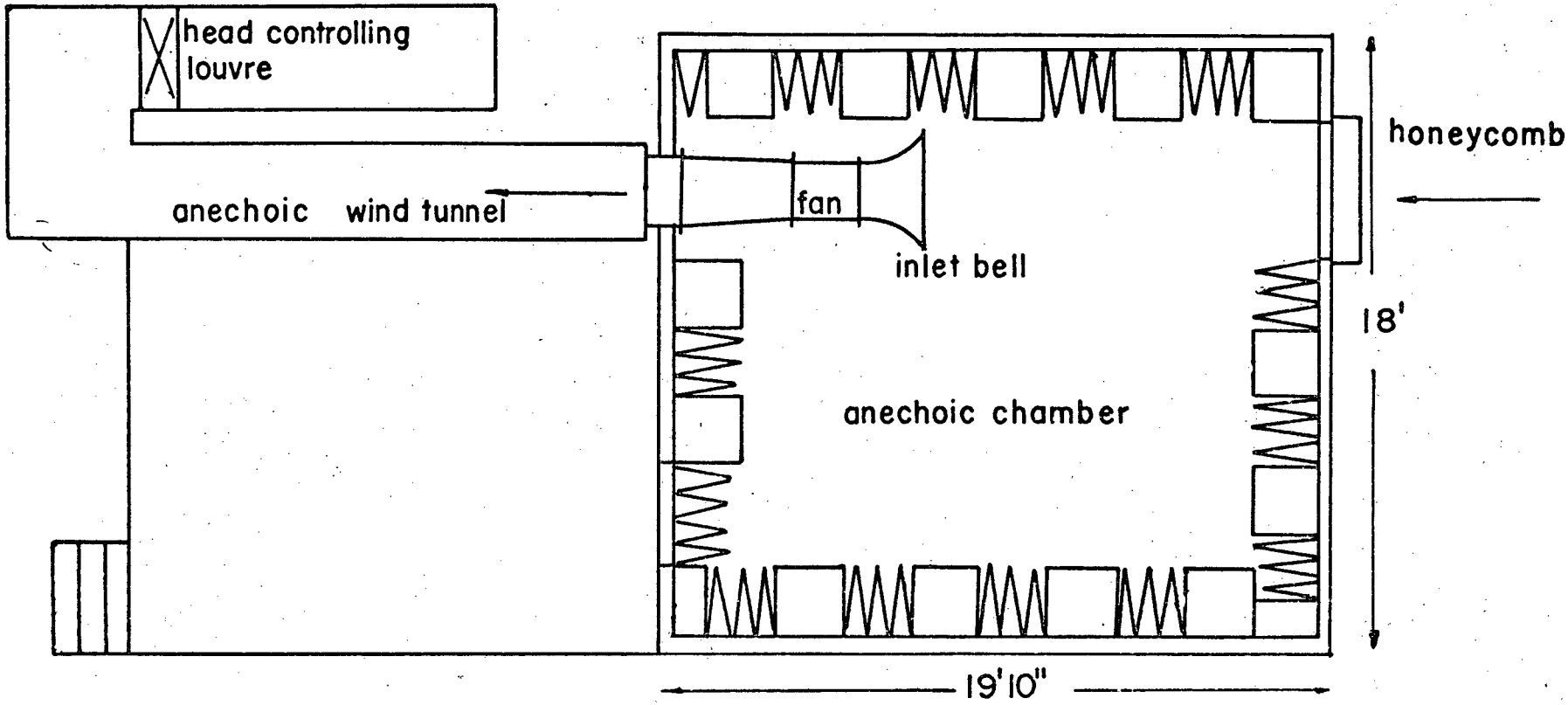

Figure 9 The UBC Fan Noise Facility

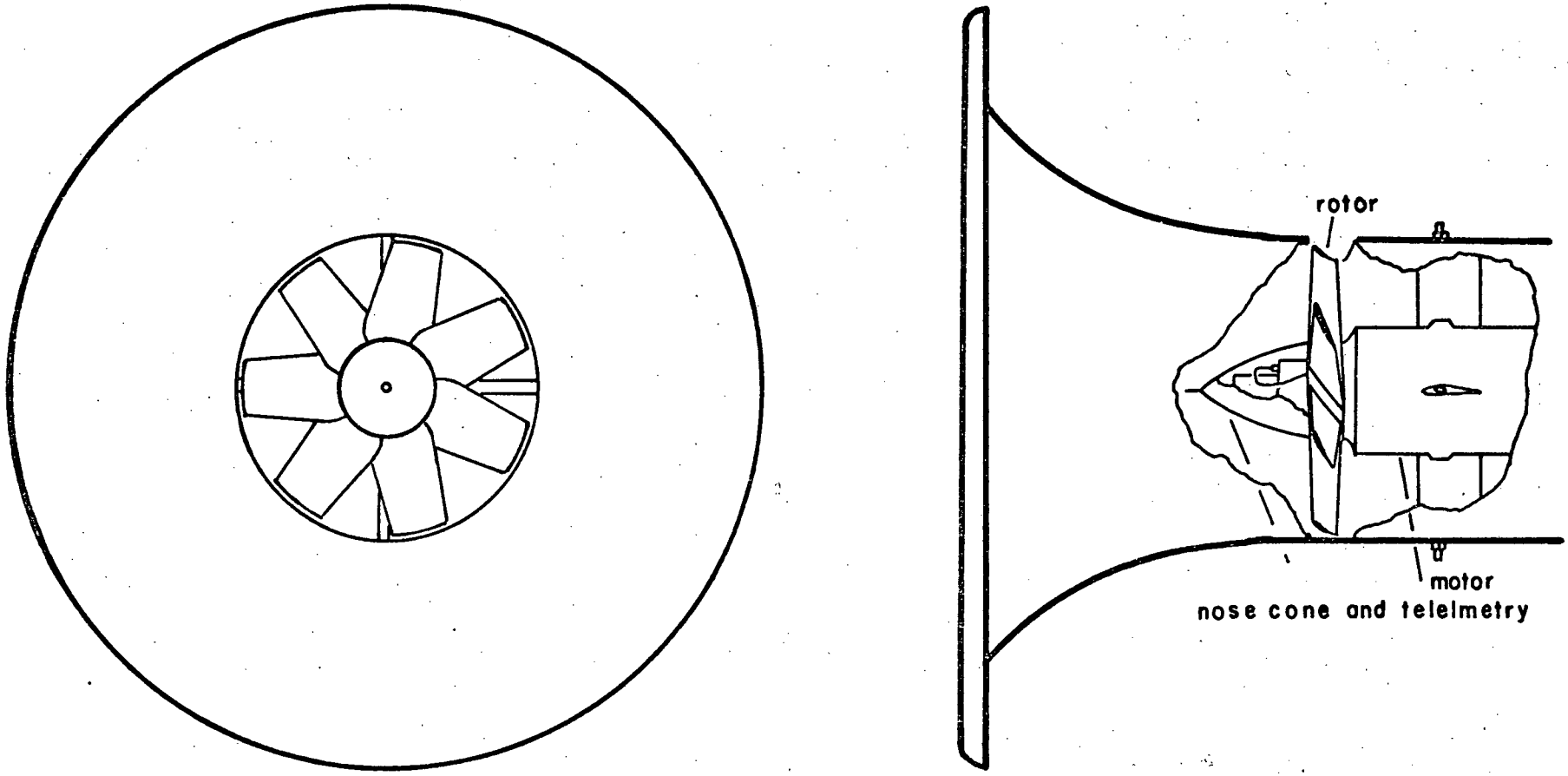

Figure 10 The Experimental Fan Apparatus

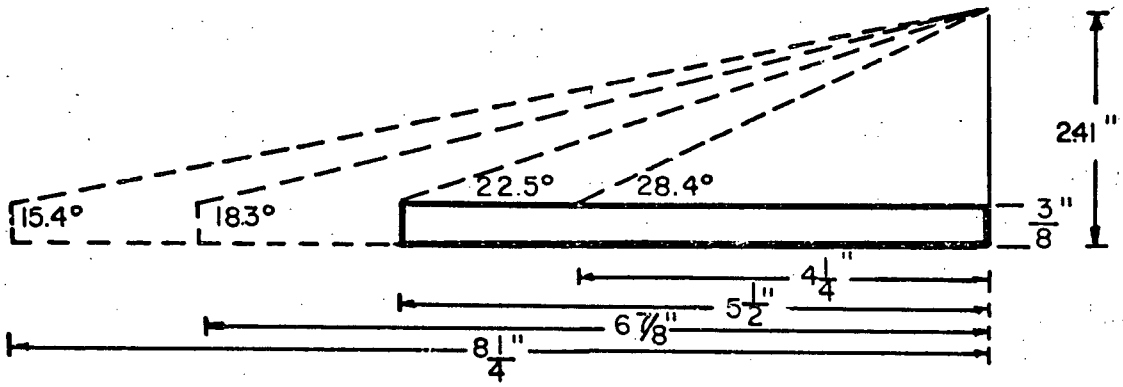

Figure 11 The Experimental Half Delta Wings

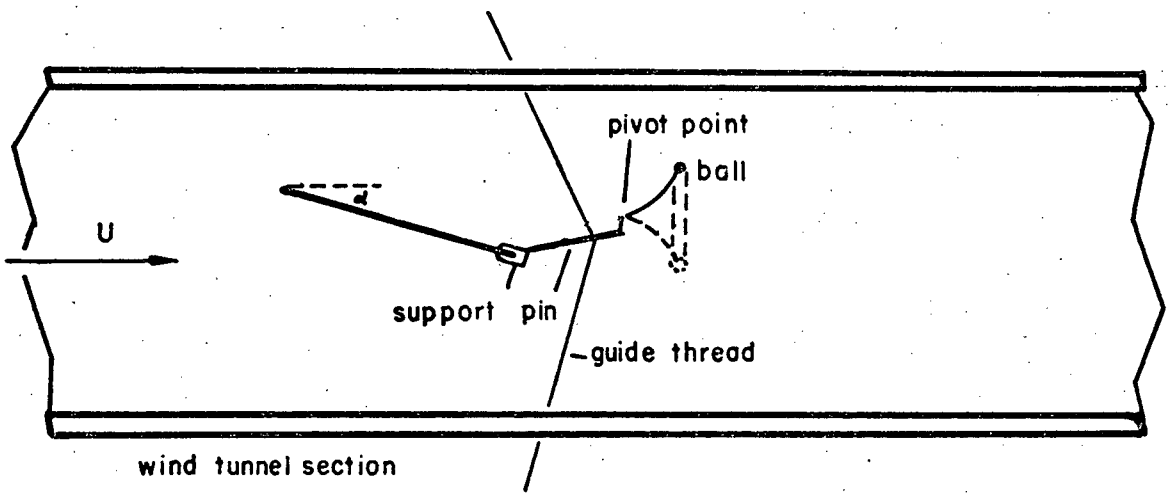

Figure 12 The Method of Determining Vortex Strength

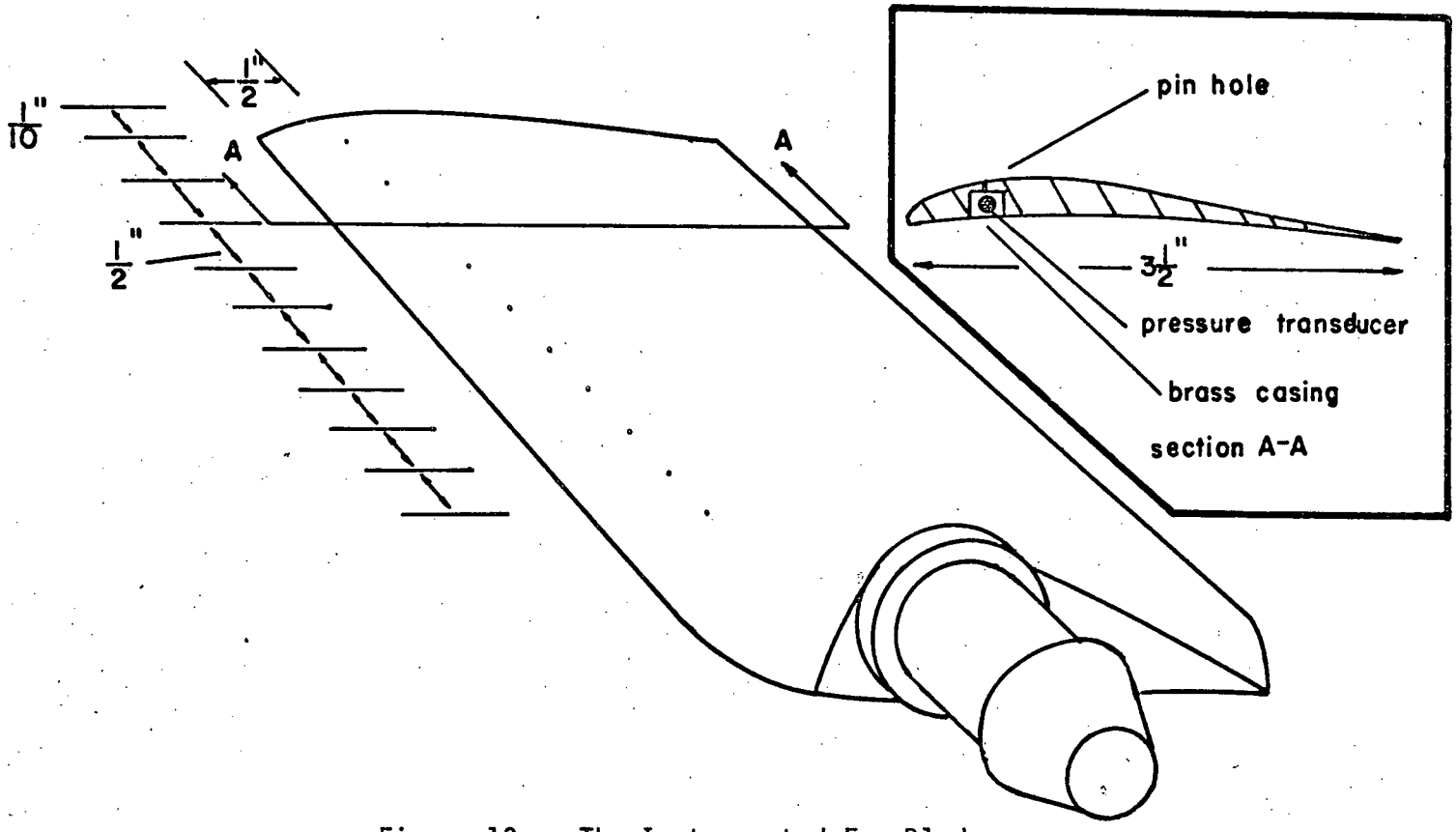

Figure 13 The Instrumented Fan Blade

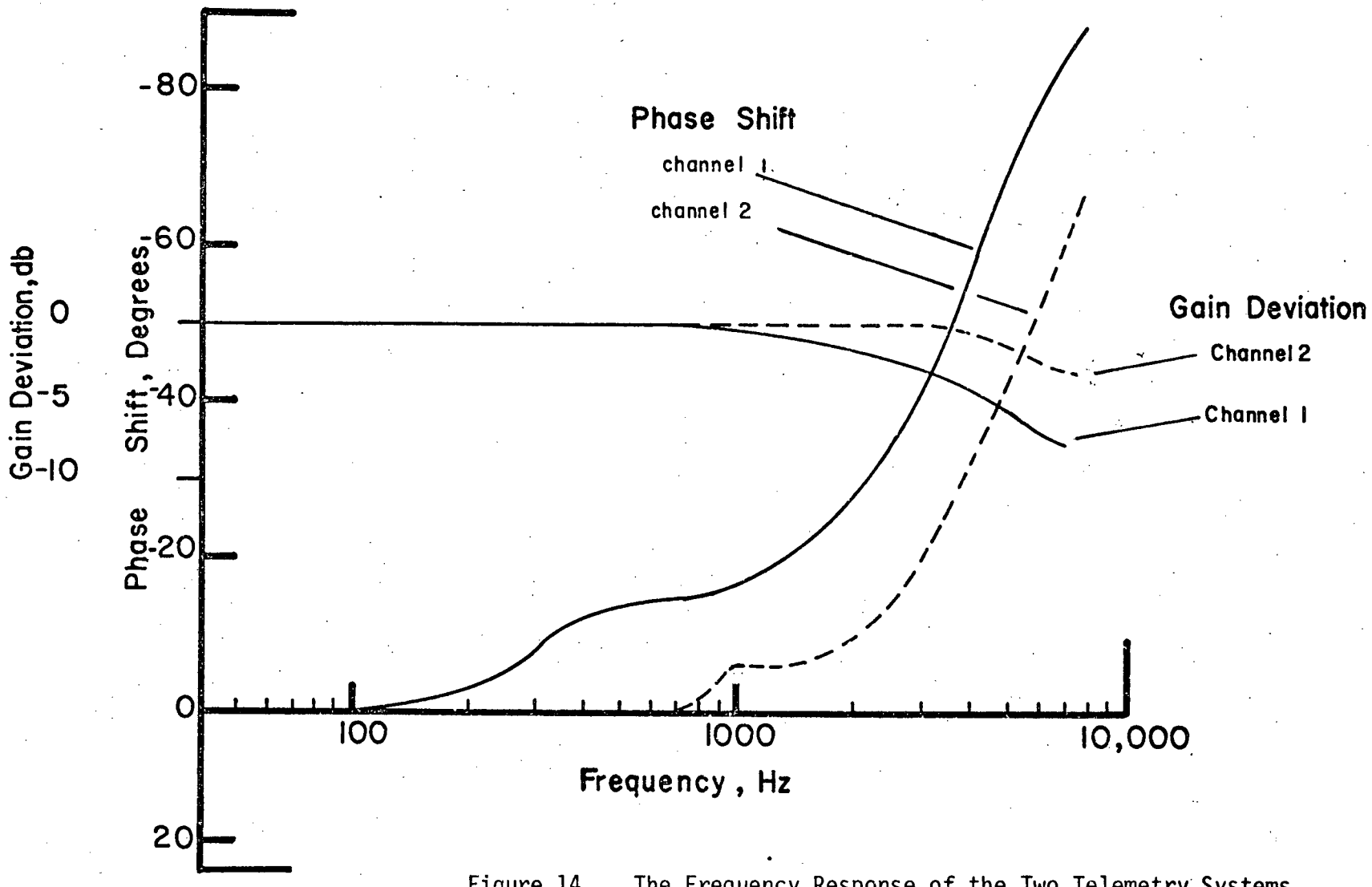

Figure 14 The Frequency Response of the Two Telemetry Systems

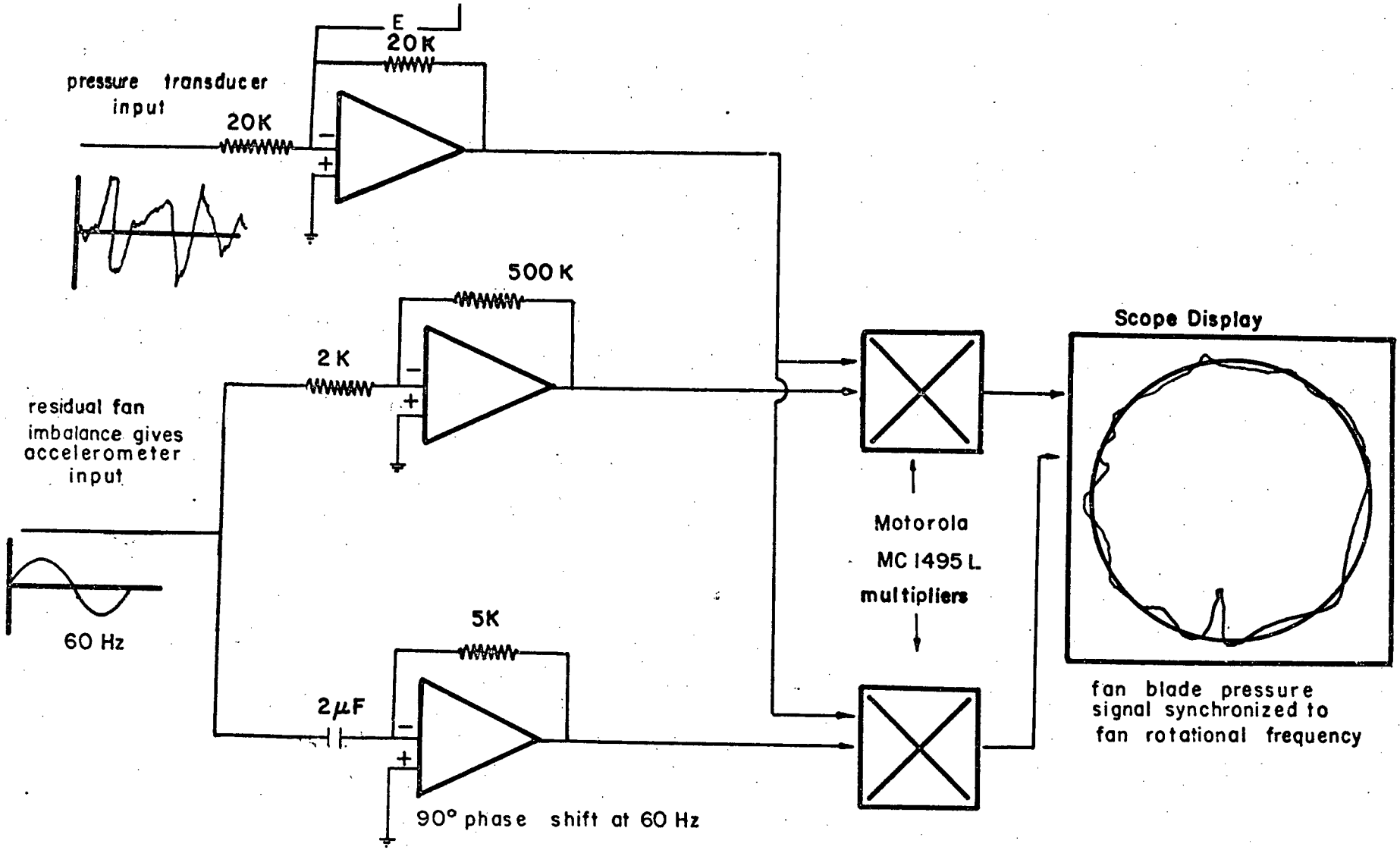

Figure 15 The Polar Plotter Configuration

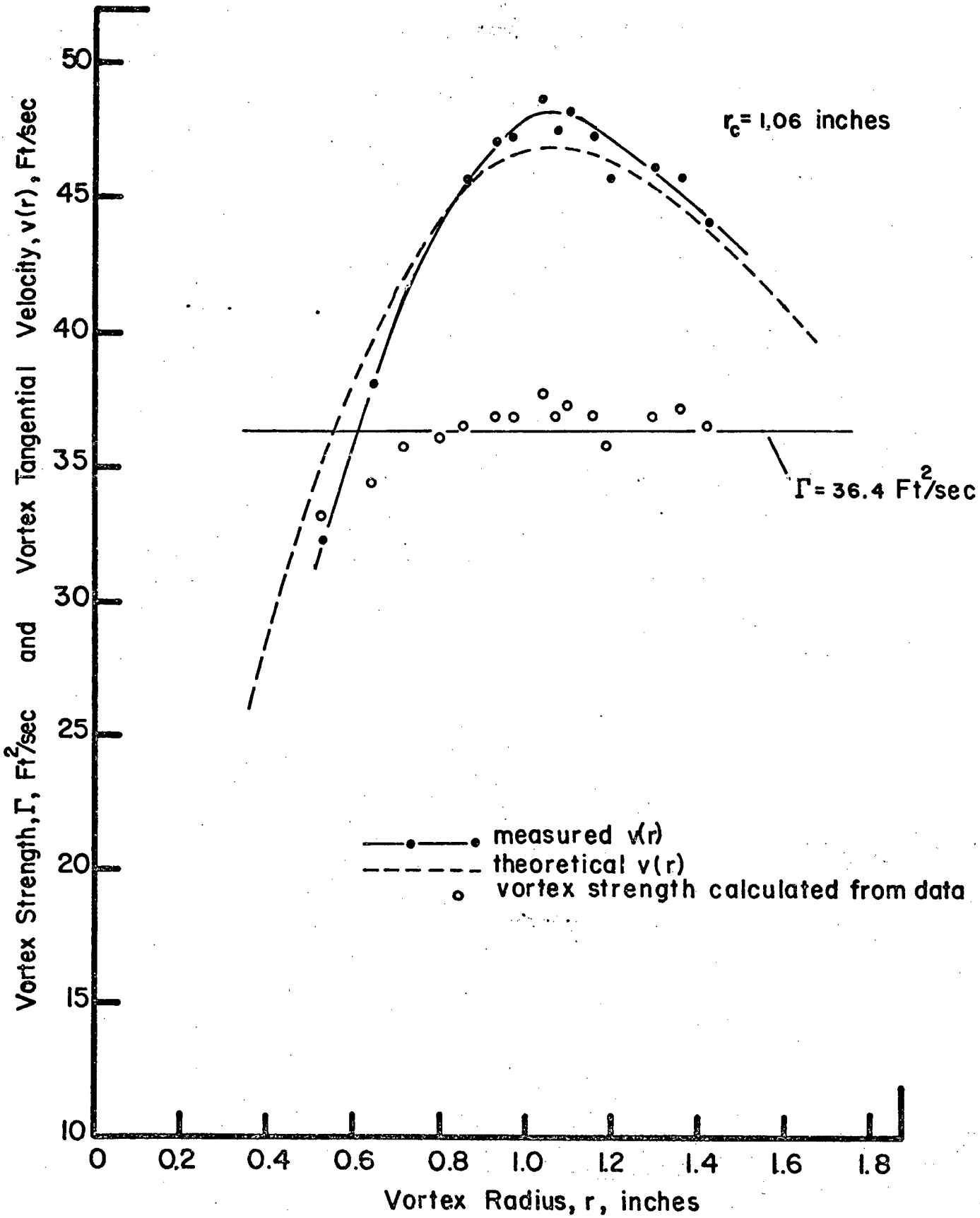

Figure 16 Comparison of Experimental and Theoretical Values of Vortex Tangential Velocity

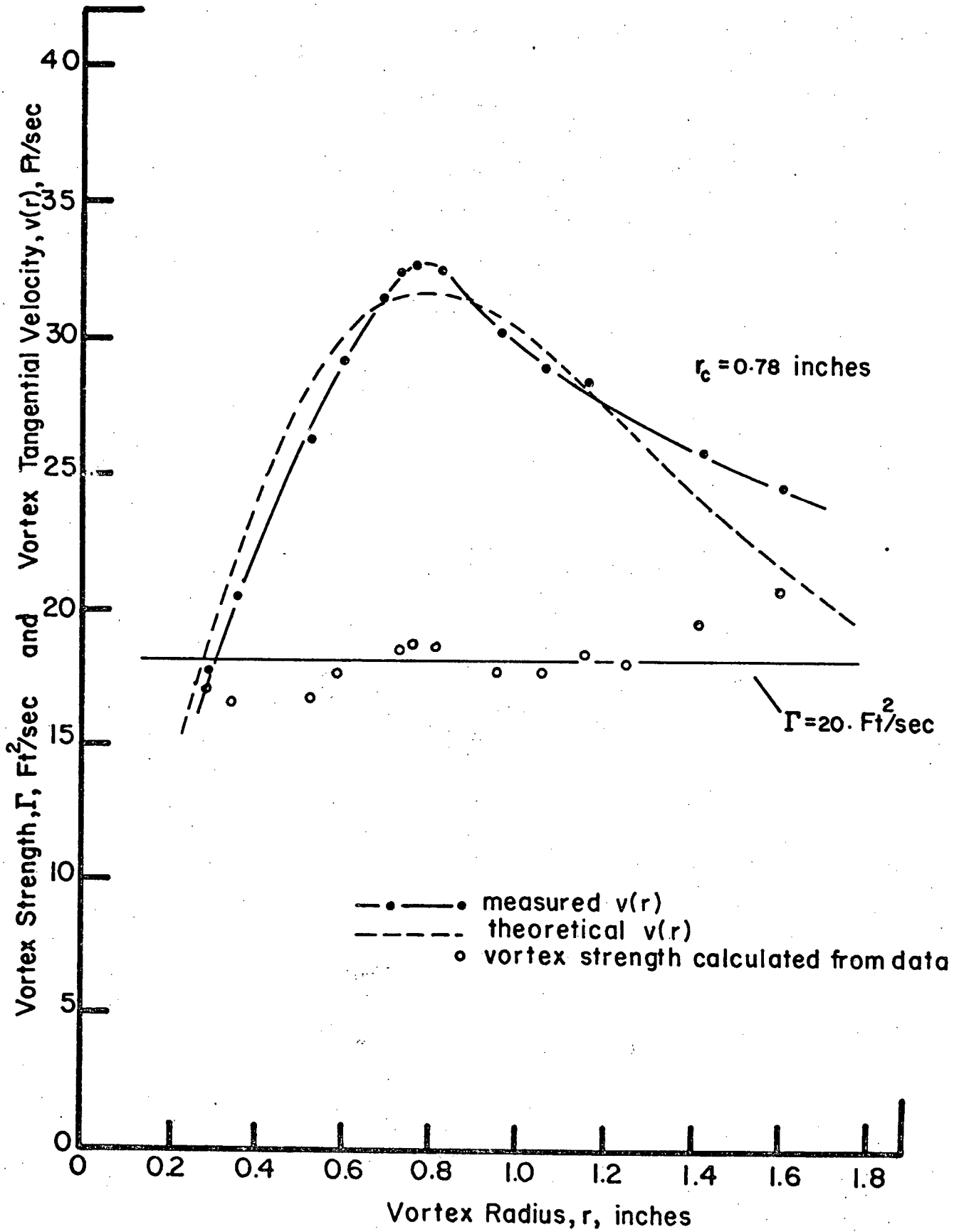

Figure 17 Comparison of Experimental and Theoretical Values of Vortex Tangential Velocity

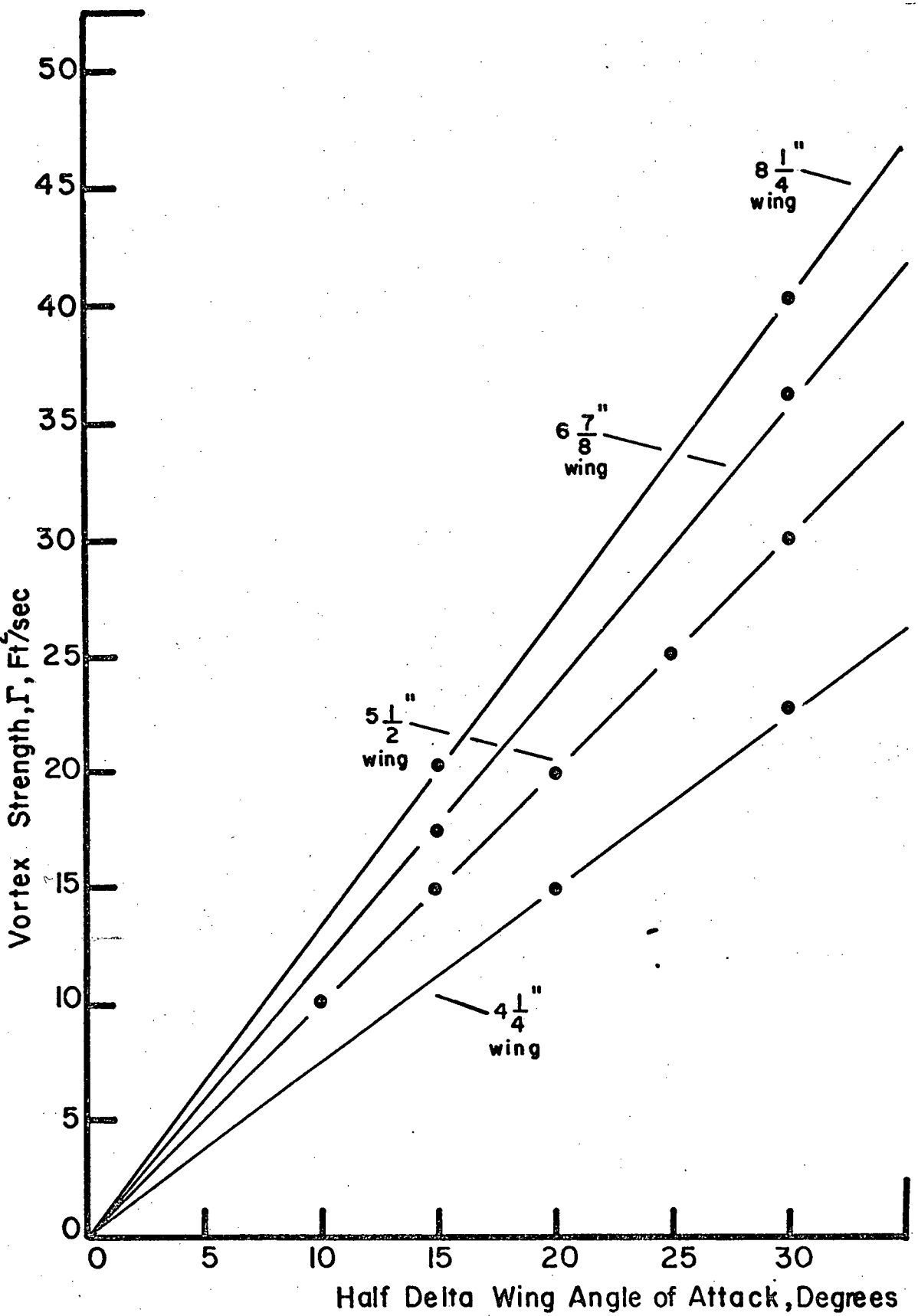

Figure 18 Vortex Strength Produced by Half Delta Wings at Various Angles of Attack

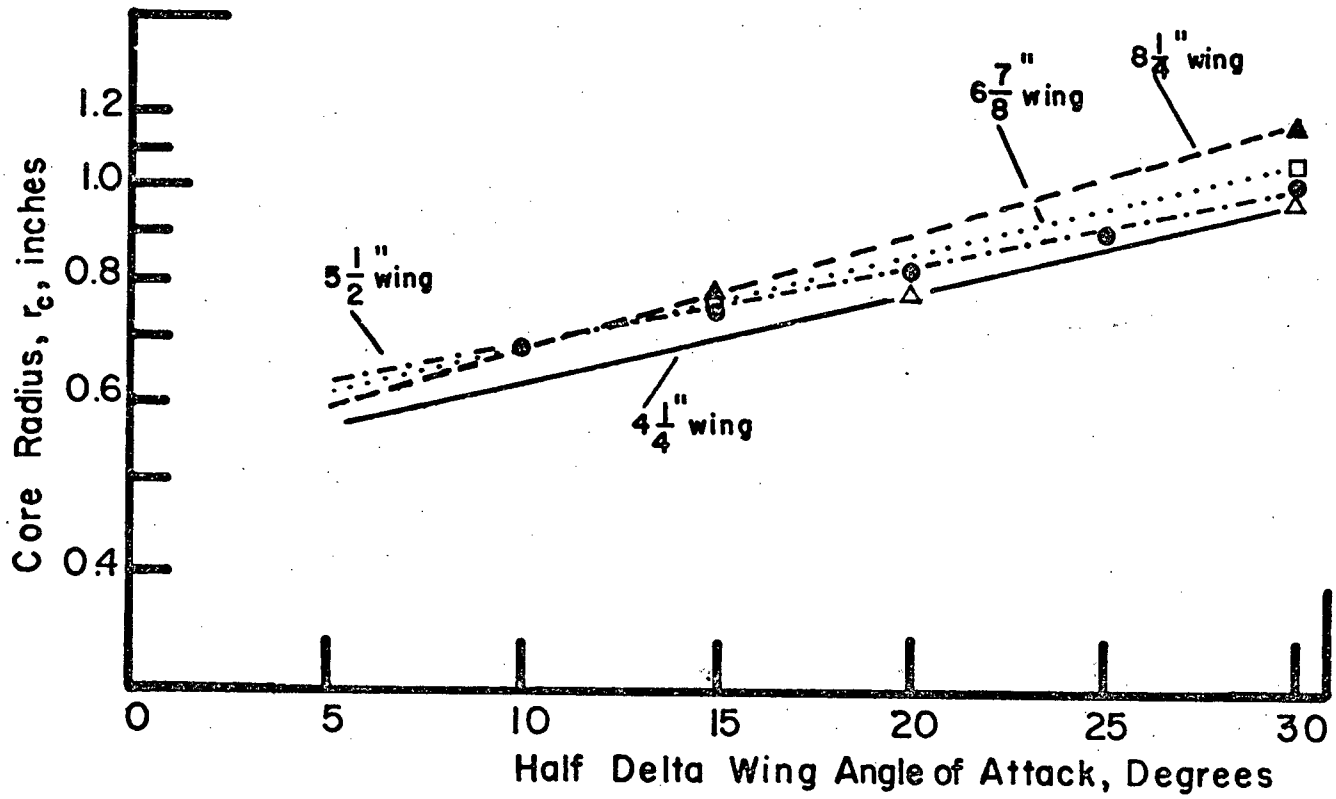

Figure 19 Variation of Core Radius of Vortices Produced by Half Delta Wings

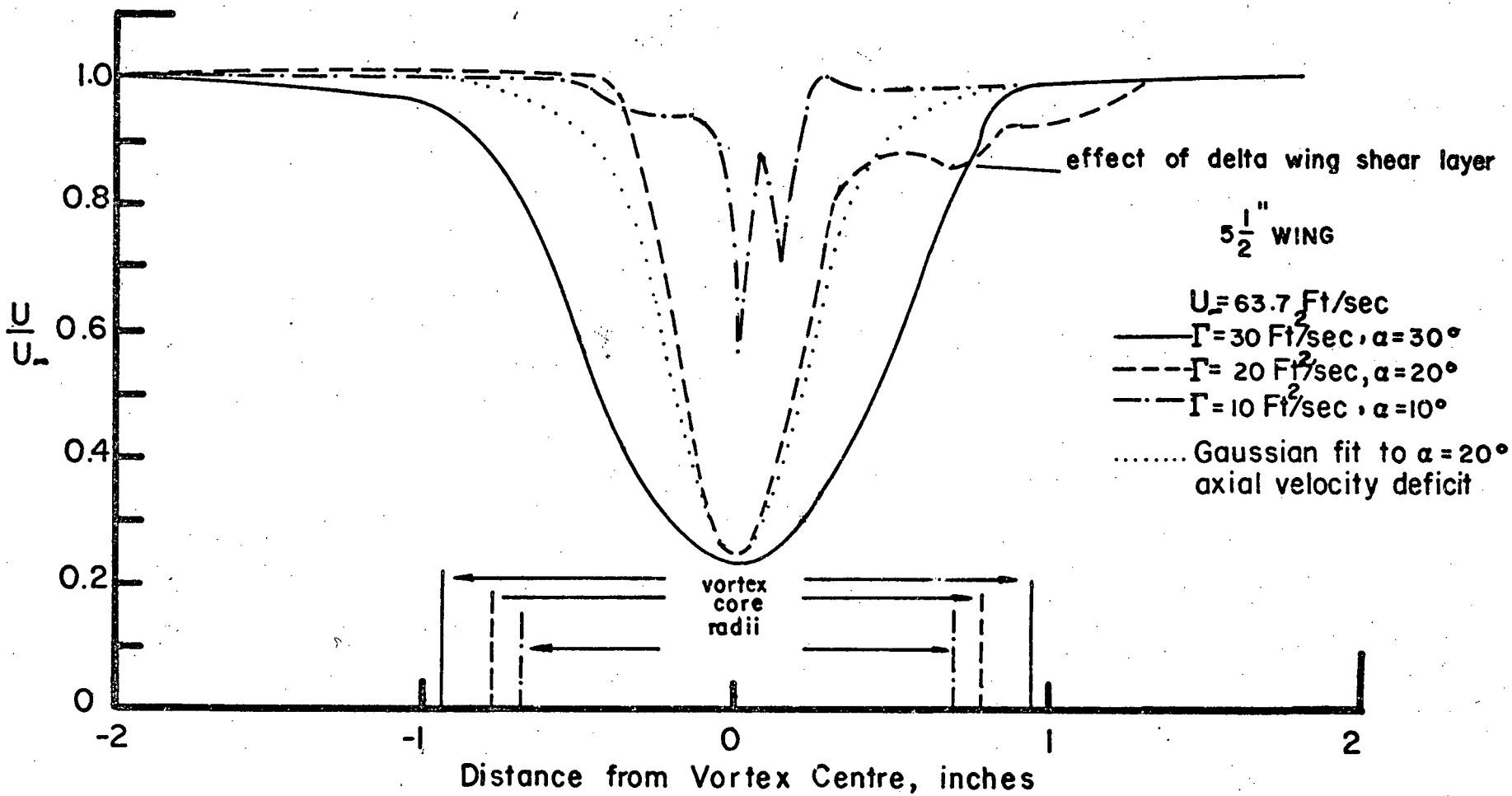

Figure 20 Axial Velocity Deficit in Vortex Core

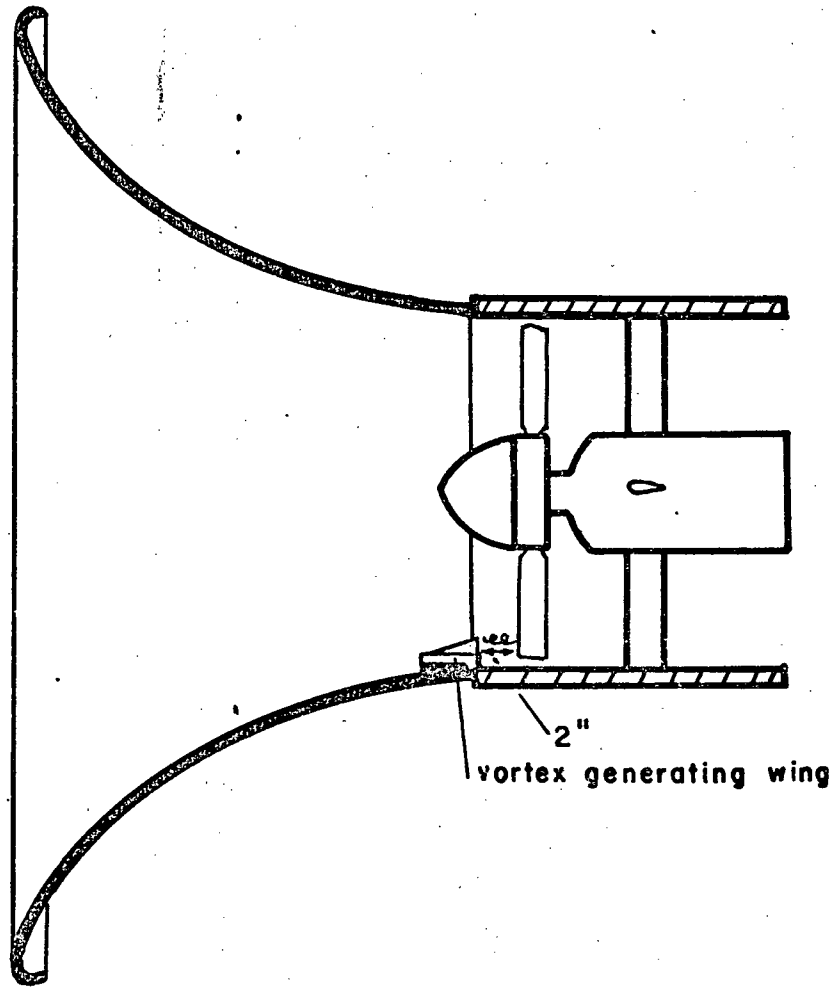

Figure 21 Half Delta Wing Mounted in Fan

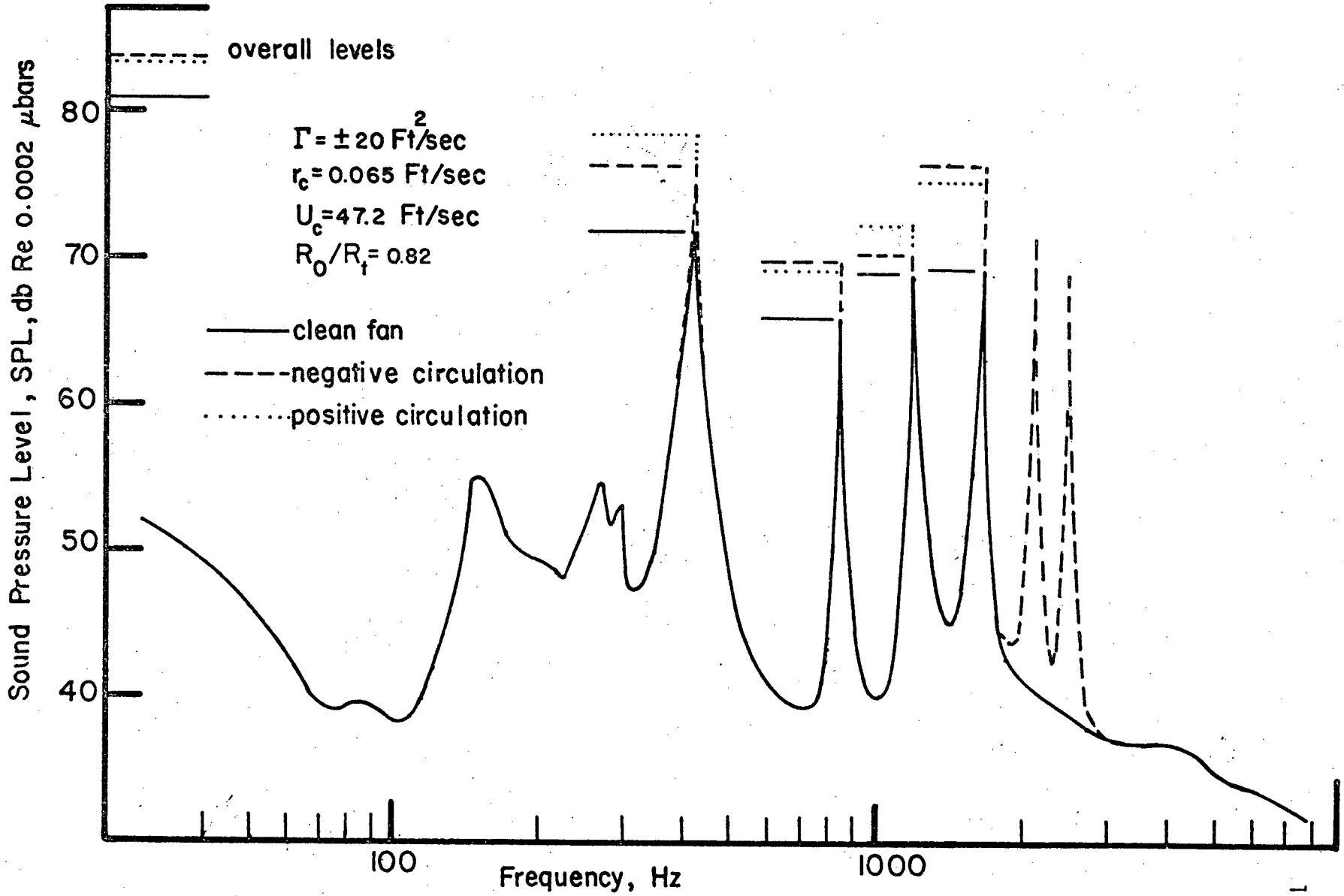

Figure 22 Effect of Imposed Vortex on the Far Field Noise Spectrum

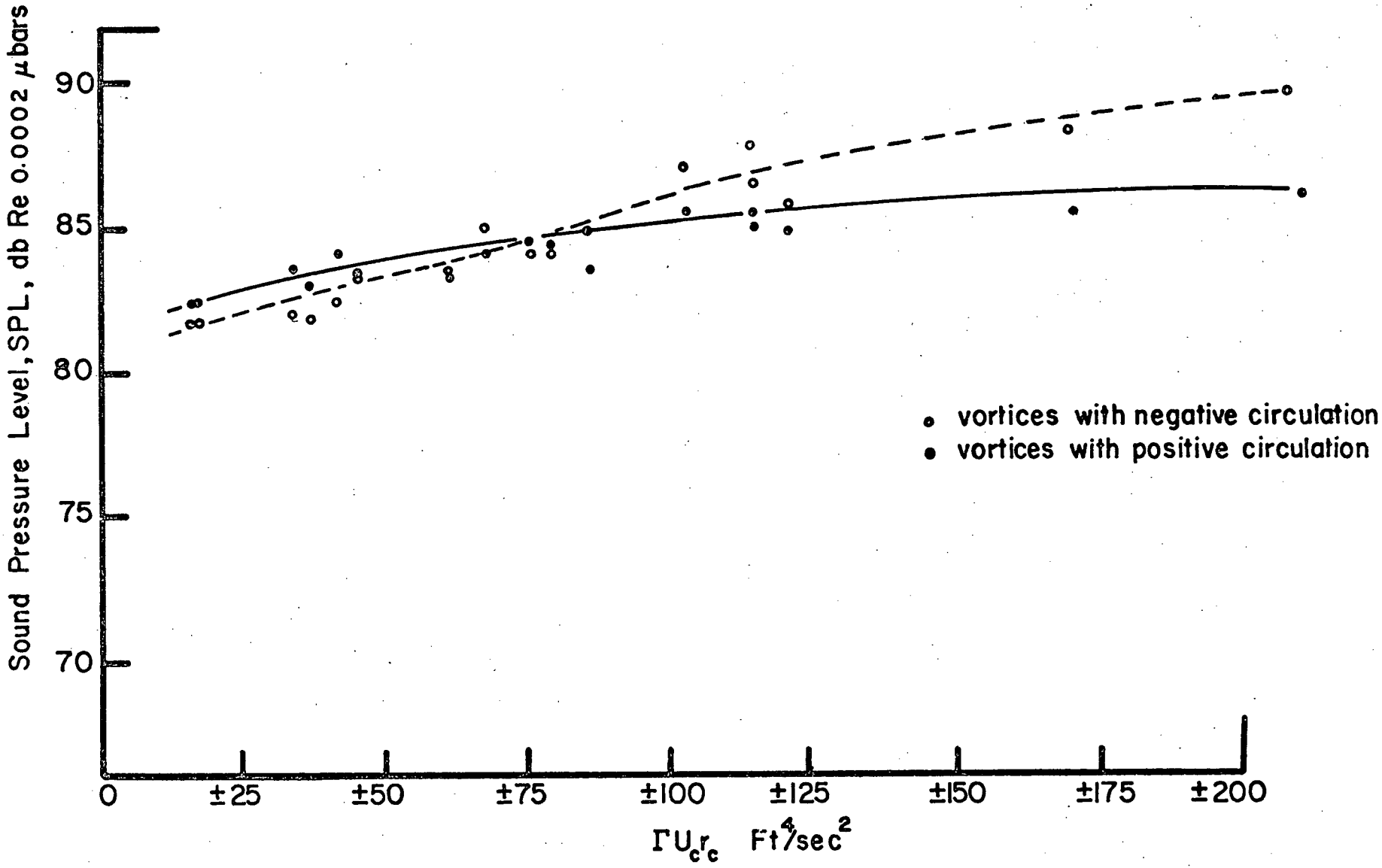

Figure 23 Collapse of Overall SPL Data Onto Parameter Groupings

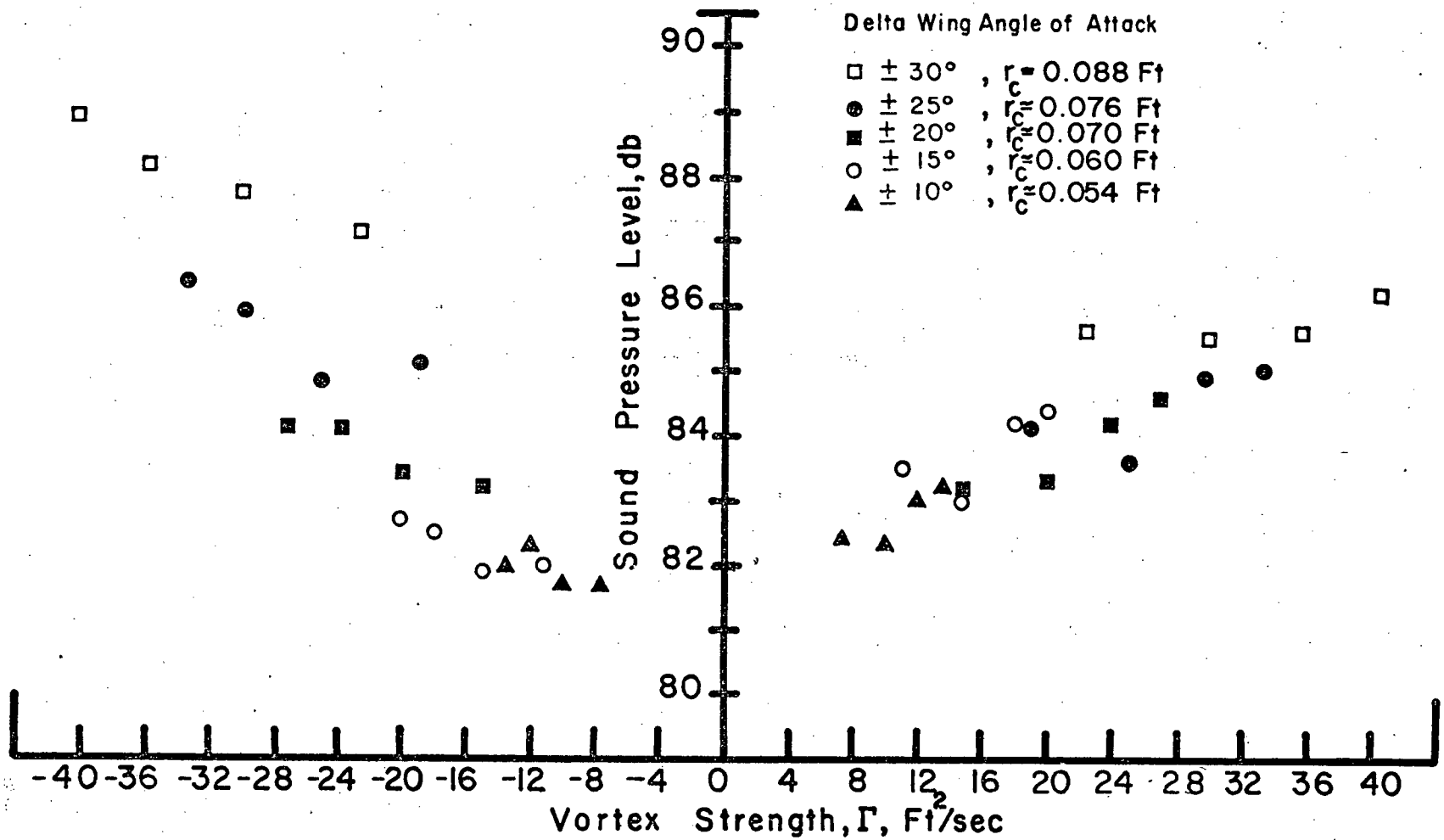

Figure 24 Experimental Dependence of Overall SPL on Vortex Strength

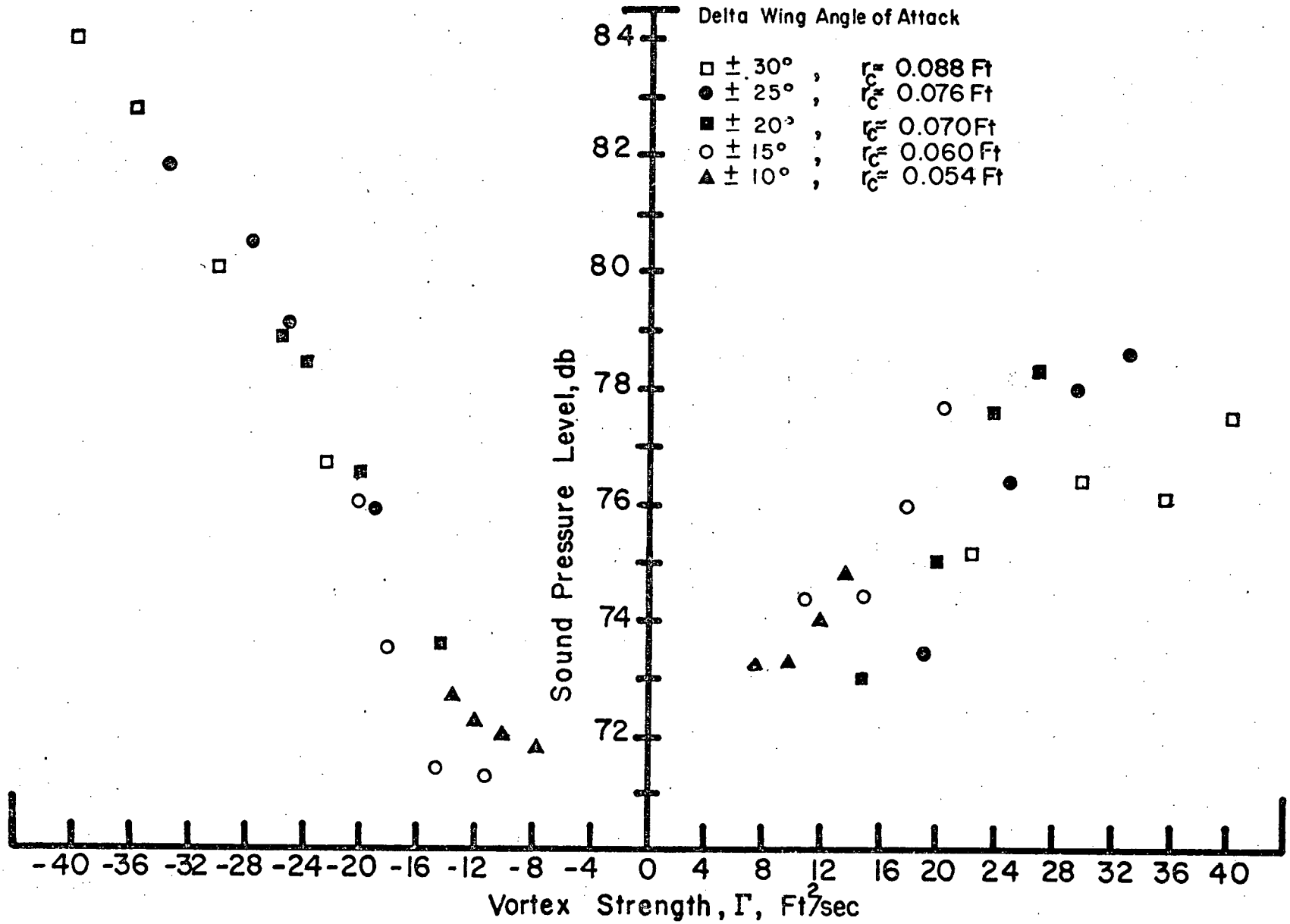

Figure 25 Experimental Dependence of 1680 Hz Harmonic on Vortex Strength

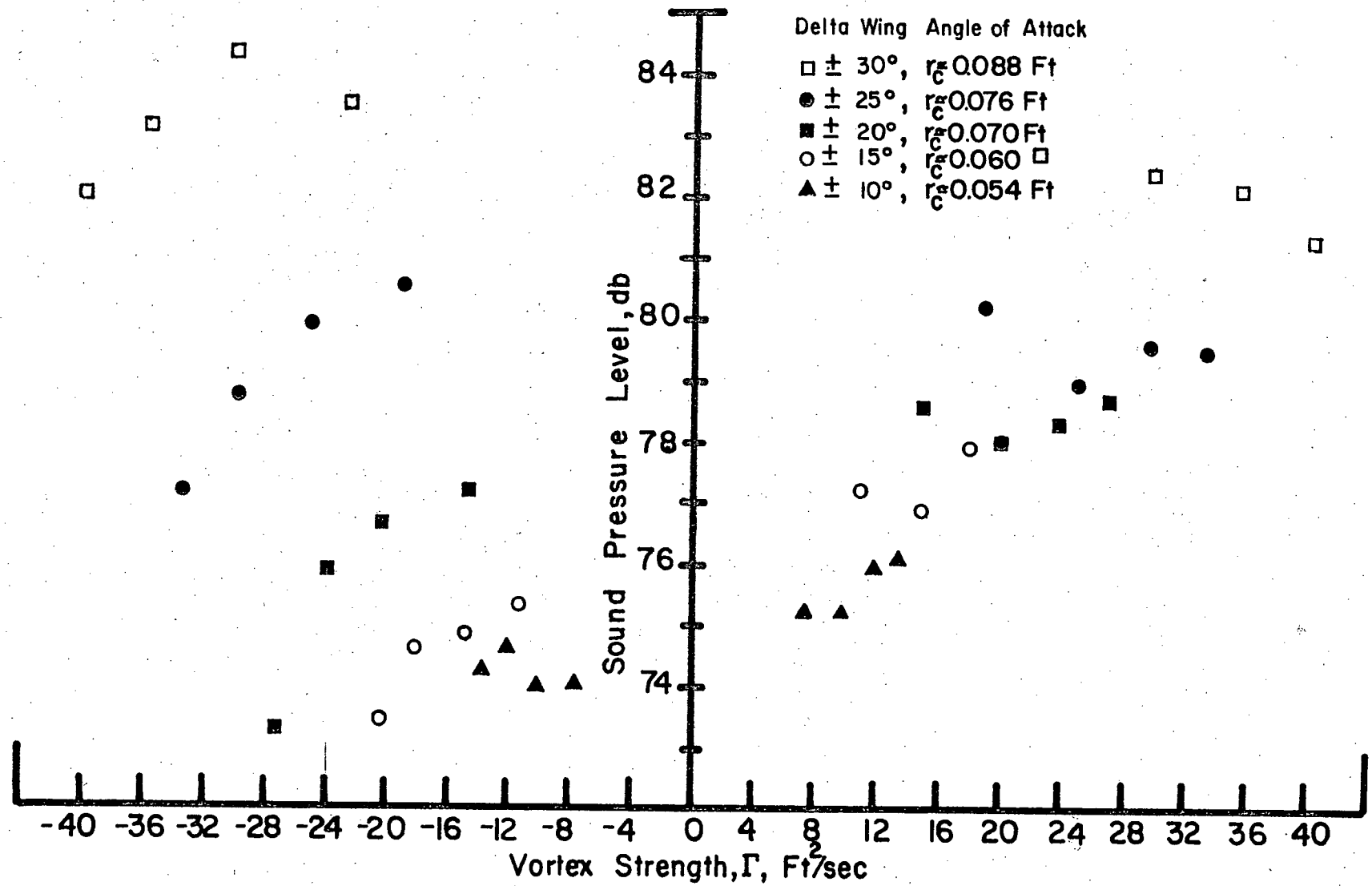

Figure 26 Experimental Dependence of 420 Hz (Fundamental) on Vortex Strength

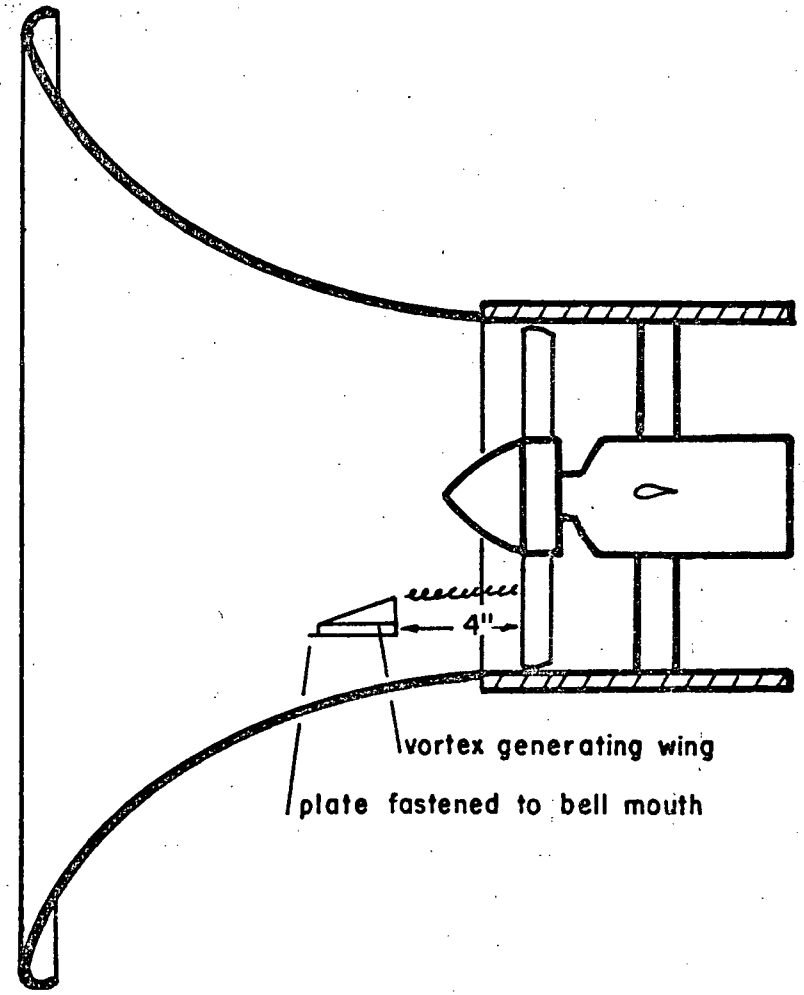

Figure 27 The Delta Wing Mounted on a Flat Plate in the Bell Mouth

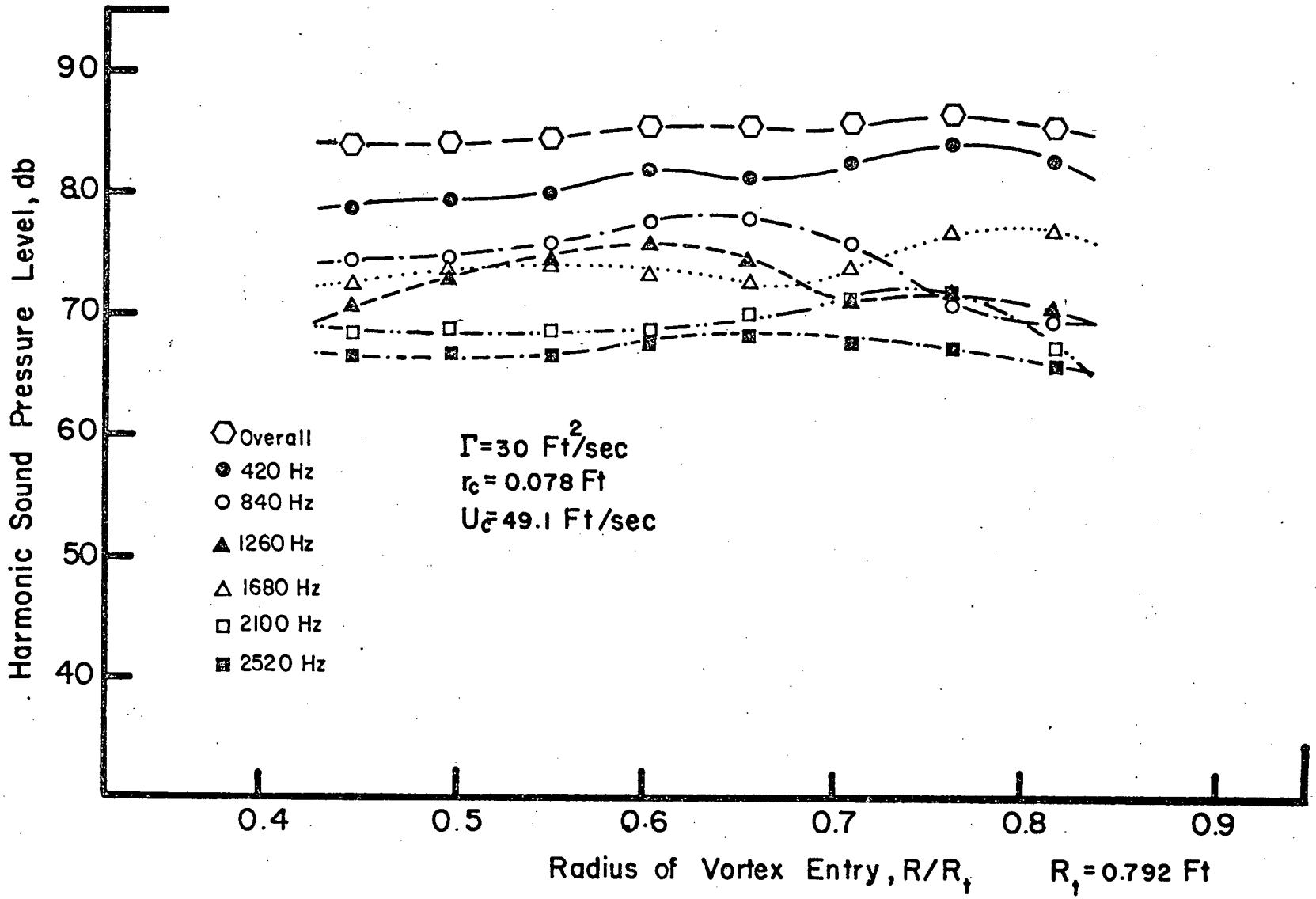

Figure 28 Variation of SPL With Radial Position of Vortex Entry (Experimental, Positive Circulation Sense)

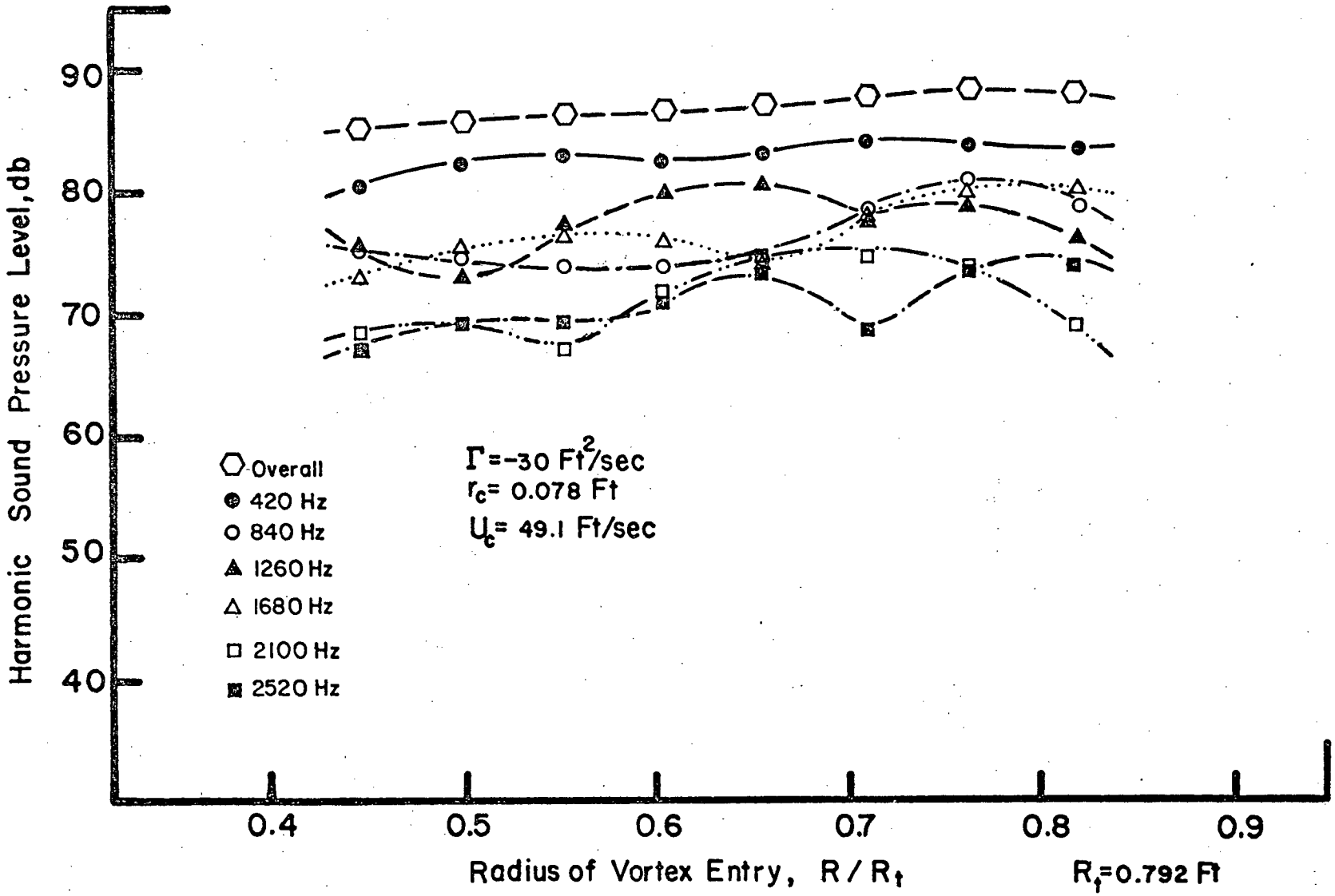

Figure 29 Variation of SPL With Radial Position of Vortex Entry (Experimental, Negative Circulation Sense)

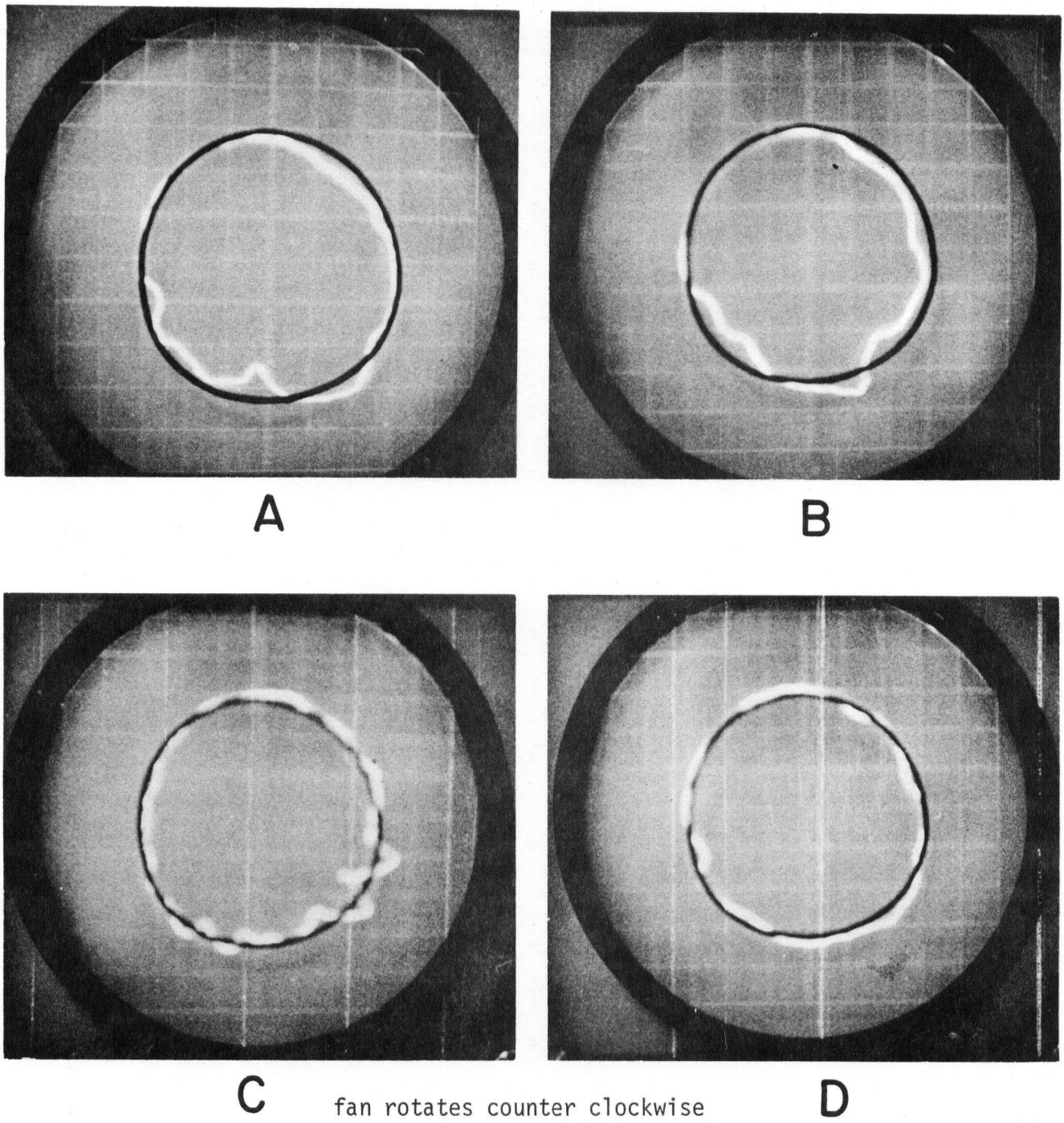

Figure 30. Blade Pressure Polar Plots

A. Negative Sense Vortex
B. Positive Sense Vortex
C. Clean Running Fan (no honeycomb)
D. Clean Running Fan (honeycomb in hatch).

(Exposure: 1/50 sec)

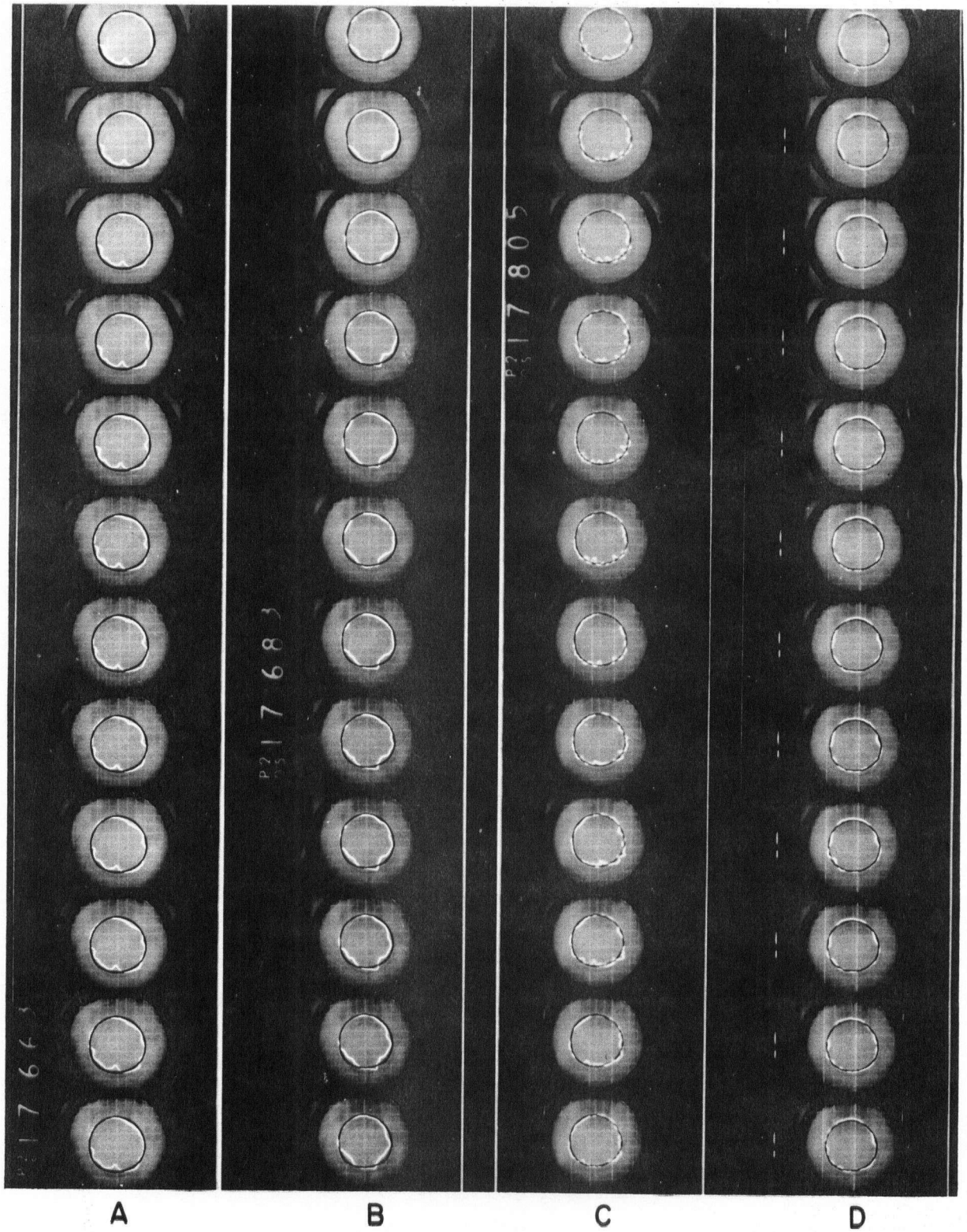

Figure 31. Sequential Blade Pressure Polar Plots

A. Negative Sense Vortex
B. Positive Sense Vortex
C. Clean Running Fan (no honeycomb)
D. Clean Running Fan (honeycomb in hatch).

(Exposure: 1/50 sec, 18 frames/sec)

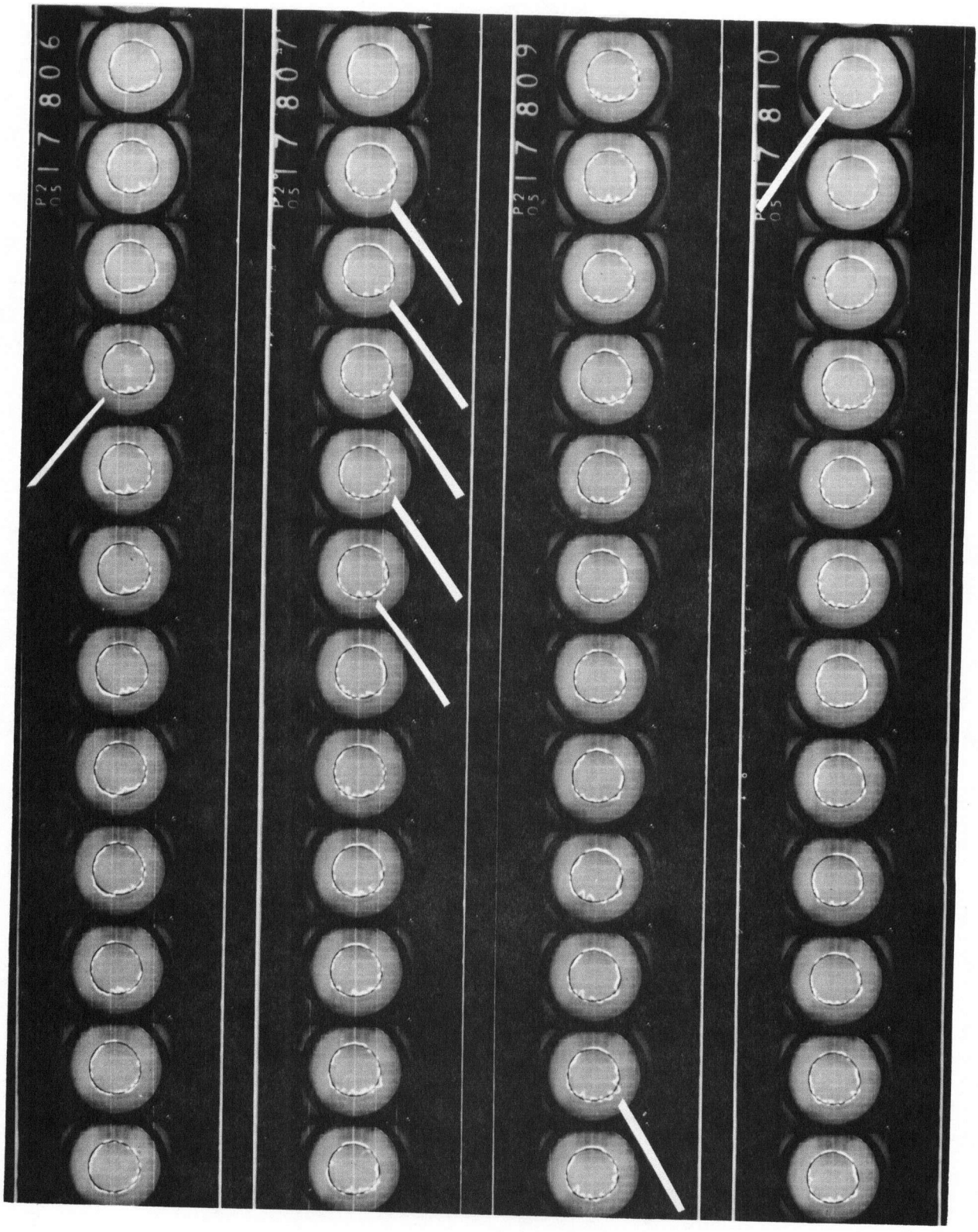

Figure 32. Sequential Blade Pressure Polar Plots. Clean Running Fan (no honeycomb).

(Exposure: 1/50 sec, 18 frames/sec)

(White markers show vortex signature.)

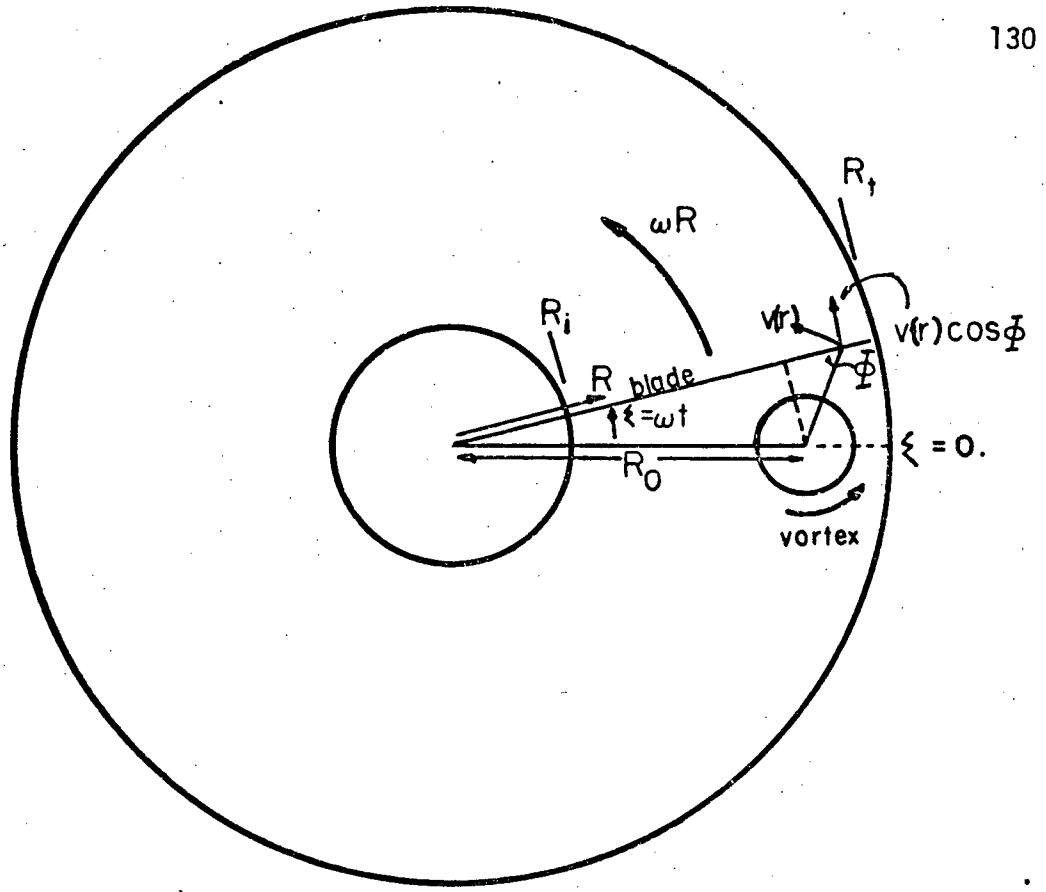

Figure 33A Fan and Vortex Positional Variables

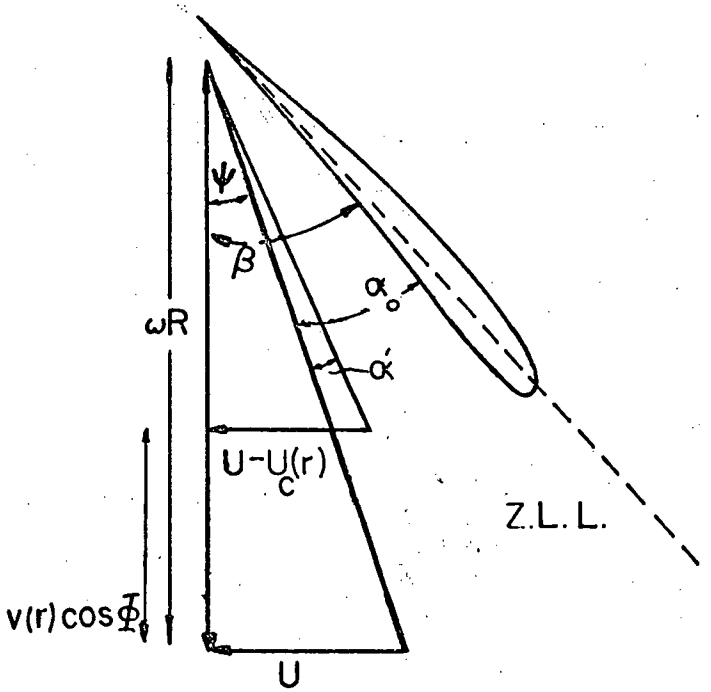

Figure 33B Superposition of Velocity Fields

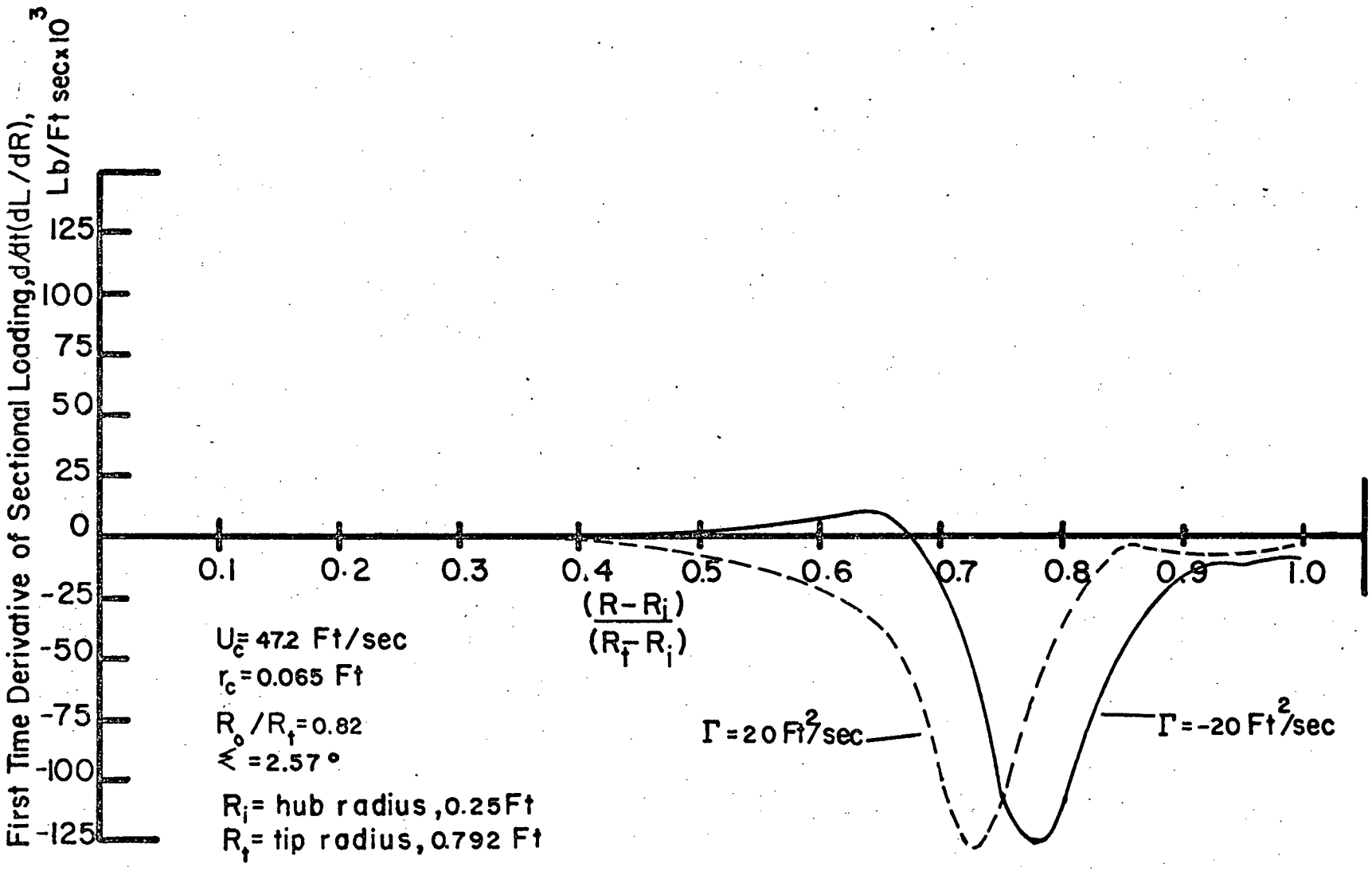

Figure 34 Variation of the Maximum Instantaneous Rate of Change of Lift Over the Span of the Fan Blade

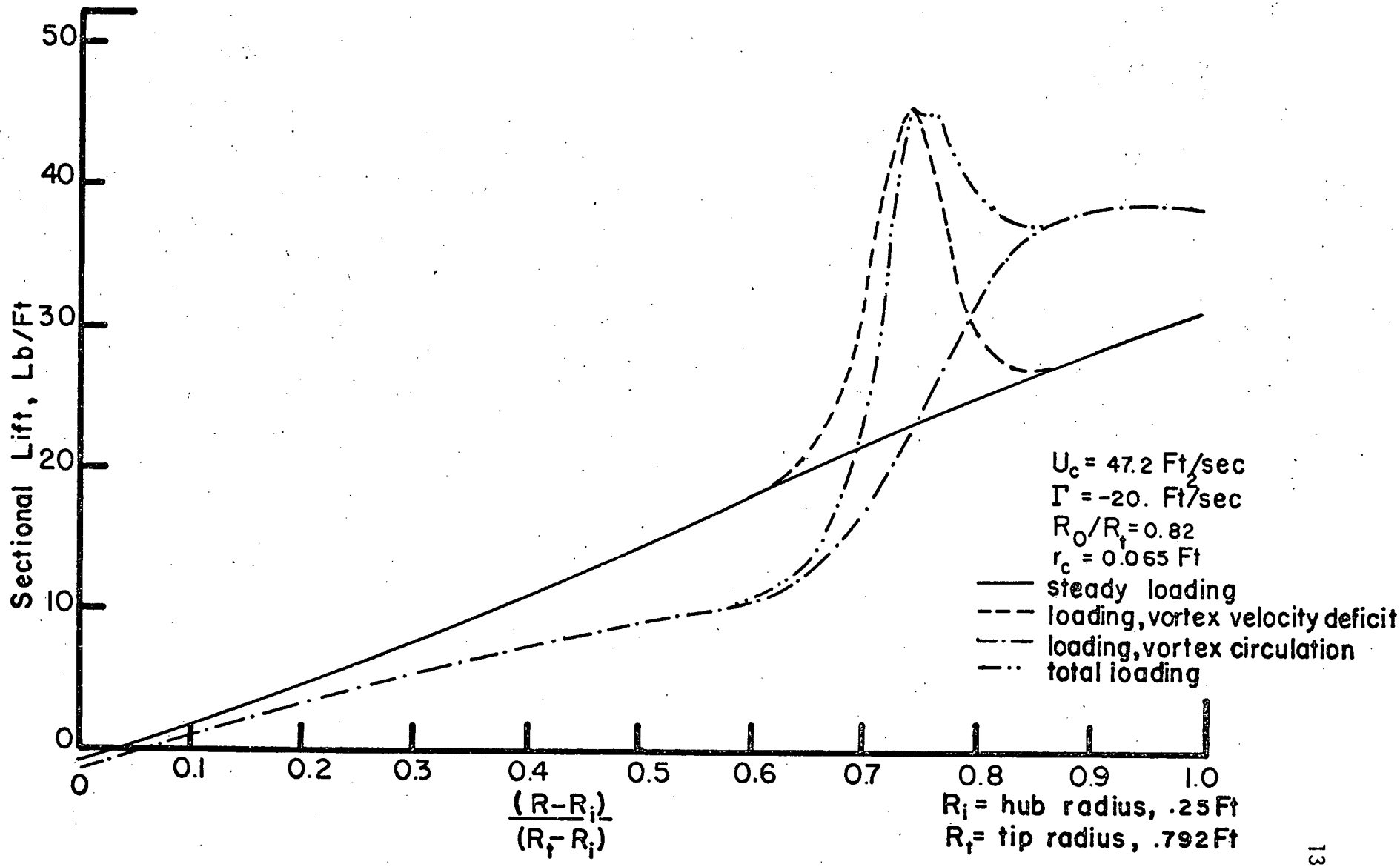

Figure 35 Blade Loading from the Axial Velocity Deficit and Circulation of Inlet Vortex

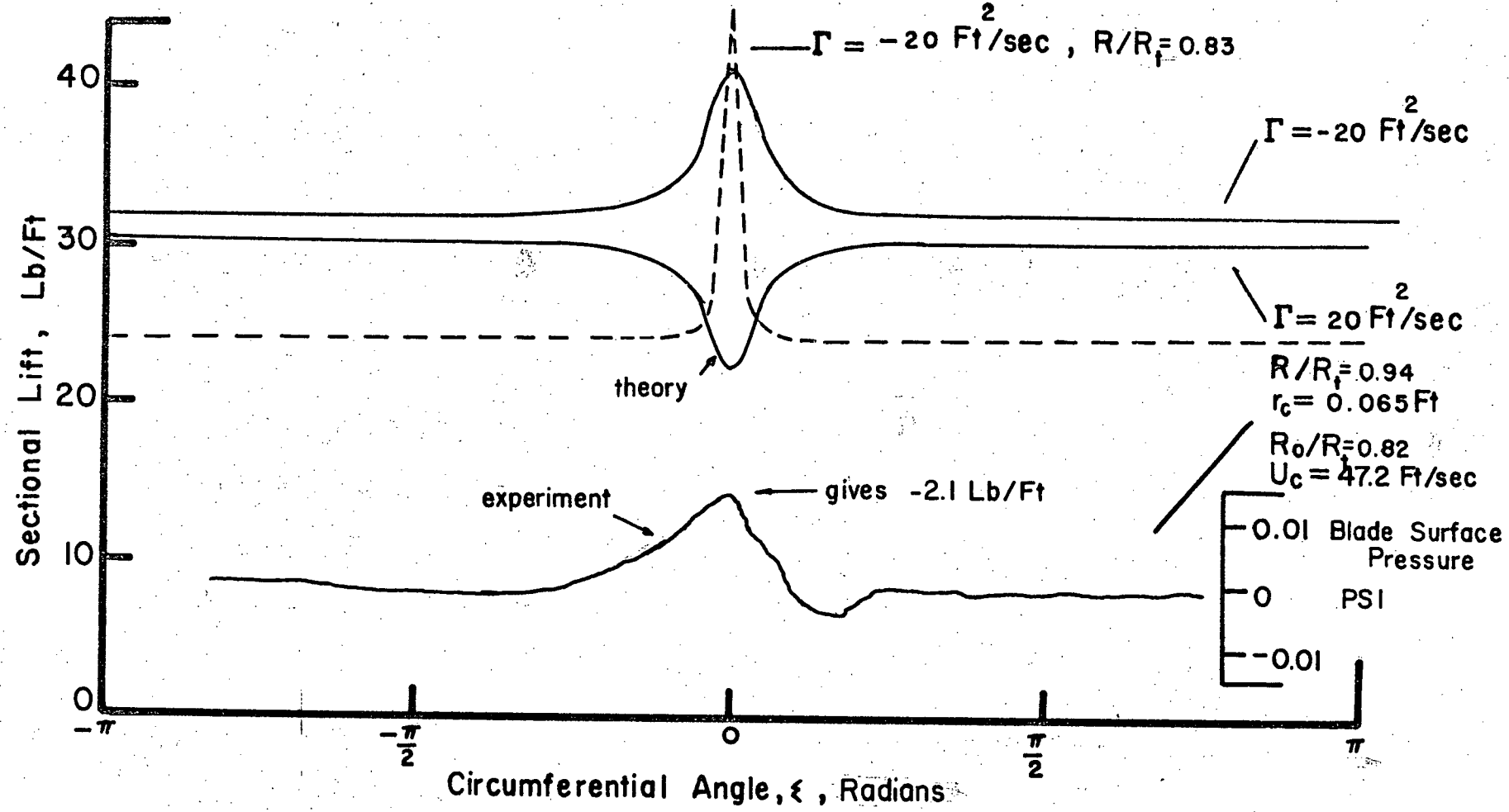

Figure 36 Circumferential Lift Variation at Two Sections and Comparison with Experiment

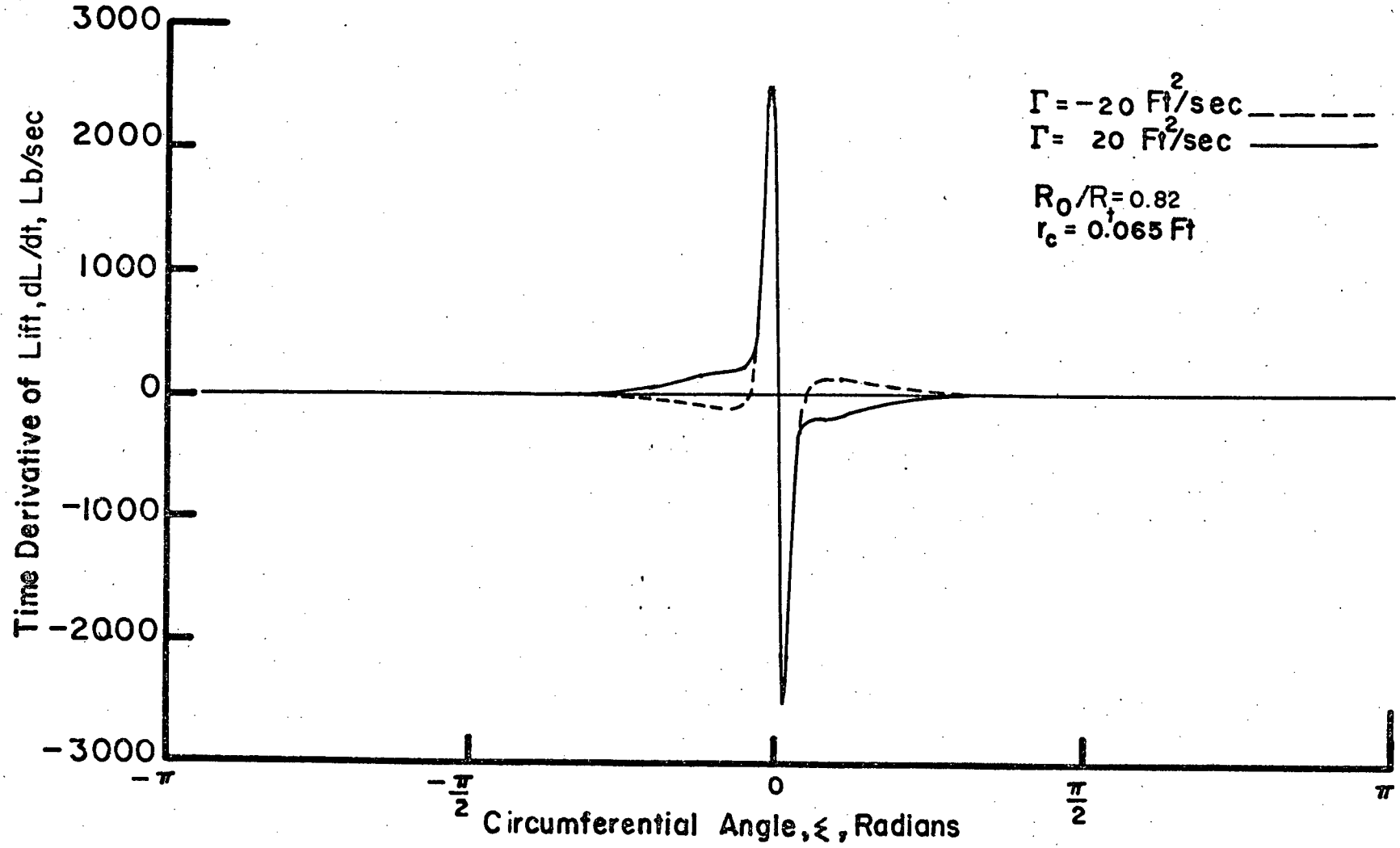

Figure 37 Variation of the Rate of Change of Blade Load Around the Fan Circumference

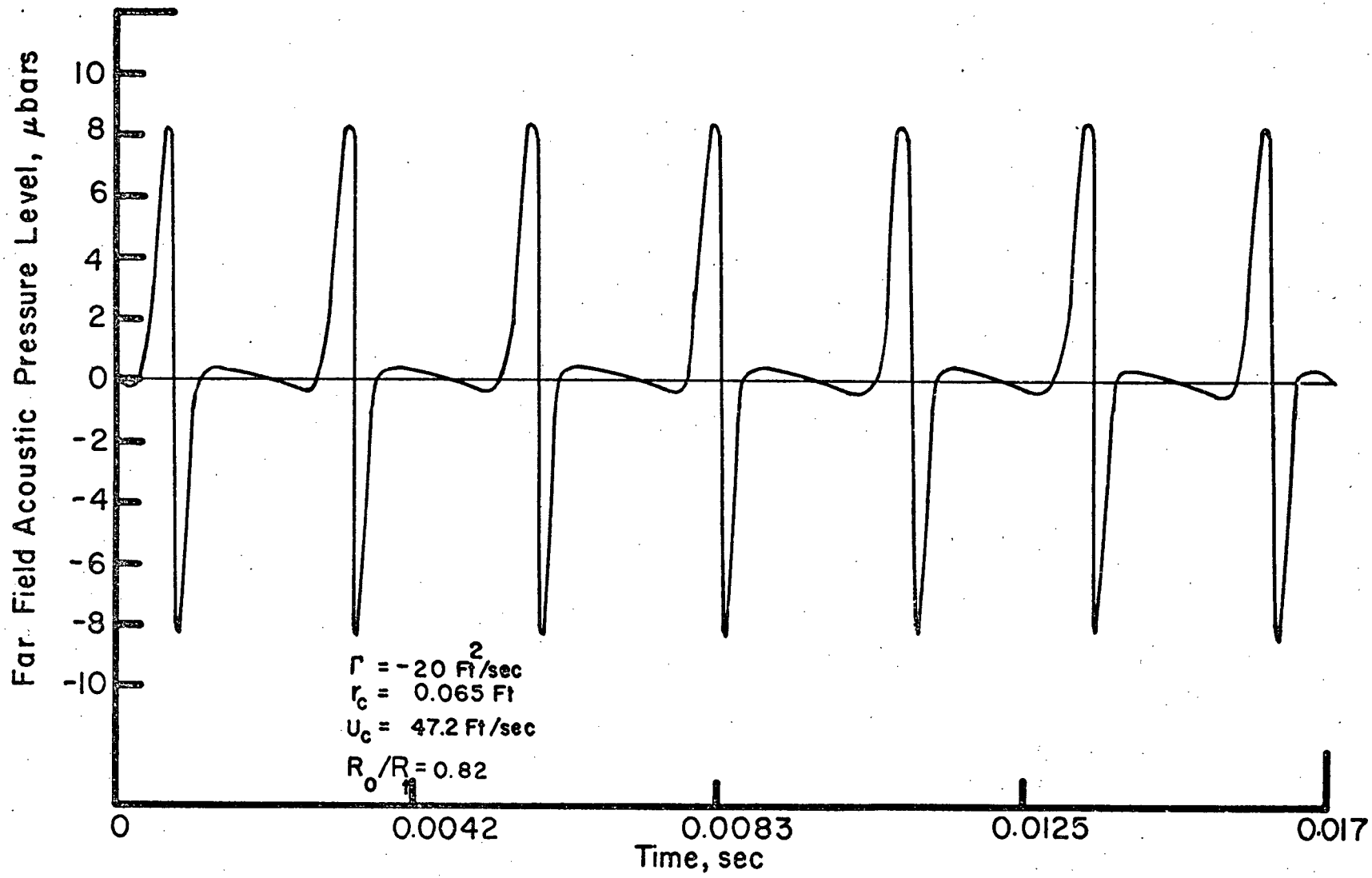

Figure 38 Far Field Pressure Signature Caused by Vortex Interaction

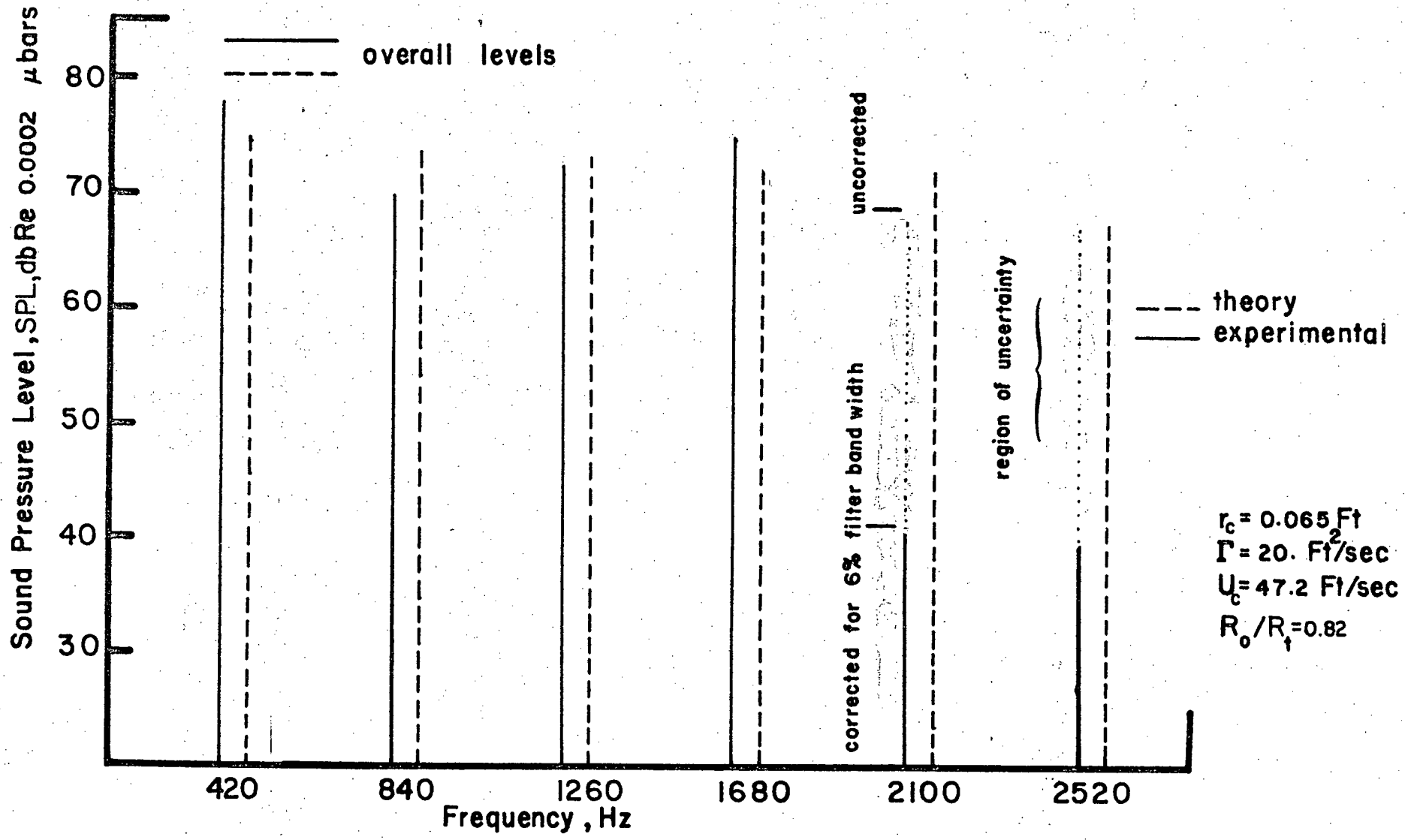

Figure 39 Comparison of Theoretical and Experimental Far Field Fan Noise Spectra. (Positive Circulation Sense)

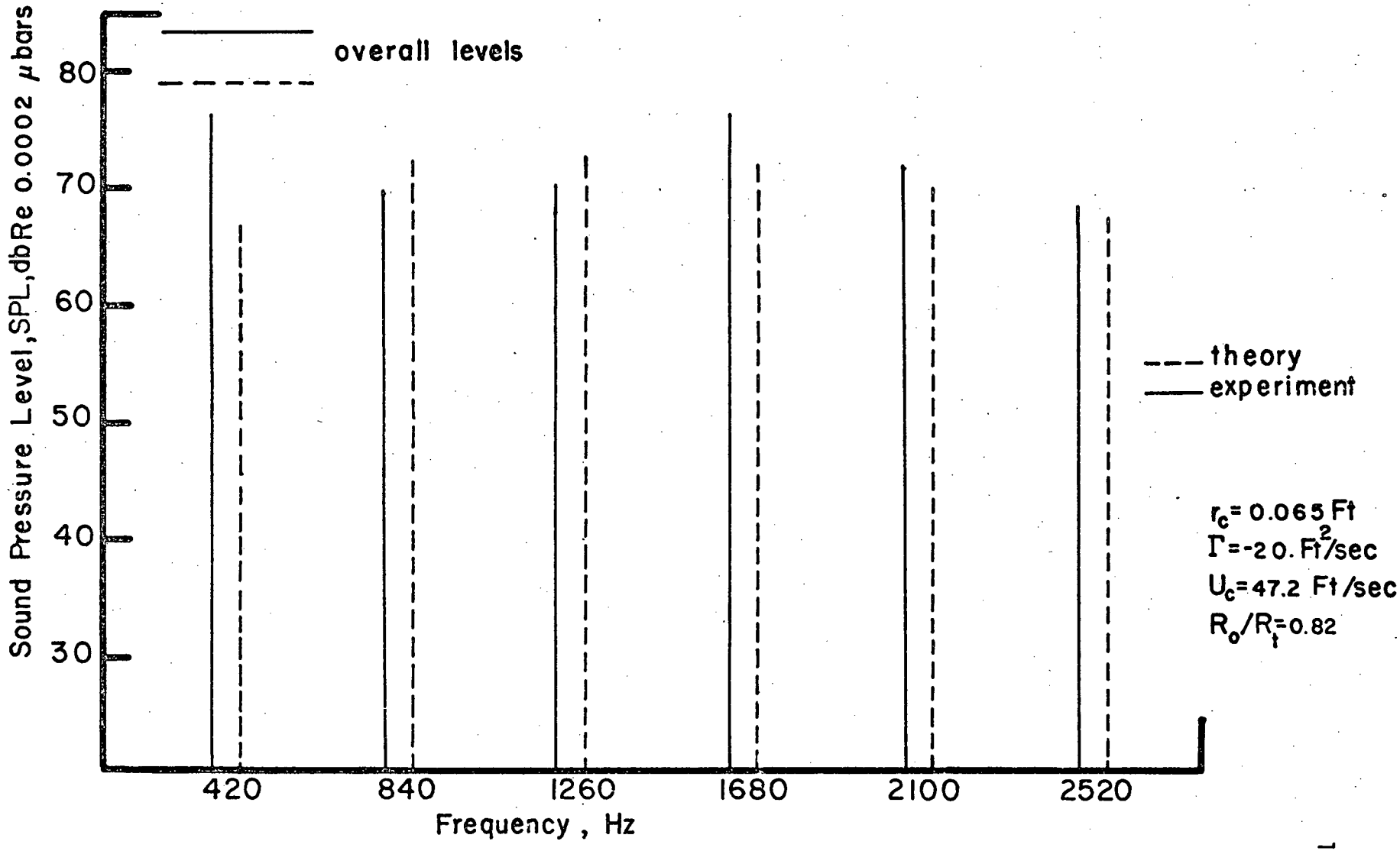

Figure 40 Comparison of Theoretical and Experimental Far Field Fan Noise Spectra (Negative Circulation Sense)

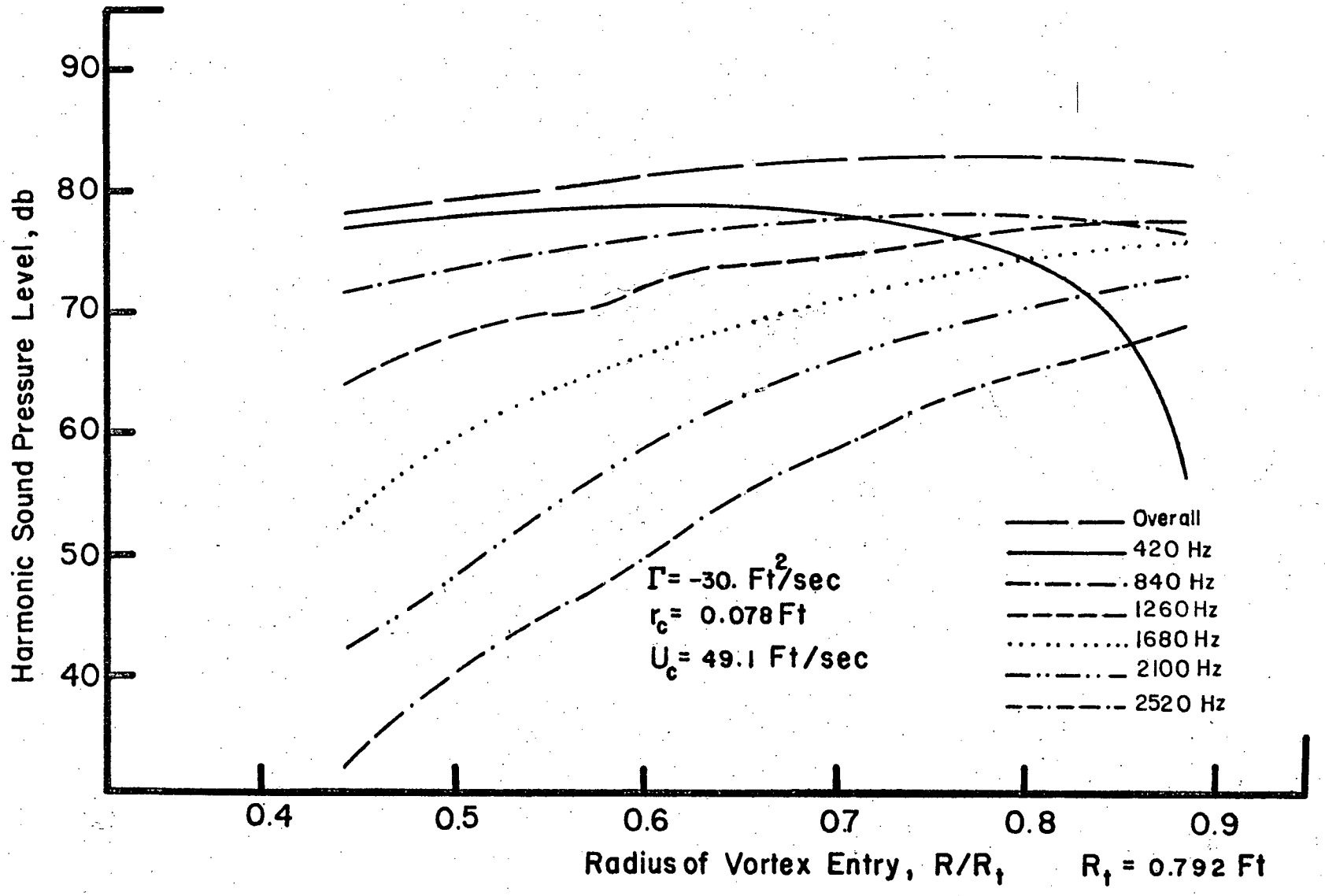

Figure 41 Variation of SPL with Radial Position of Vortex Entry (Theoretical, Negative Circulation Sense) (Compare with Figure 29 for Experimental Curves).

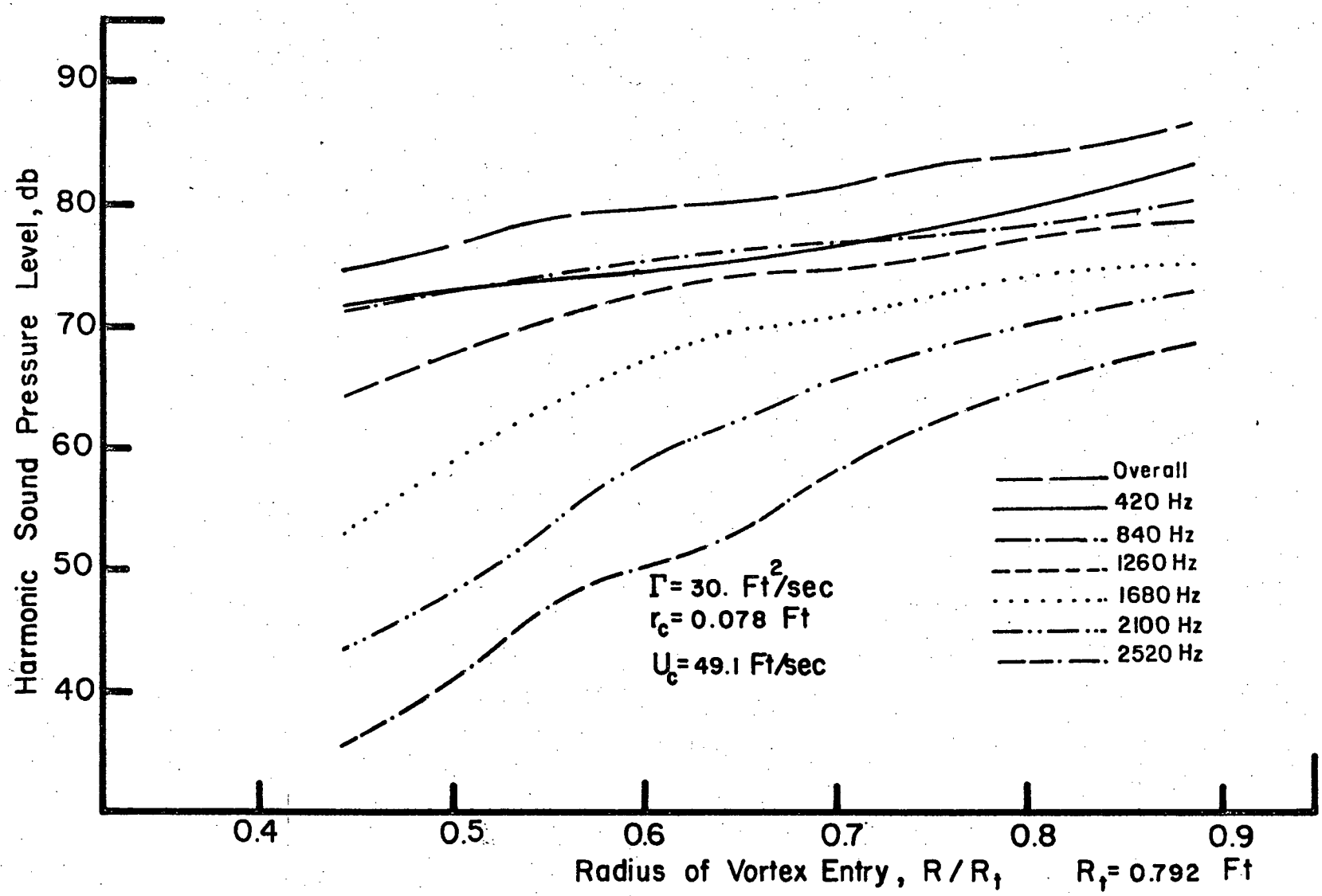

Figure 42 Variation of SPL with Radial Position of Vortex Entry (Theoretical, Positive Circulation Sense) (Compare with Figure 28 for Experimental Curves).

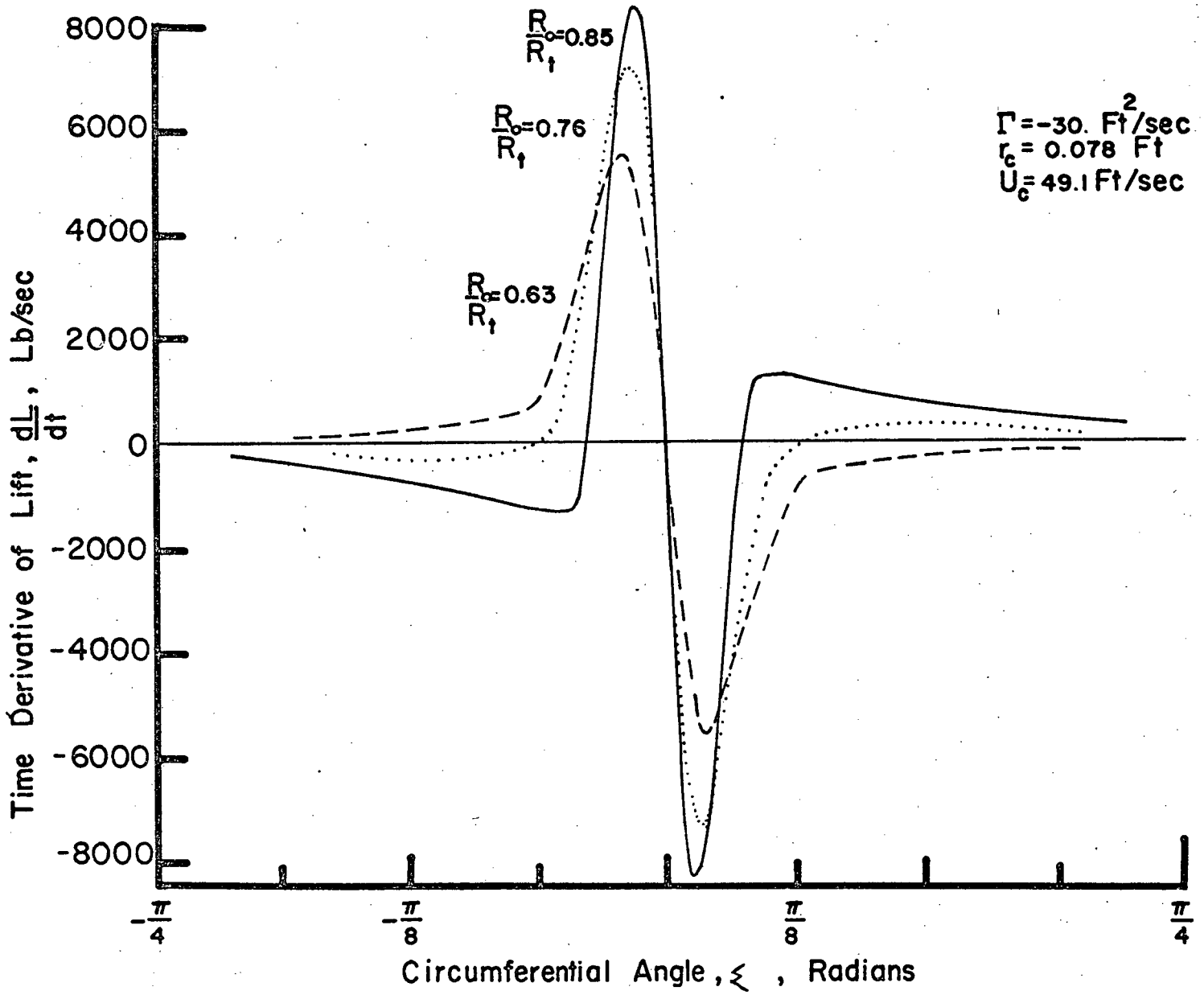

Figure 43 Change in dL/dt Curves as Vortex is Moved Radially Outwards

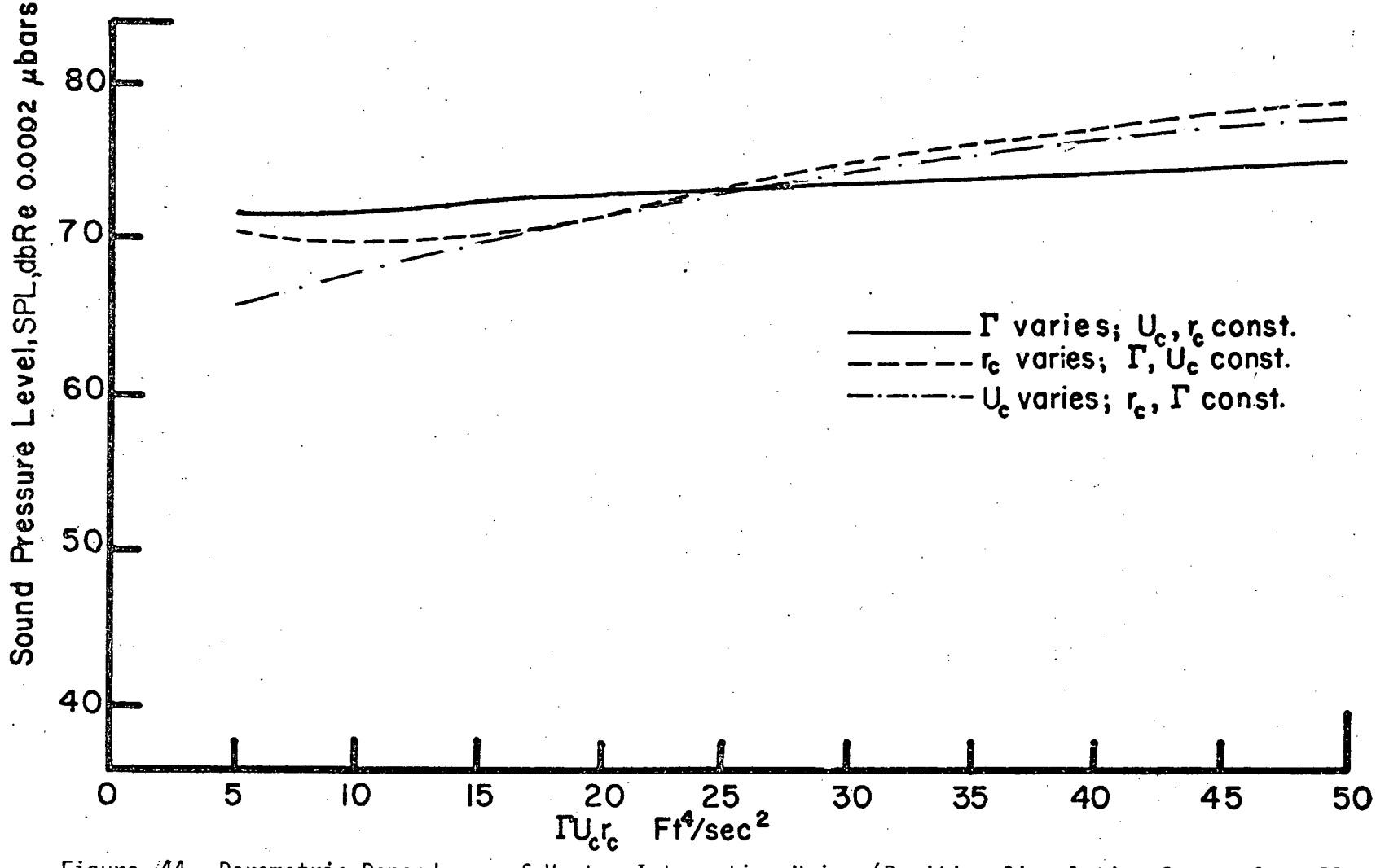

Figure 44 Parametric Dependence of Vortex Interaction Noise (Positive Circulation Sense, Overall Level)

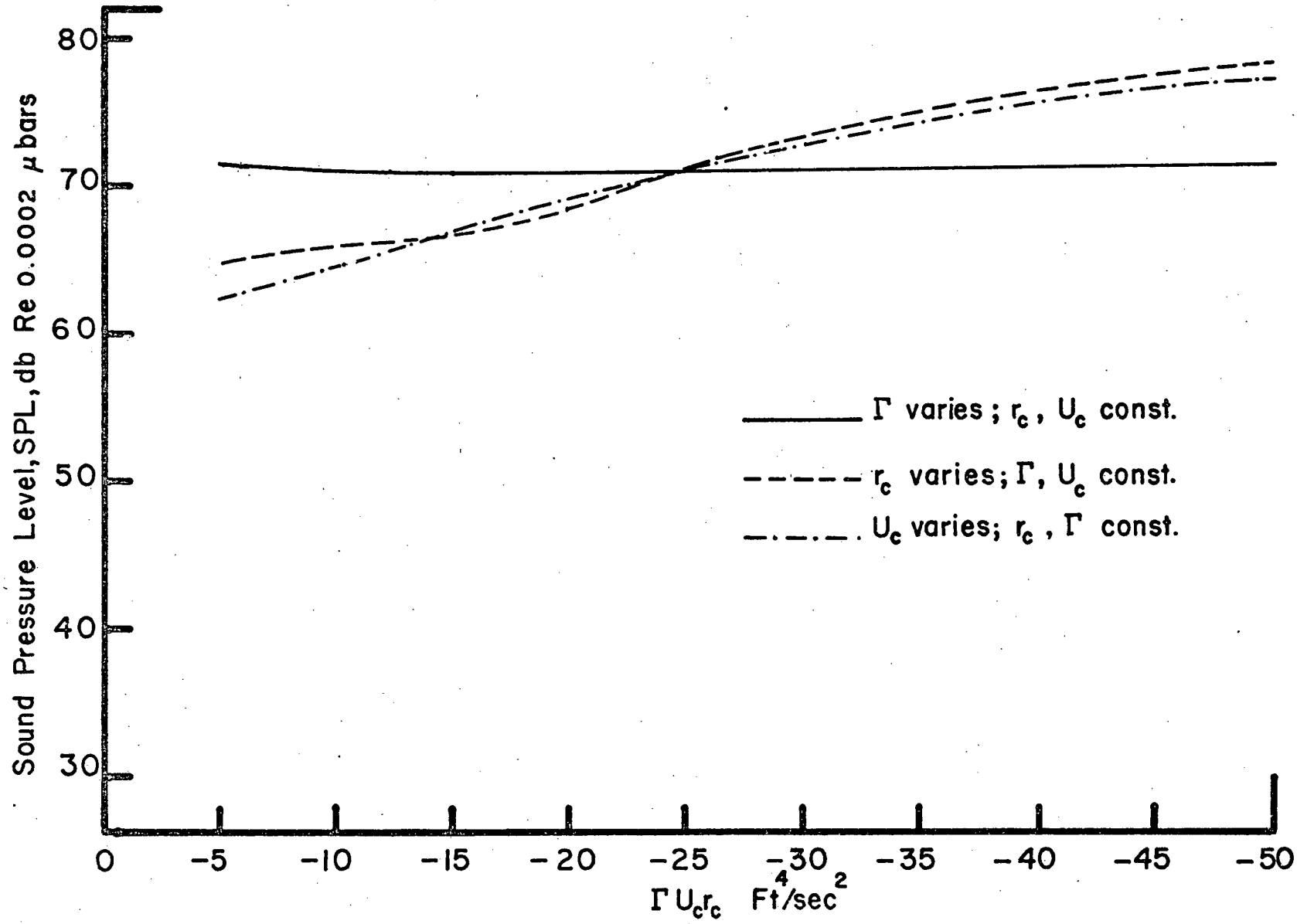

Figure 45 Parametric Dependence of Vortex Interaction Noise (Negative Circulation Sense, Overall Level)

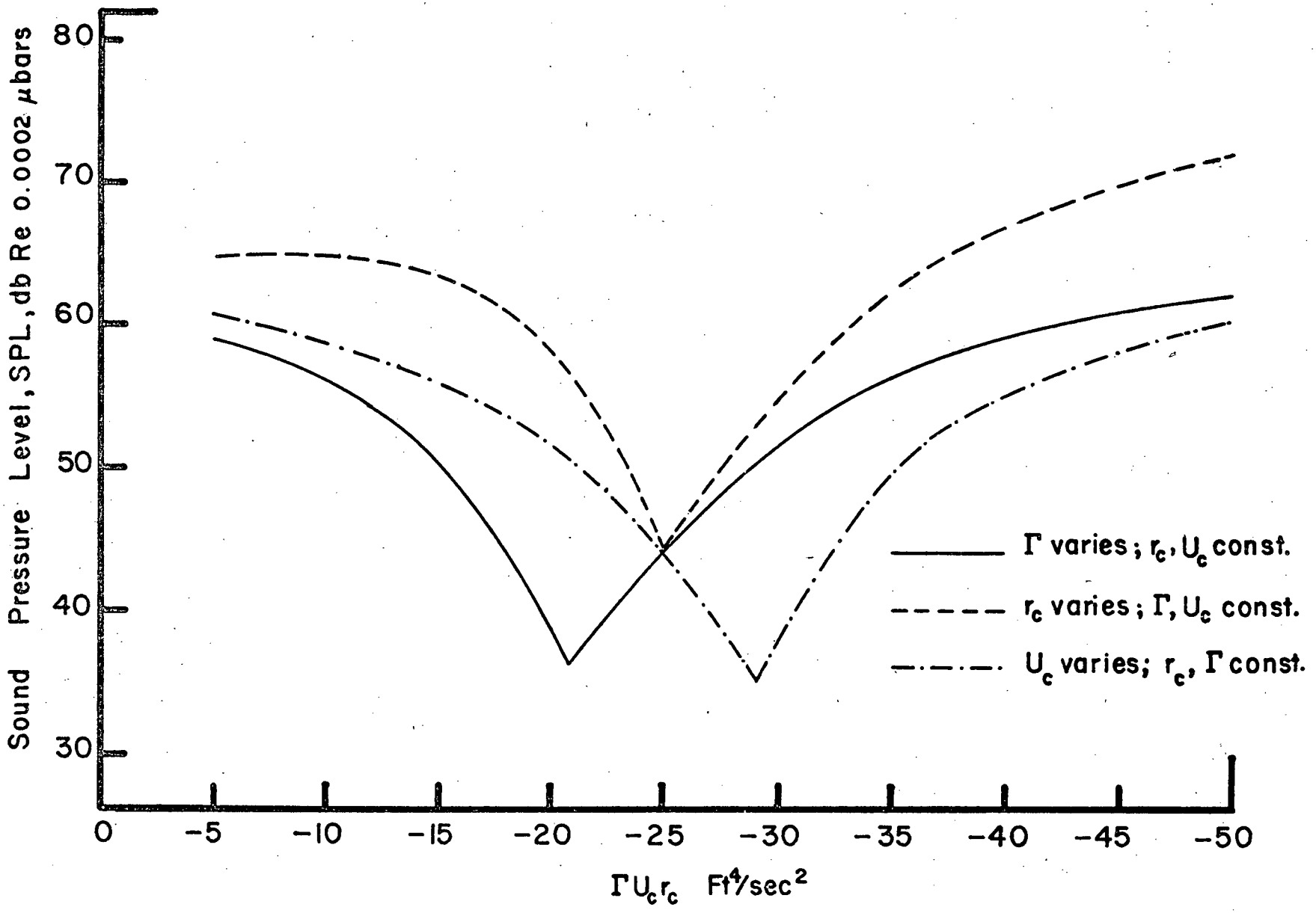

Figure 46 Parametric Dependence of Vortex Interaction Noise (Negative Circulation Sense, 420 Hz)

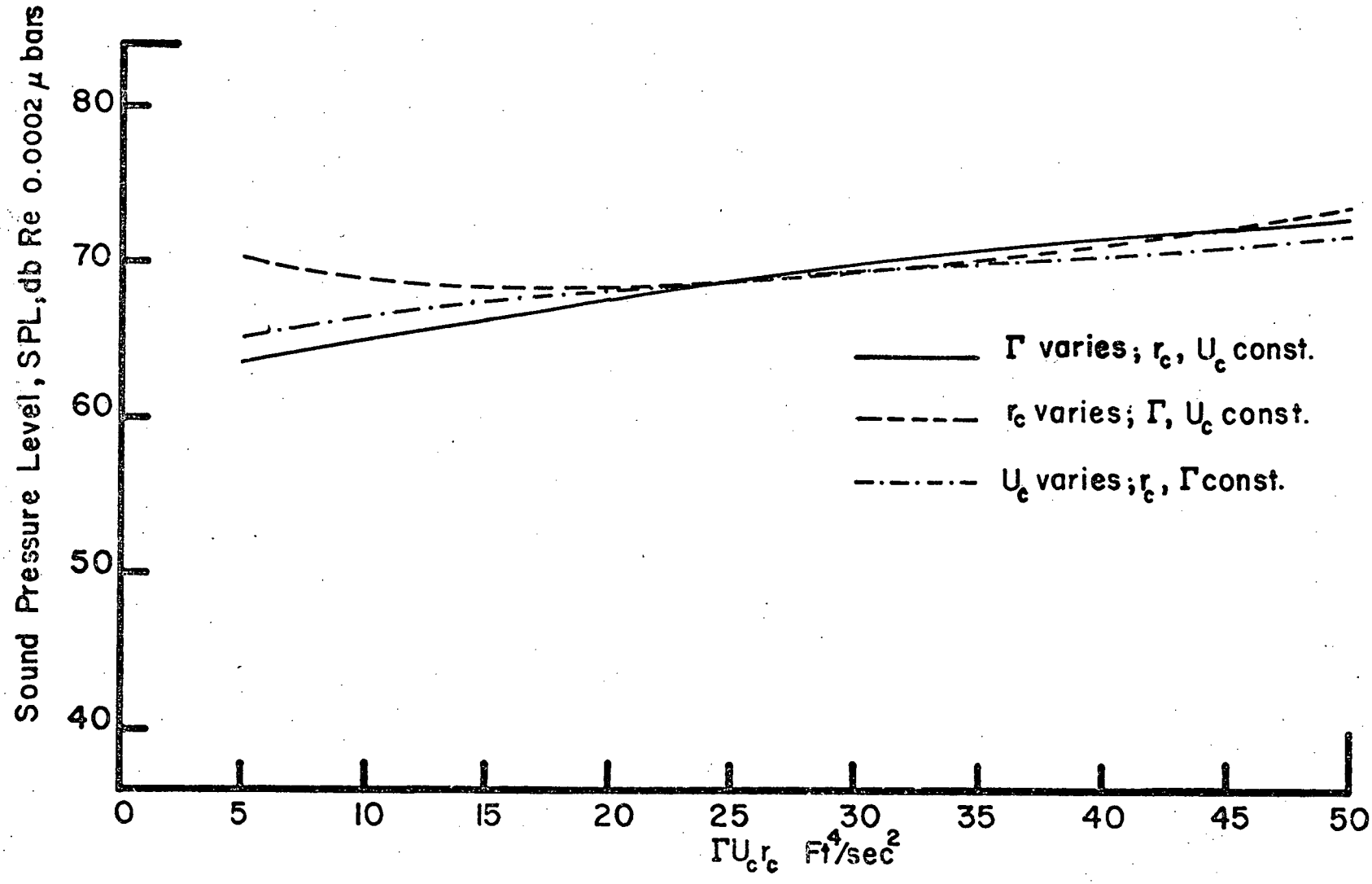

Figure 47 Parametric Dependence of Vortex Interaction Noise (Positive Circulation Sense, 420 Hz)

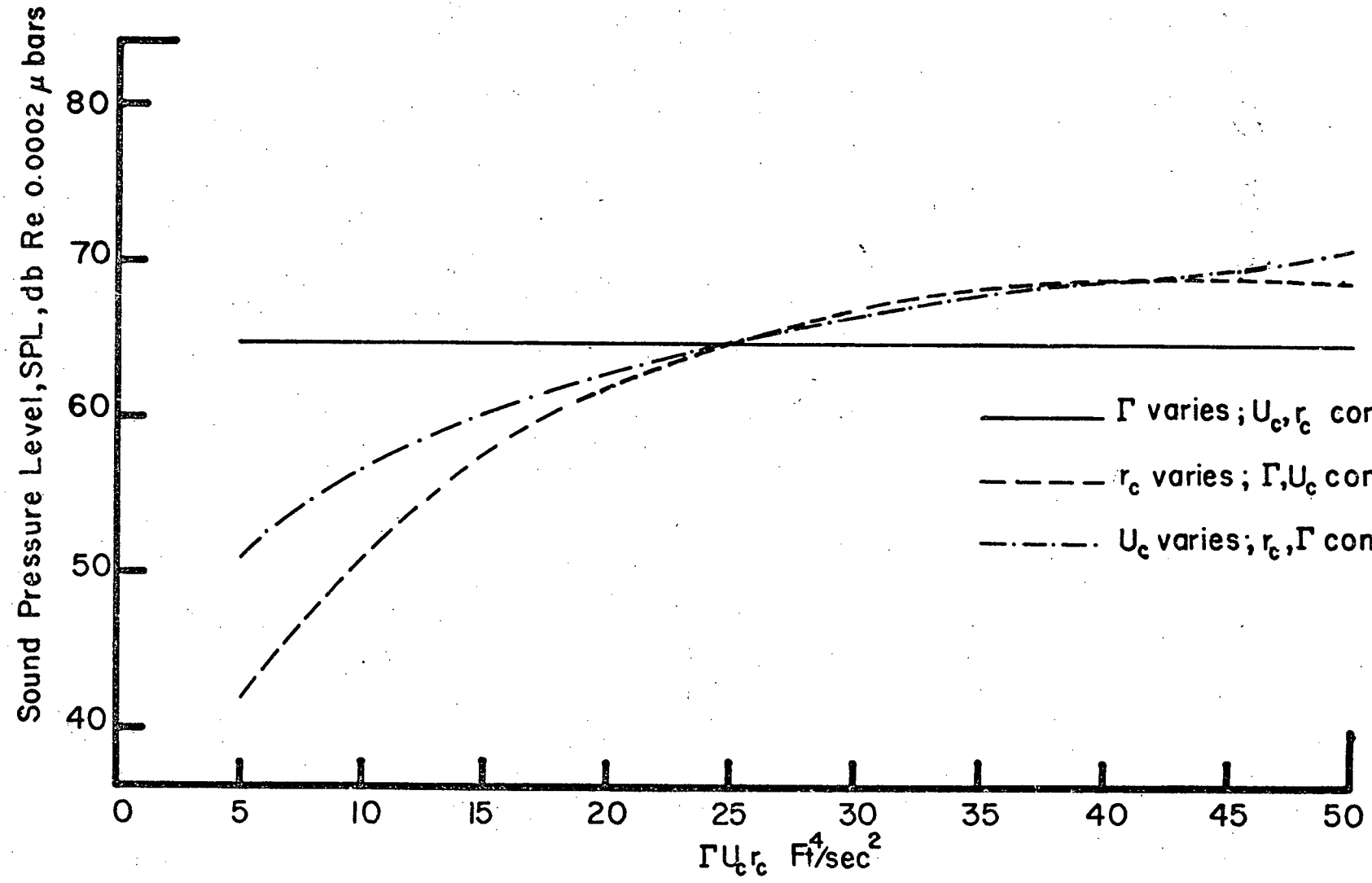

Figure 48 Parametric Dependence of Vortex Interaction Noise (Positive Circulation Sense, 1680 Hz)

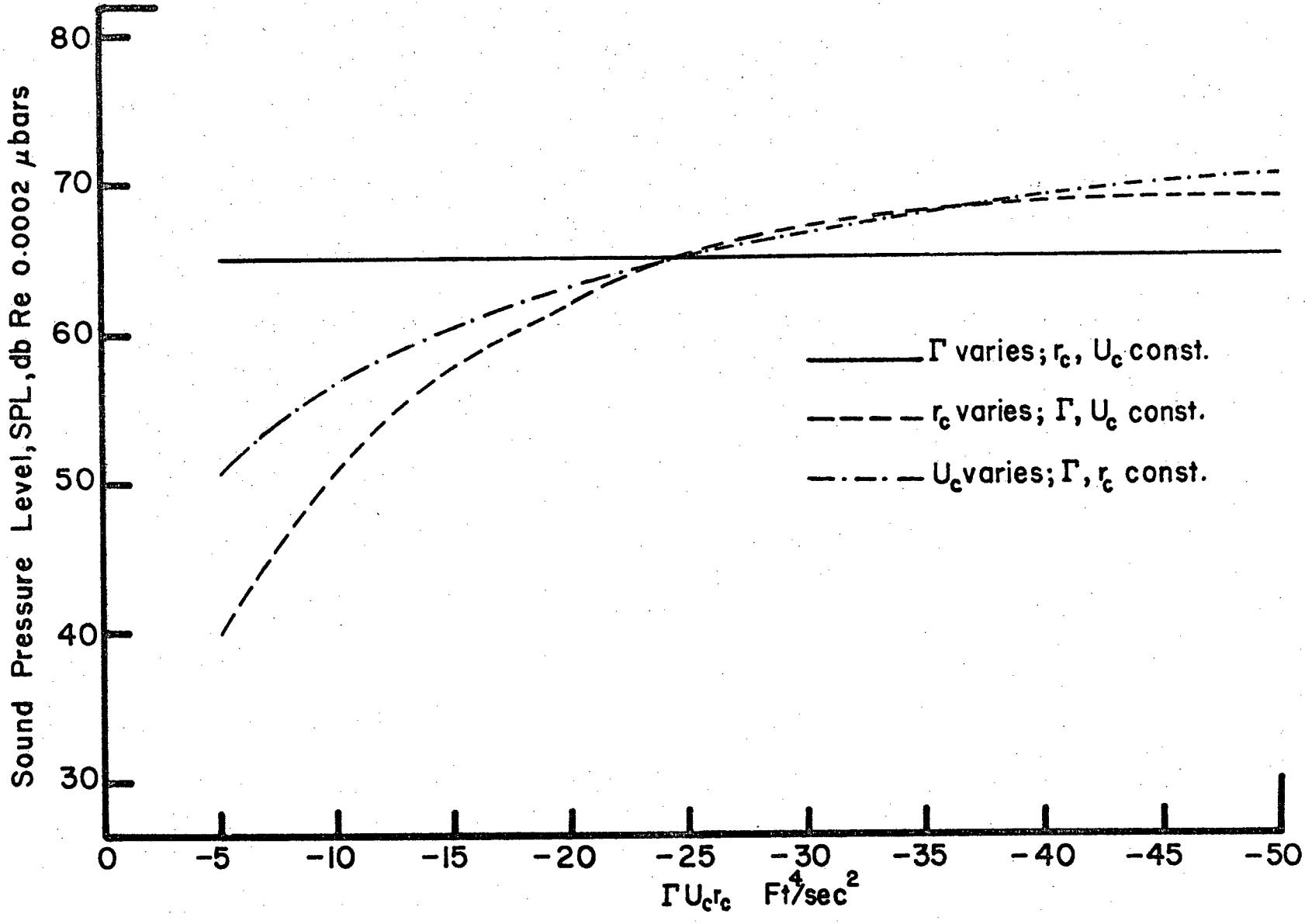

Figure 49 Parametric Dependence of Vortex Interaction Noise (Negative Circulation Sense, 1680 Hz)

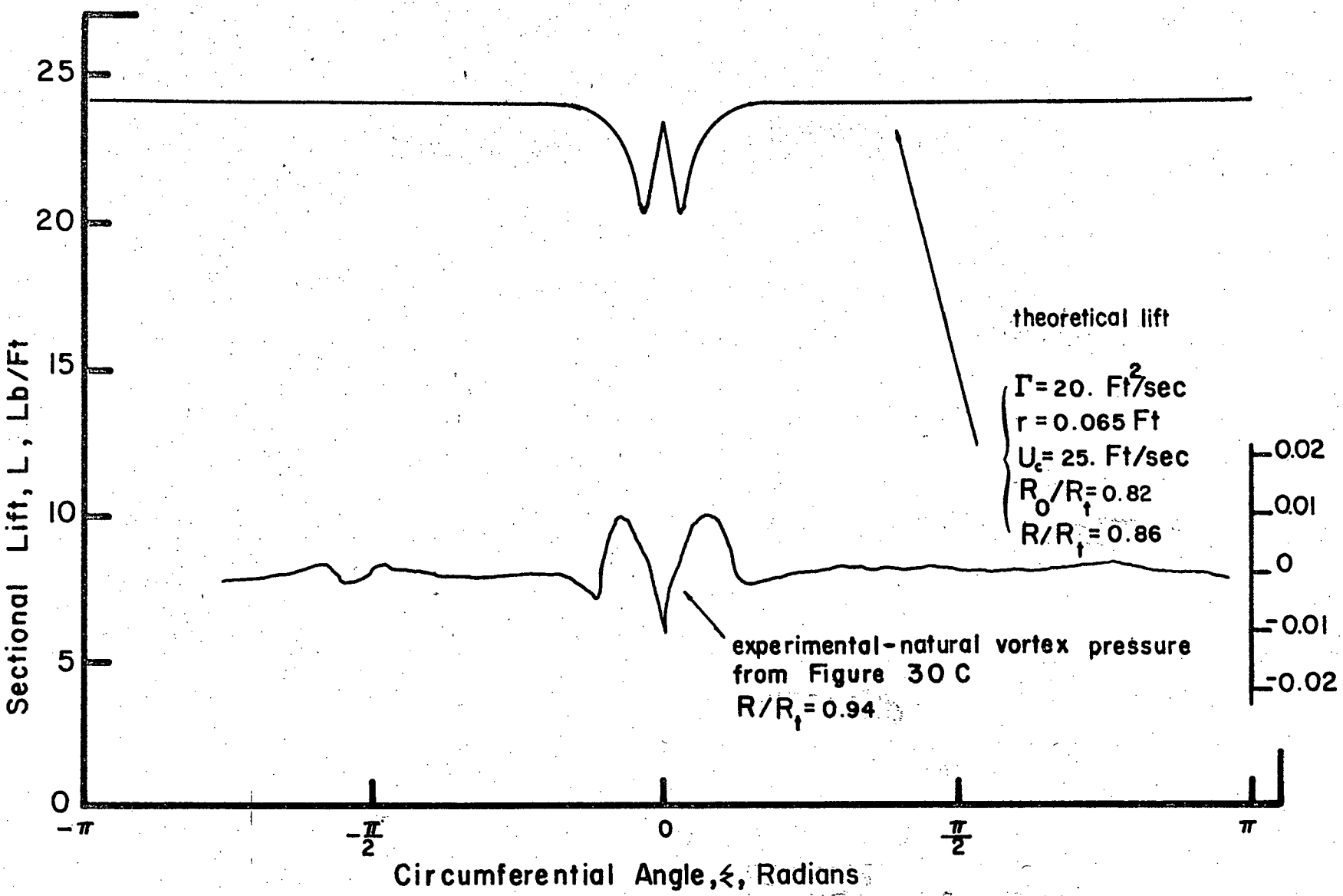

Figure 50 Circumferential Variation of Sectional Lift and Blade Pressure for Blade Sections